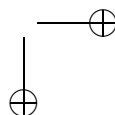
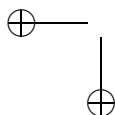
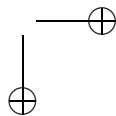
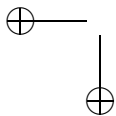
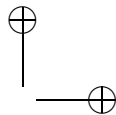
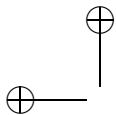
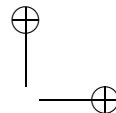
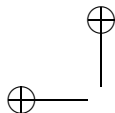


Coherent control of single atoms and Bose-Einstein condensates by light







Coherent control of single atoms and Bose-Einstein condensates by light

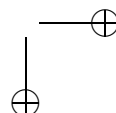
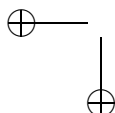
Proefschrift

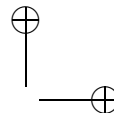
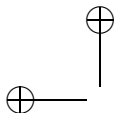
ter verkrijging van
de graad van Doctor aan de Universiteit Leiden,
op gezag van de Rector Magnificus Dr. D. D. Breimer,
hoogleraar in de faculteit der Wiskunde en
Natuurwetenschappen en die der Geneeskunde,
volgens besluit van het College voor Promoties
te verdedigen op woensdag 6 oktober 2004
klokke 15.15 uur

door

Hayk Levon Haroutyunyan

geboren te Yerevan, Armenië
op 4 februari 1975





|

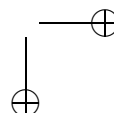
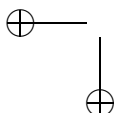
Promotiecommissie:

Promotor: Prof. dr. G. Nienhuis
Referent: Prof. dr. ir. H. B. van Linden van den Heuvell (Universiteit van Amsterdam)
Leden: Dr. P. J. H. Denteneer
Prof. dr. ir. W. van Saarloos
Dr. N. J. van Druten (Universiteit van Amsterdam)
Prof. dr. P. van der Straten (Universiteit Utrecht)
Prof. dr. P. H. Kes

—

—

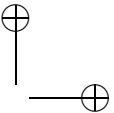
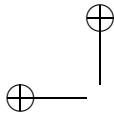
The work presented in this thesis was part of a research project supported by the
“Stichting voor Fundamenteel Onderzoek der Materie” (FOM).



|

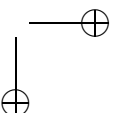
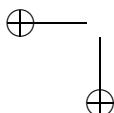
Contents

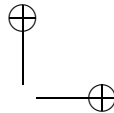
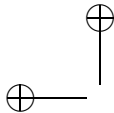
1	Introduction	3
2	Coherent control of atom dynamics in an optical lattice	5
2.1	Introduction	5
2.2	Model system	6
2.3	Operator description of evolution	8
2.4	Localized initial states	10
2.5	Constant uniform force and Bloch oscillations	12
2.6	Oscillating force	16
2.7	Discussion and conclusions	18
3	Momentum transfer for an optical transition in a prepared two-level atom	21
3.1	Introduction	21
3.2	Momentum distributions and mean momenta per atomic internal energy levels	22
3.3	The case of preparation of atomic superpositional states by scattering in the field of resonant standing wave	26
3.4	Time evolution of mean momentum per ground and excited internal energy levels in the field of travelling wave	29
3.5	Conclusions	31
4	Diffraction and trapping in circular lattices	33
4.1	Introduction	33
4.2	General framework	34
4.3	Trapping in counterrotating fields	35
4.4	Diffraction in counterrotating fields	36
4.5	Free evolution on a ring	38
4.6	Radial dispersion	42
4.7	Conclusions	44
5	Analogy between a two-well Bose-Einstein condensate and atom diffraction	47
5.1	Introduction	47
5.2	BEC in a double potential well	48
5.3	Standing-wave diffraction of atoms	50
5.4	Symmetry considerations of generic Hamiltonian	51
5.5	Pendellösung oscillations	54
5.6	Time-dependent coupling	56
5.7	Conclusions	58



2 CONTENTS

6	Resonances for coupled Bose-Einstein Condensates	59
6.1	Introduction	59
6.2	BEC in a double potential well	60
6.3	Quantum states in two wells	62
6.4	Evolution in limiting cases	64
6.5	Periodic modulation of energy difference	66
6.6	Generalization to an optical lattice	69
6.7	Periodic modulation of coupling	71
6.8	Conclusions	73
7	Phase dynamics of a multimode Bose condensate controlled by decay	75
7.1	Introduction	75
7.2	Quantum states of two boson modes	76
7.3	Decay and detection statistics of two boson modes	79
7.4	Detection statistics of two coupled boson modes	85
7.5	Linear and circular chains of modes	90
7.6	Discussion and conclusions	94
	BIBLIOGRAPHY	96
	Samenvatting	101
	Summary	105
	Curriculum Vitae	111
	Acknowledgements	113
	Publications	115





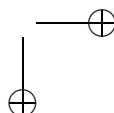
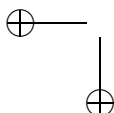
Chapter 1

Introduction

The fundamental issue of interaction between light and matter arises in several phenomena related to the manipulation of quantum matter. This is a widely studied topic, especially in recent years, triggered by the successful attempts of neutral atom cooling and trapping in light fields [1–3]. While interacting with light fields, an atom exchanges momentum and energy with the light field and experiences light forces which may confine the atom spatially and diminish the thermal component of the atomic dynamics. The recent advances in cooling and trapping techniques allow such low temperatures that the quantum features of the atomic dynamics become crucial. Besides, the light fields serve as the main tool allowing a high-quality control on properties of quantum matter such as neutral atoms. This has been implemented in several applications. The most important among them remain atomic clocks and atomic interferometers [4, 5]. Cold atoms seem to be very promising candidates to build interferometers with a sensitivity that can not be achieved by conventional, purely optical interferometric schemes. Another practical implementation of cold atoms and especially cold ions is related to their implementation in various schemes of quantum computation [6, 7].

The next step in the direction of making neutral atoms "more quantum-mechanical" has been done in 1995 after the first experimental demonstration of a Bose-Einstein Condensate (BEC) [8, 9]. Employing the technique of evaporative cooling one can access such low temperatures that most of the trapped atoms populate the one-particle ground state, giving rise to macroscopic population of a single quantum energy level. Thus, now the quantum properties of the matter are amplified and can be probed on a macroscopic level. Whereas most theories describing a sample of cold atoms neglect correlations between atoms forming the sample, one must take into account interparticle interactions between atoms forming the condensate and consider BEC as a truly multiparticle system. The early theoretical work on a single-mode condensate was based on the Gross-Pitaevskii-Bogoliubov theory, which treats the system semiclassically. This is based on analogies with the theory of superfluidity, which suggests to observe, for instance, vortices for BEC [10, 11]. In the mean time, a BEC can exhibit quantum features not covered by the semiclassical theory. Such features have been predicted [12] and observed for a multimode BEC, such as a BEC trapped in an optical lattice, in the limit where interparticle interactions are strong [13, 14]. The existence of a multimode condensate raises the important question of the relative phase between modes [15, 16].

In this thesis, we consider some examples and physical situations where light fields are employed to manipulate cold atomic samples or BECs with high degree of precision. We start with a consideration of single atoms, and then extend the discussion to multiparticle systems such as BECs.



In Chapter 2 we consider the possibilities for state preparation and state control of a single trapped atom in a tilted periodic optical potential. Normally, a periodic optical potential is formed as a result of interference between counterpropagating travelling waves. Here, in addition to the periodic potential, a uniform force is applied having arbitrary time dependence. We describe the full dynamics of the atom in such a potential on the basis of an exactly solvable model.

In the mean time, one can consider the interaction of a single two-level atom with a pulsed periodic optical potential or a single atom diffracting on a standing wave. This is described in Chapter 3. One can control the dynamics of the diffracted atoms by applying a succeeding travelling wave and appropriately choosing the interaction periods. It is also shown that the amount of momentum, that the photons transfer between the atomic internal energy levels during the interaction with a travelling wave, may be larger than the photon momentum $\hbar k$.

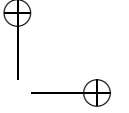
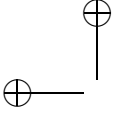
Whereas the interaction of an atom with counterpropagating travelling waves is accompanied by an exchange of linear momentum between the light field and the atom, interaction with a pair of Laguerre-Gaussian (LG) beams with opposite helicity leads to a large exchange of angular momentum. The LG beams are known to carry orbital angular momentum. The LG beams with opposite helicity form a circular lattice configuration, which has some principal advantages in comparison with a linear one. This suggests a novel scheme for atom interferometry without mirror pulses. We discuss it in Chapter 4.

Starting from Chapter 5 we consider multimode BECs. As a model problem, we take a particular physical realization in the form of a BEC trapped in a potential having a two-well geometry. Such a potential is a simple example of a two-mode system. We compare the dynamics of a BEC in such a trap with the dynamics of atoms diffracting from a standing light wave. The corresponding Hamiltonians have an identical appearance, but with a different set of commutation rules. Some well-known diffraction phenomena are shown to have analogies in the two-well case. They represent a collective exchange of a fixed number of atoms between the wells.

Then, in Chapter 6 we continue studying properties of double-well condensates. A sensitive way to probe their properties in the limit of with strong interatomic interactions is to look for resonant behavior when an external periodic perturbation acts on the system. The response of the system may be expected to be very sensitive to the value of the modulation frequency in the neighborhood of a resonance. The periodic perturbation can be implemented by modulating the form of the trapping potential. From a practical viewpoint, one can control the average number of particles in the wells by varying the parameters of the periodic perturbation.

In Chapter 7 we consider the relative phase build-up between the modes of a multimode BECs while observing the decay product from the modes in interference. We discuss exactly solvable models for this process in cases where competing observation channels drive the phases to different sets of values. We treat the case of two modes which both emit into the input ports of two beam splitters, and of a linear or circular chain of modes.

The chapters of this thesis have been written as separate papers. In order to allow a reader to read the chapters independently, some overlap between the chapters is unavoidable.



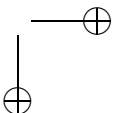
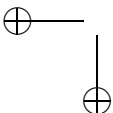
Chapter 2

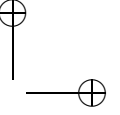
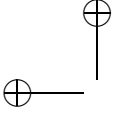
Coherent control of atom dynamics in an optical lattice

On the basis of a simple exactly solvable model we discuss the possibilities for state preparation and state control of atoms in a periodic optical potential. In addition to the periodic potential a uniform force with an arbitrary time dependence is applied. The method is based on a formal expression for the full evolution operator in the tight-binding limit. This allows us to describe the dynamics in terms of operator algebra, rather than in analytical expansions.

2.1 Introduction

The energy eigenvalues of a quantum particle moving in a periodic potential form energy bands (the Bloch bands) that are separated by band gaps. The eigenstate within a band is characterized by the quasimomentum, which determines the phase difference between two points separated by a period. An initially localized wave packet typically propagates through space, leading to unbounded motion. When an additional uniform force is applied, the Bloch bands break up into a ladder of equally spaced energy levels called the Wannier-Stark ladder. In this case, a wave packet of the particle extending over several periods can exhibit bounded oscillatory motion, termed Bloch oscillation, at a frequency determined by the level separation in the ladder. These early results of the quantum theory of electrons in solid crystals [17–20] have regained interest recently due to the advent of optical lattices for atoms. These lattices are formed when cold atoms are trapped in the periodic potential created by the superposition of a number of traveling light waves [21–24]. In contrast to the case of electrons in crystal lattices, these optical lattice fields have virtually no defects, they can be switched on and off at will, and dissipative effects can be largely controlled. The phenomenon of Bloch oscillations was first observed for cesium atoms in optical lattices [25, 26]. The uniform external force is mimicked by a linear variation of the frequency of one of the counterpropagating traveling waves, thereby creating an accelerated standing wave. By applying a modulation on the standing-wave position, Rabi oscillations between Bloch bands, as well as the level structure of the Wannier-Stark ladder have been observed for sodium atoms in an optical lattice [27–29]. Theoretical studies of transitions between ladders have also been presented [30, 31]. Bloch oscillations have also been demonstrated for a light beam propagating in an array of waveguides, with a linear variation of the refractive index imposed by a temperature gradient [32].





When the applied uniform force is oscillating in time, the motion of a particle in a periodic potential is usually unbounded. However, it has been predicted that the motion remains bounded for specific values of the ratio of the modulation frequency and the strength of the force [33,34]. Similar effects of dynamical localization, including routes to chaos, have been studied experimentally for optical lattices, including both amplitude and phase modulation of the uniform force [35]. Phase transitions have been predicted for atoms in two incompatible periodic optical potentials imposed by bichromatic standing light waves [36].

In the present paper we discuss the Wannier-Stark system with a time-dependent force, as a means of preparing the state of particles in a periodic potential. We derive an exact expression for the evolution operator of the particle, with an arbitrary time-dependent force. This allows one to apply the combination of delocalizing dynamics in the absence of the uniform force with the periodic dynamics induced by a uniform force for coherent control of the state of the particles. Exact solutions in the case of a constant uniform force have been obtained before by analytical techniques [37,38]. The operator method allows an exact and unified scheme to describe phenomena induced by an oscillating force. Examples are dynamical localization and fractional Wannier-Stark ladders.

The model is described in one dimension (1D). However, this is no real restriction. Under the assumption of nearest-neighbor interaction, the corresponding 2D or 3D problem exactly factorizes into a product of 1D solutions.

2.2 Model system

2.2.1 Periodic potential

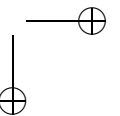
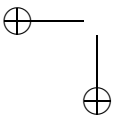
The quantum-mechanical motion of atoms in a periodic optical potential $V(x)$ with period a is described by the Hamiltonian

$$H_0 = \frac{P^2}{2M} + V(x). \quad (2.1)$$

We assume that the atoms are sufficiently cooled, so that only the lowest energy band is populated. The ground state in well n located at $x = na$ is indicated as $|n\rangle$. These states play the role of the basis of localized Wannier states. For simplicity we take the tight-binding limit, where only the ground levels in neighboring wells are coupled. When we choose the zero of energy at the ground level in a well, the Hamiltonian (2.1) projected on these ground levels is defined by

$$H_0 = \frac{1}{2} \hbar \Omega (B_+ + B_-), \quad B_{\pm} |n\rangle = |n \pm 1\rangle. \quad (2.2)$$

The raising and lowering operators B_+ and B_- are each other's Hermitian conjugates, and each one of them is unitary. The frequency Ω measures the coupling between neighboring wells, due to tunneling through the barriers. We shall allow the coupling to depend on time. The eigenstates of H_0 are directly found by diagonalizing the corresponding matrix. These states are the Bloch states $|k\rangle$, with energy $E(k) = \hbar \Omega \cos(ka)$. Their expansion in the



Wannier states and the inverse relations can be expressed as

$$|k\rangle = \sqrt{\frac{a}{2\pi}} \sum_n e^{inka} |n\rangle, \quad |n\rangle = \sqrt{\frac{a}{2\pi}} \int dk e^{-inka} |k\rangle. \quad (2.3)$$

Obviously, the states $|k\rangle$ are periodic with period $2\pi/a$, and the quasimomentum k can be chosen from the Brillouin zone $[-\pi/a, \pi/a]$. The integration in Eq. (2.3) extends over this Brillouin zone. From the translation property $\langle x|n\rangle = \langle x+a|n+1\rangle$ of the Wannier wave functions it follows that the states (2.3) do indeed obey the Bloch condition $\langle x+a|k\rangle = \exp(ika)\langle x|k\rangle$. When the states $|n\rangle$ are normalized as $\langle n|m\rangle = \delta_{nm}$, the Bloch states obey the continuous normalization relation $\langle k|k'\rangle = \delta(k-k')$.

2.2.2 Uniform force

An additional uniform force is described by adding to the Hamiltonian the term

$$H_1 = \frac{\hbar x \Delta}{a}, \quad (2.4)$$

where the (possibly time-dependent) force of size $\hbar\Delta(t)/a$ is in the negative direction. On the basis of the Wannier states, this term is diagonal, and it is represented as

$$H_1 = \hbar\Delta B_0, \quad B_0|n\rangle = n|n\rangle. \quad (2.5)$$

Hence the evolution of a particle occurs under the influence of the total Hamiltonian

$$H = H_0 + H_1, \quad (2.6)$$

with H_0 and H_1 defined by eqs. (2.2) and (2.5), in terms of the operators B_{\pm} and B_0 . We shall also need expressions for the operators B_{\pm} and B_0 acting on a Bloch state. These can be found from the definition of the operators and the expansions (2.3). One easily finds that

$$B_{\pm}|k\rangle = e^{\mp ika}|k\rangle, \quad e^{-i\beta B_0}|k\rangle = |k - \beta/a\rangle. \quad (2.7)$$

In Bloch representation the operators have the significance $B_{\pm} = \exp(\mp ika)$ and $B_0 = (i/a)(d/dk)$, which is confirmed by the commutation rules (2.8). The Wannier states may be viewed as discrete position eigenstates, with B_0 the corresponding position operator. The Bloch states play the role of momentum eigenstates, and the finite range of their eigenvalues within the Brillouin zone reflects the discreteness of the position eigenvalues.

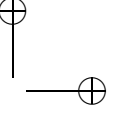
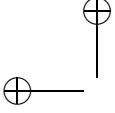
2.2.3 Operator algebra

The basic operators B_{\pm} and B_0 obey the commutation rules

$$[B_0, B_{\pm}] = \pm B_{\pm}, \quad [B_+, B_-] = 0. \quad (2.8)$$

In order to derive exact expressions for the evolution operator corresponding to the Hamiltonian (2.6), we need several operator identities involving these operators B_0 and B_{\pm} . The identities

$$e^{i\beta B_0} B_{\pm} e^{-i\beta B_0} = e^{\pm i\beta} B_{\pm} \quad (2.9)$$



directly follow from the commutation rules (2.8), and they lead the transformation rules

$$e^{i\beta B_0} \exp\left(-i\frac{1}{2}\alpha(B_+ + B_-)\right) e^{-i\beta B_0} = \exp\left(-i\frac{1}{2}\alpha(e^{i\beta} B_+ + e^{-i\beta} B_-)\right) \quad (2.10)$$

for arbitrary values of α and β . We shall also need the equalities

$$\exp\left(\frac{i}{2}\alpha B_{\pm}\right) B_0 \exp\left(-\frac{i}{2}\alpha B_{\pm}\right) = B_0 \mp \frac{i}{2}\alpha B_{\pm}, \quad (2.11)$$

which are verified after differentiation with respect to α , while using the commutation rules (2.8).

2.3 Operator description of evolution

2.3.1 Evolution operator

In this section we derive expressions for the evolution operator $U(t, 0)$, which transforms an arbitrary initial state $|\Psi(0)\rangle$ as $|\Psi(t)\rangle = U(t, 0)|\Psi(0)\rangle$. The results are valid for any time-dependence of the uniform force and the coupling between neighboring wells, as specified by $\Delta(t)$ and $\Omega(t)$. A time-dependent coupling represents the case that the intensity of the lattice beams is varied. We express the evolution operator in the factorized form

$$U(t, 0) = U_1(t, 0)U_0(t, 0), \quad (2.12)$$

where $U_1(t, 0) = \exp[-i\phi(t)B_0]$ gives the evolution corresponding to the Hamiltonian H_1 alone, in terms of the phase shift

$$\phi(t) = \int_0^t dt' \Delta(t'). \quad (2.13)$$

From the evolution equation for U with the Hamiltonian (2.6) while using the transformation (2.9) we find the evolution equation

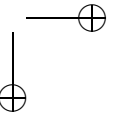
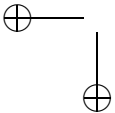
$$\frac{dU_0}{dt} = -\frac{i\Omega(t)}{2} \left(e^{i\phi(t)} B_+ + e^{-i\phi(t)} B_- \right) U_0(t). \quad (2.14)$$

Since this equation contains only the commuting operators B_+ and B_- , it can easily be integrated. In fact, the solution is given by eq. (2.10) with the time-dependent values of the real parameters α and β defined by the relations

$$\alpha(t)e^{i\beta(t)} = \int_0^t dt' \Omega(t') e^{i\phi(t')}. \quad (2.15)$$

Combining this solution with the definition of U_1 leads to a closed expression for the evolution operator $U(t, 0)$ for an arbitrary time dependence of the uniform force, in terms of the parameters α , β and ϕ defined in eq. (2.13) and (2.15). The result is $U(t, 0) \equiv R(\alpha, \beta, \phi)$, with R defined by

$$R(\alpha, \beta, \phi) = e^{i(\beta-\phi)B_0} \exp\left(-i\frac{1}{2}\alpha(B_+ + B_-)\right) e^{-i\beta B_0}. \quad (2.16)$$



This defines the unitary operator R as a function of the three parameters α , β and ϕ . The result is valid for an arbitrary time dependence of the force and the coupling, described by $\Delta(t)$ and $\Omega(t)$. The characteristics of the evolution of an arbitrary initial state are determined by the properties of the operators R as a function of α , β and ϕ . Mathematically, these operators form a three-parameter group, which is generated by the three operators B_{\pm} and B_0 .

On the basis of the Wannier states, the contribution of the operator B_0 in eq. (2.16) is trivial, whereas the effect of the exponent containing B_{\pm} can be evaluated by first expanding a Wannier state in Bloch states, for which the action of this exponent is simple. Then, reexpressing the Bloch states in Wannier states, we find

$$\exp\left(-i\frac{1}{2}\alpha(B_+ + B_-)\right)|m\rangle = \sum_n i^{-n+m} J_{n-m}(\alpha)|n\rangle, \quad (2.17)$$

where we used the defining expansion $\exp(i\xi \sin \phi) = \sum_n \exp(in\phi) J_n(\xi)$ of the ordinary Bessel functions. Hence the matrix elements of the operator (2.16) between Wannier states are

$$\langle n|R(\alpha, \beta, \phi)|m\rangle = (ie^{-i\beta})^{-n+m} e^{-in\phi} J_{n-m}(\alpha). \quad (2.18)$$

For the evolution operator (2.16) in Bloch representation we can just use the form of the operators B_{\pm} and B_0 , as given in Sec. 2.2.2. This leads to the result

$$R(\alpha, \beta, \phi)|k\rangle = e^{-i\alpha \cos(ka-\beta)}|k - \phi/a\rangle. \quad (2.19)$$

This shows that the quasimomentum as a function of time varies as $k(t) = k(0) - \phi(t)/a$, with $\phi(t)$ given in eq. (2.13). The parameter ϕ determines the shift of the quasimomentum during the evolution. The expressions (2.18) and (2.19) clarify the significance of the three parameters α , β , and ϕ that specify the evolution operator.

2.3.2 Heisenberg picture

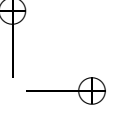
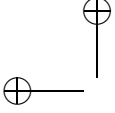
The transport properties of any initial state are conveniently described by the evolution of the operators in the Heisenberg picture. Since any evolution operator can be written in the form of $R(\alpha, \beta, \phi)$ for the appropriate values of the parameters, we can view $R^\dagger B R$ as the Heisenberg operator corresponding to any operator B . The Heisenberg operators corresponding to B_{\pm} can be expressed as

$$R^\dagger(\alpha, \beta, \phi) B_{\pm} R(\alpha, \beta, \phi) = e^{\pm i\phi} B_{\pm}, \quad (2.20)$$

which is directly shown by using eq. (2.9). Since $B_{\pm} = \exp(\mp ika)$ in Bloch representation, this confirms the significance of ϕ as the shift of the value of the quasimomentum.

After using the transformation property (2.11), one finds the Heisenberg operator corresponding to the position operator B_0 as

$$R^\dagger(\alpha, \beta, \phi) B_0 R(\alpha, \beta, \phi) = B_0 + \frac{i\alpha}{2}(e^{-i\beta} B_- - e^{i\beta} B_+). \quad (2.21)$$



This implies that the expectation value of the position after evolution is determined by

$$\langle n \rangle = \langle B_0 \rangle + \frac{i\alpha}{2} (e^{-i\beta} \langle B_- \rangle - e^{i\beta} \langle B_+ \rangle), \quad (2.22)$$

where the averages in the right-hand side should be taken with respect to the initial state. Hence no displacement of a wave packet can occur whenever $\langle B_+ \rangle = \langle B_- \rangle^* = 0$. This is true whenever the initial state is diagonal in the Wannier states $|n\rangle$. Conversely, average motion of a wave packet can occur only in the presence of initial phase coherence between neighboring Wannier states. The width of a wave packet is determined by the expectation value of the square of the Heisenberg position operator (2.21). This gives the expression

$$\begin{aligned} \langle n^2 \rangle &= \langle B_0^2 \rangle + \frac{\alpha^2}{4} (2 - e^{-2i\beta} \langle B_-^2 \rangle - e^{2i\beta} \langle B_+^2 \rangle) \\ &\quad + \frac{i\alpha}{2} (e^{-i\beta} \langle B_0 B_- + B_- B_0 \rangle - e^{i\beta} \langle B_0 B_+ + B_+ B_0 \rangle). \end{aligned} \quad (2.23)$$

2.4 Localized initial states

2.4.1 Arbitrary wave packets

A fairly localized initial state $|\Psi(0)\rangle = \sum_n c_n |n\rangle$ with a reasonably well-defined quasimomentum can be modeled by assuming that neighboring states have a fixed phase difference θ , so that

$$c_n^* c_{n+1} = |c_n c_{n+1}| e^{i\theta}. \quad (2.24)$$

Thus, the quasimomentum is initially centered around the value $k_0 = \theta/a$. For simplicity, we assume moreover that the distribution over Wannier states is even in n , so that $|c_n| = |c_{-n}|$. The initial average position of the particle is located at $n = 0$. In order to evaluate the time-dependent average position and spreading of the packet, we can apply eqs. (2.22) and (2.23). The symmetry of the distribution implies that $\langle B_0 \rangle = 0$, while $\langle B_0^2 \rangle = \sigma_0^2$ is the initial variance of the position. When we introduce the quantities

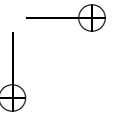
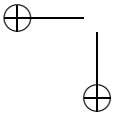
$$\sum_n |c_{n+1} c_n| \equiv b_1, \quad \sum_n |c_{n+2} c_n| \equiv b_2, \quad (2.25)$$

we obtain the simple identities

$$\langle B_+ \rangle = b_1 e^{-i\theta}, \quad \langle B_+^2 \rangle = b_2 e^{-2i\theta}, \quad \langle B_0 B_+ \rangle = -\langle B_+ B_0 \rangle = \frac{1}{2} b_1 e^{-i\theta}. \quad (2.26)$$

The last identity is proved by using the fact that the quantity $f_{2n+1} \equiv |c_{n+1} c_n|$ is even in its index (which takes only odd values). Therefore, $\sum_l l f_l = 0$, which is equivalent to the statement that $2\langle B_+ B_0 \rangle + \langle B_+ \rangle = 0$. The other expectation values occurring in eqs. (2.22) and (2.23) are found by taking the complex conjugates of the identities (2.26). This leads to the simple exact results

$$\langle n \rangle = \alpha b_1 \sin(\beta - \theta) \langle n^2 \rangle = \sigma_0^2 + \frac{\alpha^2}{2} (1 - b_2 \cos 2(\beta - \theta)), \quad (2.27)$$



so that the variance of the position is found as

$$\sigma^2 \equiv \langle n^2 \rangle - \langle n \rangle^2 = \sigma_0^2 + \frac{\alpha^2}{2} \left(1 - b_1^2 - (b_2 - b_1^2) \cos 2(\beta - \theta) \right). \quad (2.28)$$

Notice that the parameters b_1 and b_2 are real numbers between 0 and 1. In the limit of a wide initial wave packet, determined by coefficients c_n whose absolute values vary slowly with n , the parameters b_1 and b_2 will both approach 1, and the width σ will not vary during the evolution. In the opposite special case that the initial state is the single Wannier state $|0\rangle$, one finds that $b_1 = b_2 = 0$, so that the width $\sigma = \alpha/\sqrt{2}$.

In the special case that the particle is initially localized in the single Wannier state at $x = 0$, so that $|\Psi(0)\rangle = |0\rangle$, the parameters b_1 , b_2 , and σ_0 vanish, so that

$$\langle n \rangle = 0, \quad \sigma^2 = \langle n^2 \rangle = \alpha^2/2. \quad (2.29)$$

This shows that the average position of the wave packet does not change, and that its width is determined by the parameter α alone. This is in line with the fact that the population distribution over the Wannier states after the evolution is $p_n = |\langle n|R|0\rangle|^2 = J_n^2(\alpha)$, as follows from Eq. (2.18). Hence the (time-dependent) value of α determines the spreading of an initially localized particle.

2.4.2 Gaussian wave packet

When the initial distribution over the sites is Gaussian with a large width, we can evaluate the full wave packet after evolution. Suppose that the initial state is specified by the coefficients

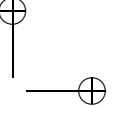
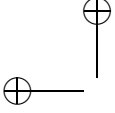
$$c_n = \frac{1}{\sqrt{\sigma_0} \sqrt{2\pi}} e^{in\theta} \exp\left(-\frac{n^2}{4\sigma_0^2}\right), \quad (2.30)$$

which obey the condition eq. (2.24). This state is properly normalized provided that $\sigma_0 \gg 1$. When the evolution operator is expressed as in (2.16), the time-dependent state is expanded as $|\Psi(t)\rangle = R|\Psi(0)\rangle = \sum_n f_n \exp[in(\theta - \phi)]|n\rangle$. Summation expressions for the coefficients f_n are directly obtained by using the expression (2.18) of R in Wannier representation. We use similar techniques to those applied in Ref. [39] in the context of the diffraction of a Gaussian momentum distribution of atoms by a standing light wave. The technique is based on differentiation of the expression for f_n with respect to n , while using the property $\alpha[J_{n+1}(\alpha) + J_{n-1}(\alpha)] = 2nJ_n(\alpha)$ of Bessel functions. When the width is sufficiently large, so that the difference $f_{n+1} - f_n$ can be approximated by the derivative, this leads to the differential equation

$$2\sigma_0^2 \frac{df_n}{dn} \approx \left(\alpha \sin(\beta - \theta) - n \right) f_n + i\alpha \cos(\beta - \theta) \frac{df_n}{dn}. \quad (2.31)$$

By solving this equation, we arrive at the closed expression

$$f_n = \frac{1}{\mathcal{N}} \exp\left(\frac{-n^2/2 + \alpha n \sin(\beta - \theta)}{2\sigma_0^2 - i\alpha \cos(\beta - \theta)}\right), \quad (2.32)$$



with the normalization constant determined by

$$\mathcal{N}^4 = \pi \left(2\sigma_0^2 + \frac{\alpha^2 \cos^2(\beta - \theta)}{2\sigma_0^2} \right). \quad (2.33)$$

We find that the distribution is Gaussian at all times, with a time-varying average position and variance. These are given by the expressions

$$\langle n \rangle = \alpha \sin(\beta - \theta), \quad \sigma^2 = \sigma_0^2 + \frac{\alpha^2}{8\sigma_0^2} (1 + \cos 2(\beta - \theta)). \quad (2.34)$$

These results are in accordance with eqs. (2.27) and (2.28), as one checks by using the approximate expressions $b_l = \exp(-l^2/8\sigma_0^2) \approx 1 - l^2/8\sigma_0^2$, while neglecting terms of order $(1/\sigma_0)^4$ and higher. The width of the packet never gets smaller than its initial value. The phase difference between neighboring sites is mainly determined by $\theta - \phi$. This shows that a phase difference can be created or modified in a controlled way, simply by imposing a time-dependent force that gives rise to the right value of ϕ . Notice that in these expressions (2.34) θ and β enter in an equivalent fashion. The position and the width of the Gaussian distribution can be controlled at will by adapting the force to the desired value of β .

We recall that the results of this section are valid for an arbitrary time-dependent force $\Delta(t)$, which determines the time-dependent values of the parameters α , β and ϕ as specified in eqs. (2.13) and (2.15). In the subsequent sections, we specialize these expressions for constant or oscillating values of the uniform force.

2.5 Constant uniform force and Bloch oscillations

2.5.1 Wannier-Stark ladder of states

The case of a constant force is the standard situation where Bloch oscillations occur. When Δ and Ω are constant, the Hamiltonian is time independent, and then it is convenient to introduce the normalized eigenstates $|\psi_m\rangle$ of H . When we expand these eigenstates in the Wannier states as $|\psi_m\rangle = \sum_n |n\rangle c_n^{(m)}$, the eigenvalue relation $H|\psi_m\rangle = E_m|\psi_m\rangle$ with $E_m = \hbar\omega_m$ leads to the recurrence relations for the coefficients

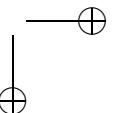
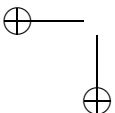
$$\frac{1}{2}\Omega(c_{n-1}^{(m)} + c_{n+1}^{(m)}) + \Delta n c_n^{(m)} = \omega_m c_n^{(m)}. \quad (2.35)$$

We introduce the generating function

$$Z_m(k) = \sqrt{\frac{a}{2\pi}} \sum_n c_n^{(m)} e^{-in ka}, \quad (2.36)$$

which is normalized for integration over the first Brillouin zone. In fact, from the expression (2.3) of the Bloch state, one notices that the generating function $Z_m(k) = \langle k | \psi_m \rangle$ is equal to the Bloch representation of the eigenstate $|\psi_m\rangle$. The relations (2.35) are found to be equivalent to the differential equation

$$\Omega \cos(ka) Z_m(k) - \frac{\Delta}{ia} \frac{d}{dk} Z_m(k) = \omega_m Z_m(k), \quad (2.37)$$



with the obvious normalized solution

$$Z_m(k) = \sqrt{\frac{a}{2\pi}} \exp\left(\frac{i}{\Delta}[\Omega \sin(ka) - ak\omega_m]\right). \quad (2.38)$$

Since the functions $Z_m(k)$ as defined by (2.36) are periodic in k with period $2\pi/a$, the same must be true for the expressions (2.38). Hence, the frequency eigenvalues must be an integer multiple of Δ , so that we can choose $\omega_m = m\Delta$, with integer m . For these values of the eigenfrequencies, the coefficients $c_n^{(m)}$ follow from the Fourier expansion of Z_m , with the result

$$c_n^{(m)} \equiv \langle n | \psi_m \rangle = J_{m-n}(\Omega/\Delta). \quad (2.39)$$

We find that the total Hamiltonian H has the same eigenvalues as H_1 . Apparently, the energy shifts due to the coupling between the Wannier states as expressed by H_0 cancel each other. Since the energy eigenvalues are integer multiples of Δ , each solution of the Schrödinger equation is periodic in time with period $2\pi/\Delta$, and the same is true for the evolution operator $U(t)$ given in eq. (2.16). This also implies that an initial localized state remains localized at all times, due to the addition of the uniform external force. The eigenstates $|\psi_m\rangle$ are the Wannier-Stark ladder of states [27–29]. They form a discrete orthonormal basis of the first energy band, and they are intermediate between the Wannier and the Bloch bases of states.

2.5.2 Oscillations of localized states

The definitions (2.13) and (2.15) show that

$$\alpha = (2\Omega/\Delta) \sin(\Delta t/2), \quad \beta = \Delta t/2, \quad \phi = \Delta t. \quad (2.40)$$

In the Wannier representation, the matrix elements of U are found from eq. (2.16) as

$$\langle n | U(t, 0) | m \rangle = i^{-n+m} e^{-i\Delta t(n+m)/2} J_{n-m}\left(\frac{2\Omega}{\Delta} \sin \frac{\Delta t}{2}\right), \quad (2.41)$$

which represents the transition amplitude from an initial state $|m\rangle$ to the final state $|n\rangle$. For the initial Wannier state $|\Psi(0)\rangle = |0\rangle$, the time-dependent state is $|\Psi(t)\rangle = \sum_n f_n(t) |n\rangle$ with

$$f_n(t) = i^{-n} e^{-i\Delta t n/2} J_n\left(\frac{2\Omega}{\Delta} \sin \frac{\Delta t}{2}\right). \quad (2.42)$$

This is in accordance with Eq. (50) of ref. [37], which was obtained by a rather elaborate analytical method, rather than an algebraic one. Equation (2.29) shows that the time-dependent average position $\langle n \rangle$ of the wave packet remains zero at all times, whereas the mean-square displacement $\sigma = |\alpha|/\sqrt{2}$ displays a breathing behavior, and returns to zero after the Bloch period $2\pi/\Delta$. Moreover, according to eq. (2.42), the phase difference between neighboring sites varies continuously with time.

This is already quite different when only two Wannier states are populated initially. Consider the initial state

$$|\Psi(0)\rangle = \frac{1}{\sqrt{2}}(|0\rangle + e^{i\theta}|1\rangle). \quad (2.43)$$

Then the average position can be evaluated from eq. (2.22), for the values of α and β given in eq. (2.40). The result is

$$\langle n \rangle = \frac{1}{2} + \frac{\Omega}{2\Delta} (\cos \theta - \cos(\Delta t - \theta)), \quad (2.44)$$

which shows that the packet displays a harmonically oscillating behavior. The amplitude of the oscillation is governed by the ratio Ω/Δ , which is one-half the maximum amplitude for Bloch oscillations of a wave packet with a large width (see Sec. 2.5.3). This amplitude must be appreciable in order that interband coupling induced by the uniform force remains negligible, as we have assumed throughout this paper.

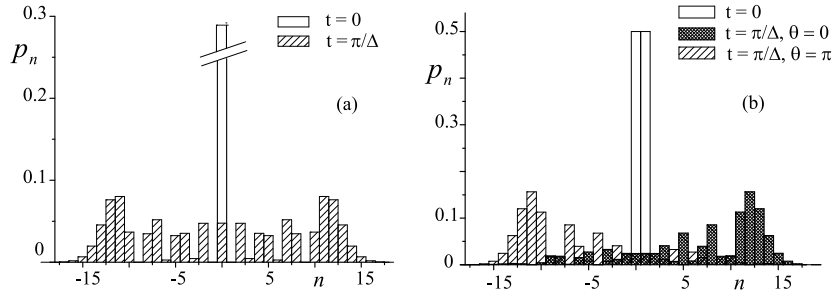


Figure 2.1: (a) Plot of the breathing population distribution for an initial Wannier state $|0\rangle$. (b) Plot of the oscillating population distribution, for two initial superpositions of Wannier states $|0\rangle$ and $|1\rangle$, and two different values of the relative phase θ . Both plots are evaluated for $\Omega/\Delta = 6$. Shaded distributions hold after one-half a Bloch period $t = \pi/\Delta$.

The distribution $p_n = |f_n|^2$ after one-half a Bloch period, both for the initial single Wannier state and for the initial state (2.43), is illustrated in Fig. 2.1. This demonstrates that a strong displacement can already be induced by evolution of a superposition state of just two neighboring Wannier states, with a specific phase difference. This displacement arises from the interference between the transition amplitudes from the two initial states to the same final state $|n\rangle$.

2.5.3 Bloch oscillations and breathing of a Gaussian wave packet

The evolution of a Gaussian wave packet as discussed in Sec. 2.4.2 is specialized to the present case of a constant force after substituting the expressions (2.40) in eqs. (2.32)-(2.34). We find for the average position $\langle n \rangle$ the identity

$$\langle n(t) \rangle = \frac{\Omega}{\Delta} [\cos \theta - \cos(\theta - \Delta t)]. \quad (2.45)$$

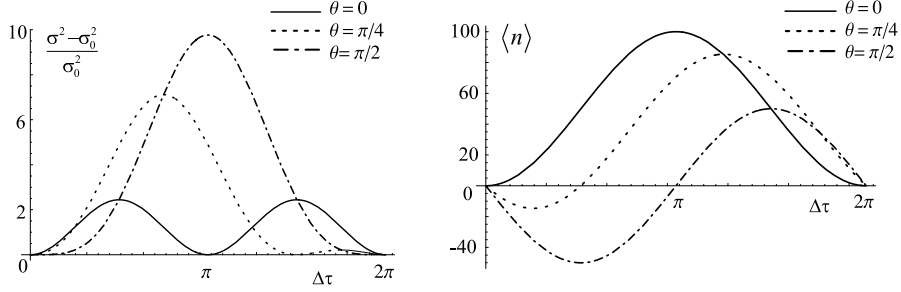


Figure 2.2: Periodic behavior of the width and the average position of a Gaussian wave packet for various initial values of the phase difference θ between neighboring states. Initial value of the width is $\sigma_0 = 4$ and $\Omega/\Delta = 50$.

This demonstrates that the wave packet oscillates harmonically in position with frequency Δ and with amplitude Ω/Δ in units of the lattice distance a . The velocity of the wave packet is found from the time derivative of eq. (2.45), with the result

$$v(t) = -a\Omega \sin(\theta - \Delta t). \quad (2.46)$$

It is noteworthy that this expression (2.46) coincides exactly with the expression for the group velocity $dE/\hbar dk$, with the derivative evaluated at the time-dependent value of the quasimomentum $(\theta - \Delta t)/a$, with $E = \hbar\Omega \cos(ka)$ the dispersion relation between energy and quasimomentum in the absence of the uniform force, as given in Sec. 2.2.1. Apparently, the expression for the group velocity retains its validity in the presence of the uniform force also. Of course, the concept of Bloch oscillations of the wave packet as a whole has significance only when the amplitude Ω/Δ of the oscillation is large compared with the width σ of the packet, which in turn must extend over many lattice sites.

The time-dependent width σ of the Gaussian packet is found from eq. (2.34) in the form

$$\sigma^2 = \sigma_0^2 + \frac{\Omega^2}{4\sigma_0^2\Delta^2} (1 - \cos \Delta t) (1 + \cos(\Delta t - 2\theta)). \quad (2.47)$$

Hence the variance of the position deviates from its initial value by an oscillating term. The amplitude of this oscillation is governed by the ratio $(\Omega/2\Delta\sigma_0)^2$. The initial width is restored whenever one of the terms in brackets vanishes. This happens twice during every Bloch period, except when $\theta = \pi/2$, when these two instants coincide. This combined breathing and oscillating behavior is illustrated in Figs. 2.2 and 2.3, for various values of the relative phase θ . Notice that the oscillation is always harmonic with the Bloch frequency Δ . This is due to the simple form of the dispersion relation for the case of nearest-neighbor interaction. The time dependence of the variance is a superposition of terms with frequencies Δ and 2Δ .

2.5.4 Zero external force

In the absence of an external force, we can take the limit $\Delta \rightarrow 0$ in the results of the previous subsections. In particular, this gives $\phi = \beta = 0$, $\alpha(t) = \Omega t$. Then the evolution of an initial

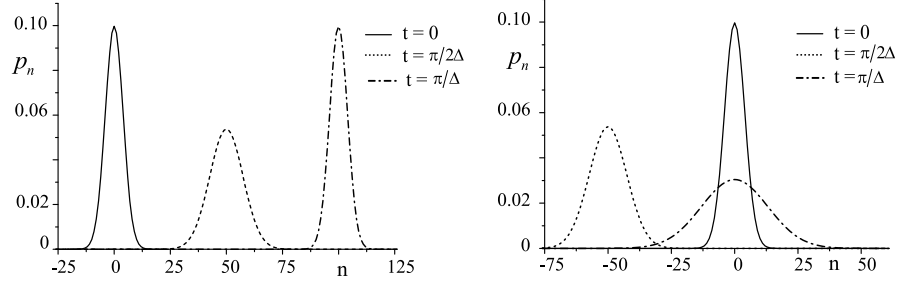


Figure 2.3: Bloch oscillation and corresponding breathing behavior of a Gaussian wave packet in a constant uniform force. Values of σ_0 , Ω , and Δ as in Fig. 2.2. Left part: $\theta = 0$. Right part: $\theta = \pi/2$.

Wannier state $|\Psi(0)\rangle = |0\rangle$ is given by

$$|\Psi(t)\rangle = R|\psi(0)\rangle = \sum_n i^{-n} J_n(\Omega t) |n\rangle, \quad (2.48)$$

which shows that the free spreading of an initial Wannier state after a time t gives Wannier populations equal to $p_n = |J_n(\Omega t)|^2$ [40]. The mean-square displacement increases linearly in time, as $\sigma = \Omega t / \sqrt{2}$. This shows that the spreading is unbounded in the absence of an external force. The self-propagator $p_0(t)$ decays to zero for large times. The phase difference between neighboring sites is $\pm\pi/2$ at all times. For only two coupled wells, the coupling would give rise to Rabi oscillations with frequency Ω . Equation (2.48) can be viewed as the generalization to the case of an infinite chain of wells.

For a Gaussian wave packet with initial width σ_0 and initial quasimomentum determined by θ , expressions (2.45) and (2.47) take the form

$$\langle n(t) \rangle = -\Omega t \sin \theta, \quad \sigma^2 = \sigma_0^2 + \frac{\Omega^2 t^2}{8\sigma_0^2} (1 + \cos 2\theta). \quad (2.49)$$

As one would expect in the absence of a uniform force, the group velocity takes the constant value $v = -a\Omega \sin \theta$, which leads to unbounded motion of the packet (except for $\theta = 0$ or $\pm\pi$). Usually, the width increases indefinitely during the propagation. However, for the special values $\theta = \pm\pi/2$ the width is constant, and the packet propagates as a solitary wave. Notice that such a phase difference between neighboring Wannier states arises spontaneously when a single Wannier state spreads in the absence of a uniform force.

2.6 Oscillating force

Other situations of practical interest arise when the uniform force has an oscillating component. Examples are the coupling between the states in the Wannier-Stark ladder [27–29], and dynamical localization for special values of the amplitude-frequency ratio of the oscillation [33–35]. The situation of an oscillating force is also described by the operator description of Sec. 2.3.1. We give some results below.

2.6.1 ac force only

The situation of a harmonically oscillating uniform force can be expressed as

$$\Delta(t) = \delta \cos(\omega t), \quad (2.50)$$

so that $\phi = (\delta/\omega) \sin(\omega t)$. Then according to (2.15) the parameters α and β are specified by the equalities

$$\alpha e^{i\beta} = \Omega t J_0\left(\frac{\delta}{\omega}\right) + \Omega \sum_{n \neq 0} J_n\left(\frac{\delta}{\omega}\right) \frac{1}{in\omega} (e^{in\omega t} - 1), \quad (2.51)$$

where we used the expansion defining the ordinary Bessel functions, given in Sec. 2.3.1.

The first term in eq. (2.51) increases linearly with time, whereas the summation is bounded and periodic in time with period $T = 2\pi/\omega$. The behavior of α and β as defined by eq. (2.51) is quite complicated in general. However, for large times the value of α , and thereby the spreading of an initial Wannier state, is the same as in the absence of the uniform force, with Ω replaced by the reduced effective coupling $\Omega J_0(\delta/\omega)$. After one period T , the values of the parameters become simple, and we find $\beta = \phi = 0$, $\alpha = \Omega T J_0(\delta/\omega)$. The evolution operator $U(T)$ during one period T is simply given by the operator R defined in eq. (2.16), at these values of the parameters. The eigenstates of the evolution operator $R = U(T)$ are simply the Bloch states $|k\rangle$. The eigenvalues can be expressed as $\exp(-i\mathcal{E}(k)T/\hbar)$, with

$$\mathcal{E}(k) = \hbar \Omega J_0\left(\frac{\delta}{\omega}\right) \quad (2.52)$$

the corresponding values of the quasienergy, which are strictly speaking defined only modulo $\hbar\omega$. The quasienergy bandwidth is reduced by the factor $J_0(\delta/\omega)$, compared with the energy bandwidth in the absence of the uniform force.

When the ratio δ/ω of the amplitude and the frequency of the oscillating force coincide with a zero of the Bessel function J_0 , no unbounded spreading occurs, and an initially localized state remains localized at all times, with a periodically varying mean-square displacement. The quasienergy bandwidth is reduced to zero in this case. This effect of dynamical localization has been discussed before for electrons in crystals [33, 34]. The related effect of an effective switch-off of atom-field coupling occurs for a two-level atom in a frequency-modulated field when the ratio of the amplitude-frequency ratio of the modulation equals a zero of the Bessel function J_0 . This effect, which leads to population trapping in a two-level atom, has recently been discussed by Agarwal and Harshawardhan [41].

2.6.2 ac and dc force

A constant uniform force creates Wannier-Stark states with equidistant energy values. An additional oscillating force can induce transitions between these states. Therefore, we consider the force specified by

$$\Delta(t) = \Delta_0 + \delta \cos(\omega t). \quad (2.53)$$

Then the values of the parameters ϕ , α , and β are

$$\phi(t) = \Delta_0 t + (\delta/\omega) \sin(\omega t), \quad \alpha e^{i\beta} = \Omega \sum_n J_n\left(\frac{\delta}{\omega}\right) \frac{1}{i(\Delta_0 + n\omega)} \left(e^{i(\Delta_0 + n\omega)t} - 1\right). \quad (2.54)$$

In general, each term in the summation is bounded and periodic, but the different periods can be incompatible. Moreover, whenever $\Delta_0 + n\omega = 0$, the corresponding summand attains the unbounded form $\Omega t J_n(\delta/\omega)$. At such a resonant value of Δ_0 , the spreading of an initially localized state becomes unbounded, and the particle becomes delocalized. This delocalization is suppressed again when the ratio δ/ω is equal to a zero of the corresponding Bessel function J_n . This is a simplified version of the phenomenon of fractional Wannier-Stark ladders, which has recently been observed and discussed [42, 43].

The quasienergy values are again determined by the eigenstates of the evolution operator $U(T)$ for one period of the oscillating force. This operator is equal to the general operator R defined in eq. (2.16), with the parameters

$$\alpha = 2\Omega \sin(\Delta_0 T/2) \sum_n J_n\left(\frac{\delta}{\omega}\right) \frac{1}{\Delta_0 + n\omega}, \quad \beta(T) = \Delta_0 T/2, \quad \phi(T) = \Delta_0 T. \quad (2.55)$$

These expressions are correct whenever $\Delta_0 + n\omega$ is nonzero for all values of n . Since these values of the parameters can be directly mapped onto the values (2.40) specifying the evolution with a constant uniform force, the eigenvectors and corresponding quasienergies are also immediately found. The eigenvectors of R can be expressed as $|\psi_m\rangle = \sum_n |n\rangle c_n^{(m)}$, with the expansion coefficients $c_n^{(m)} = J_{m-n}(\zeta)$. Here the argument ζ of the Bessel functions must be chosen as the sum

$$\zeta = \Omega \sum_n J_n\left(\frac{\delta}{\omega}\right) \frac{1}{\Delta_0 + n\omega}, \quad (2.56)$$

which replaces the simple argument Ω/Δ in eq. (2.39). The eigenvalues of $R = U(T)$ are $\exp(-i\mathcal{E}_m T/\hbar)$, with the discrete quasienergy values $\mathcal{E}_m = \hbar m \Delta_0$ (modulo $\hbar\omega$).

In the resonant case that $\Delta_0 + n_0\omega = 0$ for some integer n_0 , one summand in the expression for α and β is modified, as indicated above. When $T = t$, only this modified summand is nonzero, and the evolution operator $U(T) = R$ for one time period is characterized by the values

$$\alpha = \Omega T J_{n_0}, \quad \beta = 0, \quad \phi = -2\pi n_0. \quad (2.57)$$

The eigenvectors of R are the Bloch states $|k\rangle$, and the corresponding quasienergy values are

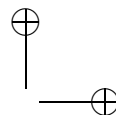
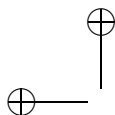
$$\mathcal{E}(k) = \hbar \Omega J_{n_0}\left(\frac{\delta}{\omega}\right). \quad (2.58)$$

2.7 Discussion and conclusions

We have analyzed the Wannier-Stark system, which is characterized by the Hamiltonian (2.6), in terms of the operators B_{\pm} and B_0 . The present interest in this model arises from the dynamics of atoms in a periodic optical potential, with an additionally applied uniform external

force. We adopted the tight-binding limit, which implied nearest-neighbor interaction only. This gives rise to an explicit simple dispersion relation between energy and quasimomentum, which makes the model exactly solvable. From the commutation properties of the basic operators we obtain eq. (2.16) for the evolution operator for an arbitrary time dependence of the uniform force, where the three parameters are defined in eq. (2.13) and (2.15). As shown in Secs. 2.3.2 and 2.4, the parameter ϕ determines the shift in the value of the quasimomentum, whereas α and β determine the evolution of the average position and the width of a wave packet. A particle starting in a single Wannier state has a uniform distribution over the quasimomentum, and cannot change its average position, whereas the width of its wave packet is simply measured by α . On the other hand, even when only two neighboring states are populated initially, the wave packet can display an appreciable motion. In Sec. 2.4.2 it is demonstrated that an initially Gaussian packet remains Gaussian at all times. This remains true when the initial state has a nonzero expectation value of the quasimomentum, which is described as an initial phase difference between neighboring Wannier states.

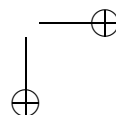
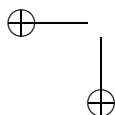
These results, which are valid for a uniform force with an arbitrary time dependence, unify and extend earlier results obtained for a constant or an oscillating uniform force. A constant force induces Bloch oscillations of a wave packet, and we obtain a simple expression for the amplitude of the oscillation and for the time dependence of the width of the wave packet. For an oscillating force, the operator method shows that the quasienergy bands can be evaluated directly in terms of the value of the parameter α after one oscillation period. This produces an exactly solvable model for dynamical localization and fractional Wannier-Stark ladders. In general, by selecting a proper time dependence of the force or of the coupling between wells, thereby realizing the desired values of the parameters α , β , and ϕ , we can coherently control the width and the position of a wave packet, as well as the phase difference between neighboring sites.



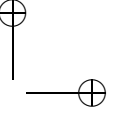
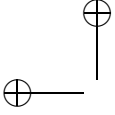
|

—

—



|



Chapter 3

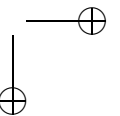
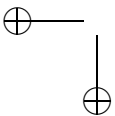
Momentum transfer for an optical transition in a prepared two-level atom

We consider the interaction of a travelling optical wave with a resonant two-level atom, which is initially in its most general superposition state, i. e. in a superposition state of the ground and excited internal energy levels with mutually different momentum distributions for each of these internal energy levels. We show that the momentum distribution per atomic internal energy level periodically gets large scale changes during the interaction. The amount of momentum that the photon transfers between the atomic internal energy levels is, in general, more than its own momentum $\hbar k$.

A special case is discussed, when the atom's preliminary superposition state is created as a result of interaction of the atom with a resonant standing wave. Also it is pointed out that the phenomenon can be considered as a transformation of the resonant Kapitza-Dirac splitting of atomic states into the Stern-Gerlach type splitting, if the interaction periods are appropriately chosen.

3.1 Introduction

When an atom interacts with a resonant travelling wave, the changes of the total momentum of the atom can not exceed one photon momentum $\hbar k$. What can be said about the distribution and the mean values of momentum for translational states per each atomic level? The answer is well-known and trivial, if the atom before the interaction is on one of the internal energy levels: the momentum distribution on the other level gets shifted by $\hbar k$ and the mean value of momentum may get shifted by $\hbar k$ as well; $\langle p_e \rangle \sim \langle p_g \rangle + \hbar k$ at certain time instants, where \bar{p}_g and \bar{p}_e are mean values of momentum, corresponding to the ground and the excited internal levels (1D case). Therefore, a photon, during an absorption or emissions, transfers between the atomic internal energy levels an amount of momentum Δp just equal to its own momentum $\hbar k$. What would happen in a general case, that is, when the atom before the interaction with a travelling wave is in the superposition state of ground and excited levels with mutually different momentum distributions? Such a state can be considered as the most general superposition state for the atom. In the further discussion this question is elucidated. We start from a general formalism and then turn to important special cases. It is shown that in general $\Delta p \neq \hbar k$, that is a photon being absorbed or emitted by an atom, transfers between the internal atomic energy levels the amount of momentum not necessarily equal and even largely exceeding the photon's own momentum.



In Sec. 2 the general conditions are discussed, when one may obtain large average momentum changes at internal energy levels for an atom interacting with a travelling wave. These redistributions are a direct consequence of interference between the amplitudes of translational states for ground and the excited internal energy levels.

In Sec. 3 we discuss the possible connection to applications. That is when the preliminary superposition state of the atom is realized by a coherent diffraction of the atom in the field of a resonant standing wave, which is being often referred as the resonant Kapitza-Dirac effect. It is pointed out, that the redistribution of momentum in the travelling wave can be considered as a transition from the resonant Kapitza-Dirac splitting to the Stern-Gerlach type splitting.

In Sec. 4 we discuss in details the temporal behavior of mean momentum corresponding to both of the internal energy levels. The results are summarized in Sec. 5, where also the possibilities of experimental observation of this phenomenon are briefly sketched.

3.2 Momentum distributions and mean momenta per atomic internal energy levels

Let's start from the discussion of a resonant interaction of a two-level atom with a radiation field [44, 45]. For the sake of simplicity, suppose that the light field has a plane wavefront and a linear polarization (these assumptions will be kept also for the standing wave in the next sections). Let's suppose that the light field amplitude is turned on instantaneously. The internal wave functions of a free two-level atom in ground (g) and excited (e) levels are noted respectively $\varphi_g(\vec{\rho}, t)$ and $\varphi_e(\vec{\rho}, t)$, where $\vec{\rho}$ is the atomic internal coordinate (the radius-vector of the optical electron, relative to the atomic center-of-mass). The wave function of an atom interacting with a light field can be presented as [44, 45]

$$\Psi = A \varphi_g(\vec{\rho}, t) + B \varphi_e(\vec{\rho}, t), \quad (3.1)$$

where A and B are the probability amplitudes of the atom to be respectively at the ground and the excited internal energy levels.

While taking into account the translational motion of the atomic center of mass, it is useful to separate the corresponding parts (wave functions) in A and B coefficients. For an atom with the well-defined momentum p , the corresponding wave function is given by the function

$$\chi(p) = \frac{1}{\sqrt{2\pi\hbar}} \exp\left(\frac{i}{\hbar} p z\right), \quad (3.2)$$

that is, by an exponential function with imaginary degree. In general, if the momentum of an atom isn't fixed at any energy level, the coefficients A and B can be expressed by the series of $\chi(p)$ -states

$$A(t, z) = \int a(p, t) \chi(p) dp, \quad B(t, z) = \int b(p, t) \chi(p) dp, \quad (3.3)$$

where the probability amplitudes $a(p, t)$ and $b(p, t)$ represent the probability for an atom to have momentum p at the time instant t while being at the ground or excited internal energy levels.

Plugging the expressions (3.1)-(3.3) into the quantum-mechanical definition of average momentum, given as

$$\langle p \rangle = \int \Psi^* \hat{p} \Psi d\vec{\rho} dz, \quad \int \Psi^* \Psi d\vec{\rho} dz = 1, \quad (3.4)$$

after standard transformations we arrive to the following expressions for the average momentum

$$\langle p \rangle = \int |a(p, t)|^2 p dp + \int |b(p, t)|^2 p dp. \quad (3.5)$$

Terms in the exp. (3.5) specify the contribution of translational states into the total momentum per internal energy levels: for the ground internal energy level

$$\langle p \rangle_g = \int |a(p, t)|^2 p dp. \quad (3.6)$$

and for the excited one

$$\langle p \rangle_e = \int |b(p, t)|^2 p dp. \quad (3.7)$$

Both momenta are time-dependent and their changes after the interaction period t are expressed as

$$\begin{aligned} \langle \Delta p \rangle_g &= \int \left(|a(p, t)|^2 - |a(p, 0)|^2 \right) p dp, \\ \langle \Delta p \rangle_e &= \int \left(|b(p, t)|^2 - |b(p, 0)|^2 \right) p dp. \end{aligned} \quad (3.8)$$

When the atom interacts with a travelling wave, the internal ground level coefficient $a(p, t)$ is related with the excited internal level coefficient $b(p + \hbar k, t)$. The relation can be represented in the form of a conserving quantity

$$|a(p, t)|^2 + |b(p + \hbar k, t)|^2 = \text{const} = |a(p, 0)|^2 + |b(p + \hbar k, 0)|^2 \quad (3.9)$$

(it can be checked by the eq. (3.17)). We can use the relation (3.9) to express $\langle \Delta p \rangle_g$ by $\langle \Delta p \rangle_e$ as follows

$$\begin{aligned} \langle \Delta p \rangle_e &= \int \left(|b(p + \hbar k, t)|^2 - |b(p + \hbar k, 0)|^2 \right) (p + \hbar k) d(p + \hbar k) = \\ &= - \int \left(|a(p, t)|^2 - |a(p, 0)|^2 \right) (p + \hbar k) d(p + \hbar k) = \\ &= - \langle \Delta p \rangle_g + \hbar k \int \left(|a(p, t)|^2 - |a(p, 0)|^2 \right) dp = - \\ &= - \langle \Delta p \rangle_g + \hbar k \Delta n_g, \end{aligned} \quad (3.10)$$

where Δn_g with

$$\Delta n_g = -\Delta n_e = \int \left(|a(p, t)|^2 - |a(p, 0)|^2 \right) dp = - \int \left(|b(p, t)|^2 - |a(p, 0)|^2 \right) dp \quad (3.11)$$

is the change of population for the internal ground level, or which is the same, the population change Δn_e of the internal excited level with the opposite sign (see (3.20)). From the equality of the first and the last terms in the exp. (3.10) a well known inequality follows directly between the momentum of the photon and the atom

$$\langle \Delta p \rangle = \langle \Delta p \rangle_g + \langle \Delta p \rangle_e = \hbar k \Delta n_g \leq \hbar k \quad (3.12)$$

Let, nevertheless, note that this "one photon demarcation" pertains to the total momentum of the atom and has nothing to do with separate average momentum changes per internal energy levels $\langle \Delta p \rangle_g$ and $\langle \Delta p \rangle_e$. In accordance with (3.8), these quantities can exhibit arbitrary changes depended on the distribution functions $|a(p, t)|^2 - |a(p, 0)|^2$ and $|b(p, t)|^2 - |b(p, 0)|^2$ in the momentum space. As it follows from the exp. (3.8), the large magnitudes for $\langle \Delta p \rangle_g$ ($\langle \Delta p \rangle_e$) are possible, if one requires to have strictly non-symmetric distributions $|a(p, t)|^2 - |a(p, 0)|^2$ (or $|b(p, t)|^2 - |b(p, 0)|^2$) relative to the replacement $p \rightarrow -p$ and the distributions are also required to have an accumulation in the range of large values of $|p|$.

And now we show that the one photon absorption/emission process in the field of a travelling wave actually allows such a behavior. The Hamiltonian of the system can be written in a dipole approximation as

$$\hat{H} = \hat{H}_0 - \hat{d}E(t, z), \quad (3.13)$$

where \hat{H}_0 is the free atom Hamiltonian, and \hat{d} is the dipole moment operator and

$$\vec{E}(t, z) = \frac{\vec{E}}{2} \exp(ikz - i\omega t) + c.c., \quad t > 0 \quad (3.14)$$

is the frequency ω of the electric field taken equal to the Bohr transition frequency ω_0 .

From the time-dependent Schrödinger equation we arrive to the system of equations for the amplitudes $A(t, z)$ and $B(t, z)$

$$\begin{aligned} i \frac{\partial A(t, z)}{\partial t} &= -\nu \exp(-ikz) B(t, z), \\ i \frac{\partial B(t, z)}{\partial t} &= -\nu \exp(ikz) A(t, z), \end{aligned} \quad (3.15)$$

As it is well-known, the system of equations (3.15) exhibits the Rabi-solutions [44, 45]

$$\begin{aligned} A(z, t) &= A(z, 0) \cos \nu t + i B(z, 0) \exp(-ikz) \sin \nu t, \\ B(z, t) &= B(z, 0) \cos \nu t + i A(z, 0) \exp(ikz) \sin \nu t, \end{aligned} \quad (3.16)$$

where $\nu = dE/2\hbar$ represents the Rabi frequency, $d = \langle \varphi_a | \hat{d} | \varphi_b \rangle$.

Performing the $\chi(p)$ -expansion in (3.16) (see Eq. (3.3)), we arrive to the expressions for the atomic amplitudes in the momentum space (3.3)

$$\begin{aligned} a(p, t) &= a(p, 0) \cos \nu t + i b(p + \hbar k, 0) \sin \nu t, \\ b(p, t) &= b(p, 0) \cos \nu t + i a(p - \hbar k, 0) \sin \nu t. \end{aligned} \quad (3.17)$$

First of all, it can be readily verified that the outcome is trivial if the atom is at one of energy levels before the interaction. Indeed, if one takes $b(p, 0) = 0$, then

$$\begin{aligned}\langle \Delta p \rangle_g &= (\cos^2 \nu t - 1) \int |a(p, 0)|^2 p dp = (\cos^2 \nu t - 1) \langle p \rangle_g |_{t=0} \\ \langle \Delta p \rangle_e &= (1 - \cos^2 \nu t) \left[\langle p \rangle_g |_{t=0} + \hbar k \right].\end{aligned}\quad (3.18)$$

This means that the contribution to the total momentum, coming from single internal energy levels, evolves periodically in time, and this evolution is merely caused by the periodic exchange of population between the internal energy levels (posed by the term $(1 - \cos^2 \nu t)$). Note also that in this case ($b(p, 0) = 0$) the momentum distributions for the internal energy levels coincide with each other after the shift $\hbar k$: $b(p + \hbar k, t) = i a(p, t) \tan \nu t$, as it is indicated in Introduction.

The situation is totally different, if the atom is initially in a superposition state of the internal ground and excited levels. Now, generally speaking, the initial momentum distributions for the internal ground and excited levels are not required to be identical with the $\hbar k$ shift: $b(p, 0) \neq \alpha a(p - \hbar k, 0)$ (α is a constant, independent on p). Then, as it follows from the exp. (3.17), the optical transition changes not only the population on the internal energy levels, it also introduces periodical changes in the form of momentum distribution. Thus, the atomic amplitudes $a(p, t)$ and $b(p, t)$ are not mutually proportional (they do not coincide after the constant shift).

To wash out the contribution coming from the evolution of population of the internal energy levels, let us introduce a pair of new quantities \bar{p}_g and \bar{p}_e , which are defined by scaling the average momentum per internal energy level by the corresponding population n_g and n_e

$$\bar{p}_g = \langle p \rangle_g / n_g, \quad \bar{p}_e = \langle p \rangle_e / n_e \quad (3.19)$$

$$n_g = \int |a(p, t)|^2 dp, \quad n_e = \int |b(p, t)|^2 dp \quad (3.20)$$

Since the \bar{p}_g, \bar{p}_e are independent on the population on the internal energy levels, their possible evolution is due to the form-deformation in the momentum distribution for the internal energy levels. Thereby, the total momentum of the atom, in addition to (3.5), can be represented in a more convenient form

$$\langle p \rangle = n_g \bar{p}_e + n_e \bar{p}_g \quad (3.21)$$

It is easy to see that the quantities \bar{p}_g and \bar{p}_e remain constant, if the atom is initially at one of the energy levels. They remain unchanged also when the initial distributions $a(p, 0)$, $b(p, 0)$ are mutually proportional with the constant $\hbar k$ shift

$$b(p, 0) = \alpha a(p - \hbar k, 0). \quad (3.22)$$

Indeed, plugging the exp. (3.22) in the relations (3.17) and performing simple substitutions, we arrive to the following relation for the internal ground energy level

$$\bar{p}_g = \frac{|\cos \nu t - i\alpha \sin \nu t|^2 \int |a(p, 0)|^2 p dp}{|\cos \nu t - i\alpha \sin \nu t|^2 \int |a(p, 0)|^2 dp} = \bar{p}_g |_{t=0},$$

and the same is true for the internal excited energy level. So, if the condition (3.22) holds, only a population exchange takes place between the internal energy levels, and the scaled average momenta \bar{p}_g and \bar{p}_e do not change.

Nevertheless, in the general case the state evolution forms as a result of interference between non-similarly distributed amplitudes. The atomic amplitudes distributions per internal energy levels aren't proportional to each other and subsequently the mean momenta \bar{p}_e and \bar{p}_g exhibit non-trivial temporal evolution.

Now we turn to the issue of a more concrete and quantitative picture for the developed formalism. This can be important for various applications in atom optics and interferometry [4, 46]. As an example, we study the coherent scattering of atoms in a resonant field of a standing wave. This example is particularly important, because it is the main routine to prepare a widespread momentum distribution in atom optics. The probability amplitudes, prepared in such a way, principally can not satisfy the "undesirable" condition (3.22). The reason is well-known: any state with momentum p at one of internal energy levels is connected to two states with momenta $p - \hbar k$ and $p + \hbar k$ simultaneously at the other internal energy level in the field of a standing wave. Therefore, any atom prepared by means of the resonant Kapitza-Dirac effect is forced to change implicitly the momentum distribution at the internal energy levels while interacting with a travelling wave.

3.3 The case of preparation of atomic superpositional states by scattering in the field of resonant standing wave

We consider a coherent interaction of an atom with a resonant ($\omega = \omega_0$) standing wave [47–52] during the time interval τ_s followed by the interaction with a travelling wave. We restrict ourselves to a relatively simple case, when the interaction proceeds by the well known scheme of mutually orthogonal atom-standing wave beams. Moreover, the Raman-Nath approximation is applied, which allows to leave out the kinetic energy term in Hamiltonian (3.13) (note that the kinetic energy term has not been included also in eq. (3.15)). Although the scheme of calculations is well known and presented elsewhere in details (see, for example [4, 46–52]), we find it appropriate to give here an overview of the main intermediate formulas, too.

To describe the interaction in the preparing standing wave, the electric field (3.14) in the Hamiltonian (3.13) must be substituted by the following one

$$E(t, z) = E_s \cos kz \exp(-i\omega t) + c.c., \quad -\tau_s \leq t \leq 0. \quad (3.23)$$

Now, the atomic amplitudes $A_s(z, t)$ and $B_s(z, t)$ have to satisfy (3.15)-type equations where the following replacements are made: $\nu \rightarrow 2\nu_s = 2dE_s/\hbar$ (which is mean Rabi frequency in the standing wave), $\exp(\pm ikz) \rightarrow \cos kz$. Allowing the atom initially ($t < -\tau_s$) to be at the ground level, we arrive to the following expressions for the amplitudes $A_s(z, t)$, $B_s(z, t)$ after the atom interacts with the standing wave (3.23)

$$\begin{aligned} A_s(z, t) &= \cos(2\nu_s(t + \tau_s) \cos kz), \\ B_s(z, t) &= i \sin(2\nu_s(t + \tau_s) \cos kz). \end{aligned} \quad (3.24)$$

The multiphoton nature of the standing wave diffraction is evident, if one performs the $\chi(p)$ -expansion for the amplitudes $A_s(z, t)$ and $B_s(z, t)$ (3.24) [53]

$$\begin{aligned} A_s(z, 0) &= \cos(2\nu_s \tau_s \cos kz) = \sum_{m=-\infty}^{\infty} i^{2m} J_{2m}(2\nu_s \tau_s) \exp(i2mkz), \\ B_s(z, 0) &= i \sin(2\nu_s \tau_s \cos kz) = \sum_{m=-\infty}^{\infty} i^{2m+1} J_{2m+1}(2\nu_s \tau_s) \exp(i(2m+1)kz), \end{aligned} \quad (3.25)$$

where m is the number of photons reemitted from one into the other of the counterpropagating waves, $J_m(x)$ is the Bessel function of m -th order.

At $t = 0$ the standing wave is turned off, the amplitudes (3.24) serve as initial amplitudes for the subsequent interaction with the travelling wave. For the atomic center-of-mass motion probability amplitudes $a(p, t)$ and $b(p, t)$ at $t > 0$ the following expressions can be easily evaluated using (3.3, 3.16)

$$\begin{aligned} a(2m\hbar k, t) &= i^{2m} [\cos \nu t J_{2m}(2\nu_s \tau_s) - \sin \nu t J_{2m+1}(2\nu_s \tau_s)], \\ b((2m+1)\hbar k, t) &= i^{2m+1} [\cos \nu t J_{2m+1}(2\nu_s \tau_s) + \sin \nu t J_{2m}(2\nu_s \tau_s)], \\ a((2m+1)\hbar k, t) &= b(2m\hbar k, t) = 0. \end{aligned} \quad (3.26)$$

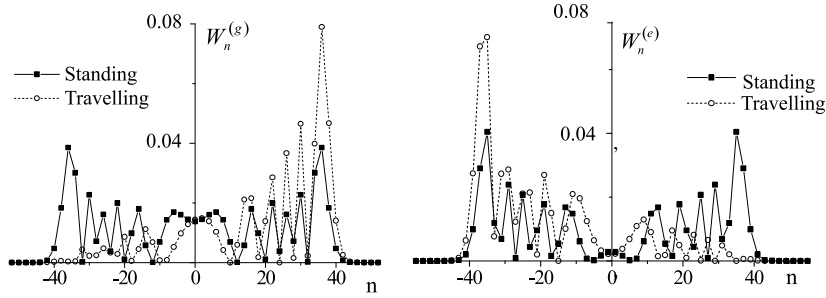


Figure 3.1: Probability distribution is plotted in the momentum space for the ground and excited internal energy levels. State is prepared symmetrically in the momentum space. The chosen parameters are $2\nu_s \tau_s = 40$, $|A(-\tau_s)|^2 = 1$, $|B(-\tau_s)|^2 = 0$, $\nu t = \pi/4$.

We see that the superposition state, created as a result of the interaction with the standing wave, represents discrete manifolds of states, where the space between the adjacent values of momentum is $2\hbar k$, herewith the manifolds for the ground and excited internal energy levels are shifted with respect to each other by $\hbar k$ [47–52].

The formulas (3.26) contain explicitly the aimed result about the evolution of momentum distribution. To demonstrate it, first of all we note, that the initial momentum distribution for any of internal energy levels is symmetric relative to the middle point $p = 0$. Indeed, the distribution functions are given by the functions $i^{2m} J_{2m}(\cdot)$ and $i^{2m+1} J_{2m+1}(\cdot)$ respectively for the ground and excited energy levels and remain symmetric relative to the transformation

$2m \rightarrow -2m$, $2m + 1 \rightarrow -(2m + 1)$, that is relative to the value $m = 0$ ($p = 0$). This symmetry proves that the average momentum per each internal energy level is zero before interacting with the travelling wave [47–52].

Nevertheless, in accordance with (3.26), the symmetry breaks down when the travelling wave acts. So, one photon absorption/emission process transforms the momentum distribution for internal energy levels to an asymmetric form for both of the internal energy levels. Both distributions are peaked in the opposite directions for the ground and excited internal energy levels. The sign of asymmetry per each internal energy level changes periodically.

A typical form of the initial distribution and the subsequent transformation (due to a single-photon process) are plotted on the Fig. 3.1 for the ground and the excited energy levels. To be more precise, the quantities $W_m^{(g)} = |a(2m\hbar k, t)|^2$ and $W_m^{(e)} = |b((2m + 1)\hbar k, t)|^2$ are plotted on the Fig. 3.1 at two time instants, namely before and after the travelling wave. Single-photon induced large-scale momentum changes are apparent.

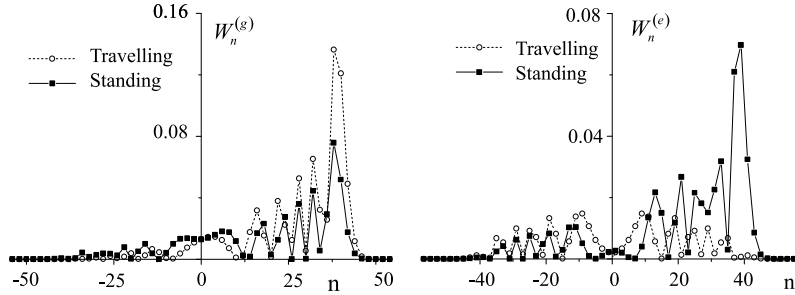


Figure 3.2: Probability distribution is plotted in the momentum space for the ground and excited internal energy levels. State is prepared asymmetrically in the momentum space. The chosen parameters are $2\nu_s\tau_s = 40$, $|A(-\tau_s)|^2 = 1/2$, $|B(-\tau_s)|^2 = 1/2$, $\nu t = \pi/4$.

Now let us notice that we obtain almost one-side distributions for conditions taken for Fig. 3.1. The translational states with positive momentum prevail at the ground internal energy level, and the opposite ones are mostly at the excited internal level. So, the state of the atom is split into two subgroups, where one subgroup represents the ground-level atoms with positive momentum, and the second subgroup is related to the excited-level atoms. Obviously, this is a Stern-Gerlach type splitting. Thus, one-photon optical transition transforms the resonant Kapitza-Dirac splitting into the Stern-Gerlach type splitting.

The phenomenon of one-photon coherent accumulation of momentum on the internal energy levels (OP-CAMEL) can be generalized, if the initial momentum distributions for the atom are taken in an asymmetric form. Such distributions can also be built by a standing wave, but only if a travelling wave precedes the standing wave [54, 55]. This is a typical situation, if the standing wave is formed by means of reflection of a laser pulse from a mirror (see, for example [56]). In order to keep the discussion short, we give the main features of the asymmetric OP-CAMEL in figures.

In Fig. 3.2 we plot the evolution of a maximally asymmetric distribution for the ground and the excited internal energy levels. As it can be seen from the figures, OP-CAMEL manifests itself as an accumulation of an asymmetry for one internal energy level (ground in this case), whereas the asymmetry of the other internal energy level (excited) is strongly sup-

pressed.

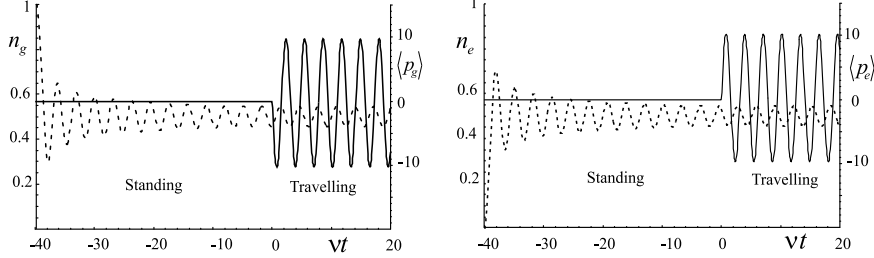


Figure 3.3: The temporal evolution of average momentum per ground and excited internal energy level, while the atom interacts with the standing and the travelling waves. Population changes per energy levels are plotted by dashed lines. All parameters are taken the same as for Fig. 3.1.

3.4 Time evolution of mean momentum per ground and excited internal energy levels in the field of travelling wave

Let us now discuss the evolution of momenta \bar{p}_g and \bar{p}_e after the sequence of two pulses, namely standing wave-travelling wave pulse sequence. Using the expressions for \bar{p}_g and \bar{p}_e (3.6, 3.7, 3.19, 3.20), we can easily calculate the average momentum and the population of the internal ground energy level

$$\begin{aligned} \langle p \rangle_g &= \hbar k \sum_{m=-\infty}^{\infty} 2m [\cos \nu t J_{2m}(u) - \sin \nu t J_{2m+1}(u)]^2 = \\ &= -\hbar k \left[\frac{1 - J_0(2u)}{2} \sin^2 \nu t + \frac{u - J_1(2u)}{4} \sin 2\nu t \right], \end{aligned} \quad (3.27)$$

$$\begin{aligned} n_g &= \sum_{m=-\infty}^{\infty} [\cos \nu t J_{2m}(u) - \sin \nu t J_{2m+1}(u)]^2 = \\ &= \frac{1}{2} + \frac{J_0(2u)}{2} \cos 2\nu t - \frac{J_1(2u)}{2} \sin 2\nu t \end{aligned} \quad (3.28)$$

and the same for the excited one

$$\begin{aligned} \langle p \rangle_e &= \hbar k \sum_{m=-\infty}^{\infty} (2m+1) [\cos \nu t J_{2m+1}(u) + \sin \nu t J_{2m+2}(u)]^2 = \\ &= \hbar k \left[\frac{1 + J_0(2u)}{2} \sin^2 \nu t + \frac{u + J_1(2u)}{4} \sin 2\nu t \right], \end{aligned} \quad (3.29)$$

$$\begin{aligned}
n_e &= \sum_{m=-\infty}^{\infty} [\cos \nu t J_{2m+1}(u) + \sin \nu t J_{2m}(u)]^2 = \\
&= \frac{1}{2} - \frac{J_0(2u)}{2} \cos 2\nu t + \frac{J_1(2u)}{2} \sin 2\nu t = 1 - n_g,
\end{aligned} \tag{3.30}$$

where we use a notation $u = 2\nu_s \tau_s$.

The last relations (3.27)-(3.30) are derived using Bessel function summation formulas [57]) for the initial conditions are assumed to be $\langle p \rangle_g|_{t=0} = 0$, $\langle p \rangle_e|_{t=0} = 0$, (the same is true for \bar{p}_g and \bar{p}_e), so their values at any time instant coincide with their changes: $\langle \Delta p \rangle_g = \langle p \rangle_g$, $\langle \Delta p \rangle_e = \langle p \rangle_e$.

On the Fig. 3.3 the temporal evolution of the average momenta is plotted, while the atom interacts with the travelling (accumulating) wave. Population changes, which contribute also to the time evolution of average momentum, are plotted by dashed lines. For the case presented on the figures, the population on the internal energy levels is practically unchanged during the interaction period with the travelling wave. Indeed, it immediately follows from the exp. (3.28) and (3.30), if one takes $u \gg 1$, the Bessel functions $J_{0,1}(2u)$ are negligible.

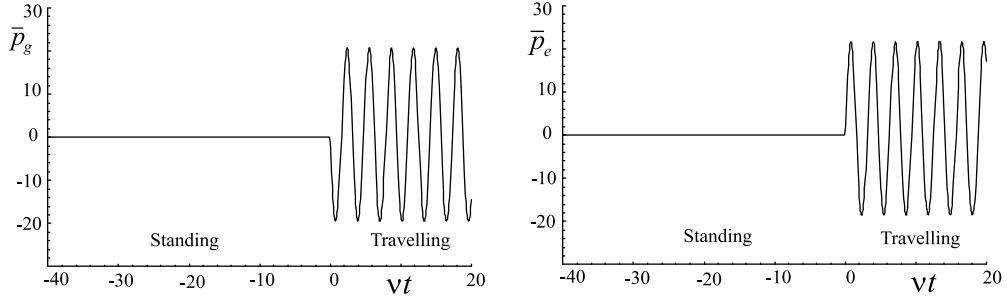


Figure 3.4: Temporal behavior of the scaled mean momentum per ground internal energy level (left plot) and the excited internal energy level (right plot).

Respectively, the temporal evolution of the scaled average momentum \bar{p}_g and \bar{p}_e is conditioned only by the redistribution of momentum between the internal energy levels, as it is shown in Fig. 3.4. The parameters of the preparing standing wave are the same as in Fig. 3.1, where the distance between the left-hand and right-hand maxima (the width of momentum distribution) is about $70 \hbar k$. Such magnitudes for the resonant Kapitza-Dirac splitting are totally in limits of experimental realization (for example [52]).

Note also, that the comparison between the deviation of \bar{p}_g or \bar{p}_e (from the Fig. 3.4) and the width of momentum distribution (from the Fig. 3.1) shows the same order of magnitude for them. The widespread character of the momentum distribution comes from the multiphoton nature of the phenomenon (multiphoton process of photon reemission from one wave into the counterpropagating one takes place), so the large-scale variations in OP-CAMEL may be named as "multiphoton".

The multiphoton character of OP-CAMEL can be made more transparent, if we consider the limit of a sufficiently wide initial momentum distribution, that is $\Delta p \gg \hbar k$, then $u = 2\nu_s \tau_s \gg 1$. The last estimate comes from the theory of resonant Kapitza-Dirac effect, where the connection between momentum width δp and the number of Rabi-flops $2\nu_s \tau_s$ is given as

$\delta p \approx 2\nu_s \tau_s \hbar k$. Taking into account also that $J_{1,0}(2u) \leq 1$, we conclude that the terms $\frac{1}{4} \hbar k u \sin 2\nu t$ (3.27) and $-\frac{1}{4} \hbar k u \sin 2\nu t$ (3.29) stand out as the prevailing terms for respectively $\langle p \rangle_g$ and $\langle p \rangle_e$

$$\langle p \rangle_g \approx -\frac{u}{4} \hbar k \sin 2\nu t, \quad \langle p \rangle_e \approx \frac{u}{4} \hbar k \sin 2\nu t.$$

Since $u \gg 1$, the changes of $\langle p \rangle_g$ and $\langle p \rangle_e$ per Rabi period, which are in the order of $u/2\hbar k$ largely exceed the momentum $\hbar k$ of a single photon.

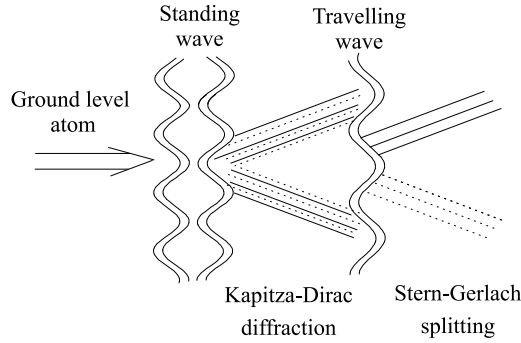


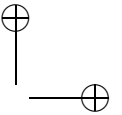
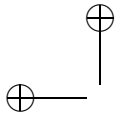
Figure 3.5: The atom at a ground internal energy level with a fixed momentum (zone 1) changes its state into a superposition while coherently interacting with a resonant standing wave (zone 2). The next interaction with the travelling wave leads to large-scale changes in the momentum distribution per internal energy level. Solid lines represent the atoms at the ground level and the dotted lines represent the atoms at the excited internal energy level.

3.5 Conclusions

We presented a simple theoretical picture for an optical transition of a single two-level atom for general conditions, when the atom is in a superposition state of ground and excited internal energy levels. When these levels initially have different momentum distributions, the one-photon optical transition leads to significant asymmetric changes in the form of momentum distributions per internal energy level. In other words, the photon induces a change of the mean momentum for each internal energy level and this change is larger than the momentum of the photon itself.

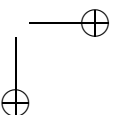
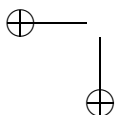
For an important case, when the preliminary superposition state of the atom is prepared by a coherent scattering at the resonant standing wave, the phenomenon can be considered as a transition from the resonant Kapitza-Dirac splitting of atomic translational states into the Stern-Gerlach type splitting. This is sketched schematically on the Fig. 3.5.

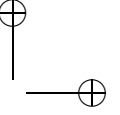
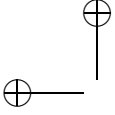
Finally, let's make some remarks on possibilities of the experimental observation of the phenomenon. First of all, the "non-optical" methods, which detect the atom in total (for example, the "hot-wire" method), can't be used for our purposes. It is because the phenomenon



deals with individual internal energy level. The momentum distribution of the total atom doesn't change, or rather, it changes only in limits of one-photon momentum.

Preferably, other detecting methods can be used, which deal only with one of resonantly connected internal energy levels, such as adjacent optical transitions. Then the phenomenon appears as asymmetry in the profile of the Doppler broadening, relative to the Bohr frequency. The other proposal is to use long-living energy levels, so the atomic translational states can be distinguished in space before the spontaneous emission (zone 3 in Fig. 3.5). In this case the space-sensitive schemes of spontaneous emission collection or probe pulse absorption may lead to the desired result.





Chapter 4

Diffraction and trapping in circular lattices

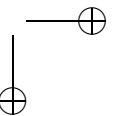
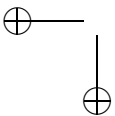
When a single two-level atom interacts with a pair of Laguerre-Gaussian beams with opposite helicity, this leads to an efficient exchange of angular momentum between the light field and the atom. When the radial motion is trapped by an additional potential, the wave function of a single localized atom can be split into components that rotate in opposite direction. This suggests a novel scheme for atom interferometry without mirror pulses. Also atoms in this configuration can be bound into a circular lattice.

4.1 Introduction

It is well-known that light may carry both angular and linear momentum. When a light field interacts with matter, exchange of momentum and angular momentum between light and matter can occur. Laguerre-Gaussian (LG) light modes are known to carry orbital angular momentum. If one employs the paraxial approximation for the light field, simple expressions for the field amplitudes and its average angular momentum can be derived [58]. An easy way to produce such beams is using spiral phase plates [59].

Another important question is the separability of the total angular momentum into 'orbital' and 'spin' parts [60]. The orbital part is associated with the phase distribution of the light field, and the spin part is connected with its polarization. This question is essential in the context of momentum transfer from light to the atom when one includes atomic internal degrees of freedom. It has been shown that 'spin' and 'orbital' angular momentum of the photon are transferred from the quantized light field to, respectively, the internal and the external angular momentum of the atom. The interaction with a LG mode is a possible way to entangle internal and external degrees of freedom of an atom [61]. The transfer of the angular momentum of light to particles has been also experimentally demonstrated in [62], where trapped massive particles are set into rotation while interacting with the light field. Other authors have studied the cooling properties for atoms using LG beams [63]. Also LG beams have been proposed as a $2D$ trapping potential for Bose condensates [64].

Whereas angular momentum exchange between light and matter is a relatively new topic, the linear momentum exchange is a well-established issue [47, 48, 65]. It is well-known that two counterpropagating waves lead to a more efficient exchange of linear momentum between an atom and the light field than a single travelling wave. Using quantum language for a classical light field, one can describe such an interaction as a sequence of successive single photon absorption and emission events. This suggests that one may expect more efficient angular momentum exchange between a light field and an atom if one uses two LG modes with opposite helicity, e.g. counterrotating waves.



4.2 General framework

We start with radiation fields propagating along the z -axis with wave number k and carrying orbital angular momentum (Laguerre-Gaussian beams). If one considers the paraxial limit of these waves, the expressions for the light fields are particularly simple [58]

$$E(\rho, z, \phi, t) = E_0(\rho, z) e^{i(kz - \omega t + l\phi)} + c.c., \quad (4.1)$$

where ρ, z, ϕ are the cylindrical coordinates, ω is the frequency and the integer index l indicates the helicity of the LG beam. For two Laguerre-Gaussian beams with opposite helicity, namely l and $-l$, the total field can be written as

$$E(\rho, z, \phi, t) = 2E_0(\rho, z) \cos l\phi e^{i(kz - \omega t)} + c.c. \quad (4.2)$$

We indicated already in the Introduction, that one expects a more efficient exchange of angular momentum between the light field and the atom in the configuration (4.2) than in a single LG mode. This expectation is based on the corresponding situation of momentum exchange between an atom and a standing light wave. In addition to the light field (4.2), the atomic motion in the radial direction is assumed to be confined by an extra trapping potential $U(\rho)$ with cylindrical symmetry.

The z -dependence of the amplitude $E_0(\rho, z)$ is slow and can be ignored. Properly shaping the LG mode, the radial dependence of $E_0(\rho, z)$ can be ignored on the characteristic width of the trapping potential $U(\rho)$. Thus, we assume that $E_0(\rho, z) \simeq E_0$ is constant. For a two-level atom the Hamiltonian in the rotating-wave approximation can then be written as

$$\hat{H} = \hat{H}_0 + U(\rho) + 2\hbar\omega_R \cos l\phi \left(e^{i(kz - \omega t)} |e\rangle \langle g| + e^{-i(kz - \omega t)} |g\rangle \langle e| \right), \quad (4.3)$$

where ω_R is the Rabi frequency of each of the travelling waves that create the standing wave, ω is the laser frequency, and

$$\hat{H}_0 = \frac{\hat{P}^2}{2M} + \frac{\hbar\omega_0}{2} (|e\rangle \langle e| - |g\rangle \langle g|) \quad (4.4)$$

is the Hamiltonian for a free atom, with \hat{P} the momentum operator of the atom, $|g\rangle$ and $|e\rangle$ indicate the ground and excited states, and $\omega_0 = (E_e - E_g)/\hbar$ defines the transition frequency of a free atom.

The dynamics of the atom is rather simple if the laser is far detuned. We assume that

$$|\Delta| \gg \omega_R, \quad (4.5)$$

where the detuning Δ is defined as $\Delta = \omega_0 - \omega$. For an atom in the ground state, the excited state can be adiabatically eliminated, which leads to an effective Hamiltonian in the well-known form

$$\hat{H} = \frac{\hat{P}^2}{2M} + U(\rho) + V(\phi), \quad (4.6)$$

where the light-shift potential is specified by

$$V(\phi) = -\hbar\Omega \cos^2 l\phi \quad (4.7)$$

with $\Omega = \omega_R^2/\Delta$.

4.3 Trapping in counterrotating fields

Some general conclusions on the bound states of the Hamiltonian (4.6) directly follow from its symmetry properties. We introduce the unitary translation operator \hat{T} defined as

$$\hat{T}|\phi\rangle = \left|\phi + \frac{\pi}{l}\right\rangle, \quad (4.8)$$

where $|\phi\rangle$ indicates the states with fixed azimuthal angle. Since the Hamiltonian (4.6) is invariant for rotation about an angle π/l , it follows from a rotational version of the Bloch theorem that the eigenstates of this Hamiltonian are also eigenstates of \hat{T} . The eigenvalue relation can be expressed as

$$\hat{T}|\Psi_q\rangle_j = e^{-i\frac{\pi}{l}q}|\Psi_q\rangle_j, \quad (4.9)$$

where q is referred to as angular quasimomentum and j identifies the energy band. We consider a single energy band, and we suppress the index j . We can restrict q to the first Brillouin zone given as

$$-l \leq q < l. \quad (4.10)$$

The eigenstates $|\Psi_q\rangle$ should be periodic in ϕ with period 2π , because a rotation over 2π must leave the wave function invariant. The finite range of ϕ leads to a discretization of angular quasimomentum. On the other hand, a rotation over 2π is equivalent to the action of the operator \hat{T}^{2l} . Since it follows from Eq. (4.9) that

$$\hat{T}^{2l}|\Psi_q\rangle = e^{-2i\pi q}|\Psi_q\rangle,$$

we conclude that the only possible values of the angular quasimomentum are determined from the condition

$$e^{-2i\pi q} = 1.$$

Hence q must be integer, and each band contains $2l$ Bloch states. For example, for $l = 2$ the first Brillouin zone contains only the four values $q = -2, -1, 0, 1$ of the angular quasimomentum.

Also, in analogy to the case of an infinite linear lattice, one can introduce localized Wannier states $|\Theta_n\rangle$ in the usual manner, as Fourier transforms of the Bloch states

$$|\Psi_q\rangle = \frac{1}{\sqrt{2l}} \sum_{n=-l}^{l-1} e^{iq\frac{\pi}{l}n} |\Theta_n\rangle.$$

Obviously, the number of Wannier states within an energy band is equal to $2l$, just as the number of Bloch states.

In Fig. 4.1 we plot the trapping potential (4.7) $V(x, y)/\hbar\Omega$ for $l = 2, 4$ in Cartesian coordinates. When the potential is sufficiently deep, atoms can be bound in the angular wells, and the Wannier states are confined to a single well. An additional confining potential $U(\rho)$ is required to trap particles in the radial direction, and to avoid their escape. Then the potential (4.7) can create a circular lattice, where particles are located near the minima of the periodic potential. A circular optical lattice has many applications, as discussed recently by several authors [66–68].

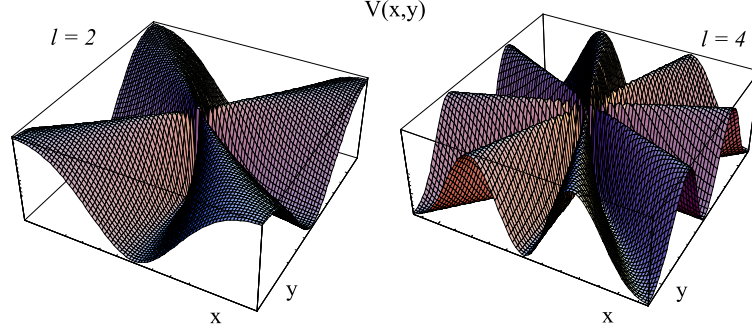


Figure 4.1: Circular lattice structure due to the trapping potential $V(x, y)$. The plot shows $V(x, y)/\hbar\Omega$ for $l = 2, 4$ in Cartesian coordinates.

4.4 Diffraction in counterrotating fields

Since the potentials have a cylindrical symmetry, it is convenient to express the kinetic energy in cylindrical coordinates, and we write

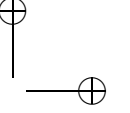
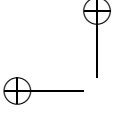
$$\frac{\hat{p}^2}{2M} = -\frac{\hbar^2}{2M} \left(\frac{\partial^2}{\partial z^2} + \frac{1}{\rho} \frac{\partial}{\partial \rho} \rho \frac{\partial}{\partial \rho} + \frac{1}{\rho^2} \frac{\partial^2}{\partial \phi^2} \right). \quad (4.11)$$

The dynamics along the z axis is completely free. For simplicity, we assume that the radial potential $U(\rho)$ is narrow, so that the radial motion is restricted to a ring with radius ρ_0 , and we ignore radial dispersion in the present Section. We return to it in Sec. VI, where the effect of the radial dispersion is estimated. The motion of an atom in the angular direction is then described by the one-dimensional Hamiltonian

$$\hat{H} = -\frac{\hbar^2}{2I} \frac{\partial^2}{\partial \phi^2} - \hbar\Omega \cos^2 l\phi, \quad (4.12)$$

which has the azimuthal angle as the only coordinate. The quantity $I = M\rho_0^2$ is the moment of inertia. This Hamiltonian is the circular counterpart of the Hamiltonian for simple linear diffraction. The main difference is that the coordinate ϕ is periodic, which forces the angular wave number l to be integer. Diffraction of a single atom described by such a linear Hamiltonian has been extensively studied theoretically and experimentally by several groups [47, 48, 65].

Just as is usually done for linear diffraction, we consider the situation that an initially localized atom interacts with the optical potential during a small interaction interval $[-\tau, 0]$, where the atom picks up momentum from the lattice. The transition from the near field immediately after the interaction and the far field is described by free evolution. We assume the atom to be initially in its ground state and situated in a small segment of the ring. Since the angular wave function $\Phi(\phi)$ of the atom must be periodic at all times, we cannot represent a localized wave packet by a Gaussian. The initial state at the beginning of the interaction



interval is taken as

$$\Phi(\phi, -\tau) = C_N \cos^{2N} \frac{\phi}{2}, \quad (4.13)$$

with N to be a large natural number, and C_N is the normalization constant

$$C_N = \frac{2^{2N}}{\sqrt{2\pi \binom{4N}{2N}}}. \quad (4.14)$$

The state (4.13) can be written as a Fourier series, which is just an expansion in the angular-momentum eigenstates. This gives

$$\Phi(\phi, -\tau) = \frac{1}{\sqrt{2\pi}} \sum_{m=-N}^N \psi_m e^{im\phi}, \quad (4.15)$$

with

$$\psi_m = \frac{1}{\sqrt{\binom{4N}{2N}}} \binom{2N}{N+m}. \quad (4.16)$$

The initial state (4.13) is localized around $\phi = 0$, which is clear from the asymptotic form

$$\cos^{2N} \frac{\phi}{2} \simeq \exp \left\{ -\frac{N \phi^2}{4} \right\}, \quad (4.17)$$

for large N . The half width in the azimuthal angle is of the order of $\sqrt{2/N}$. From the asymptotic form of the binomial coefficient

$$\binom{2N}{N+m} \simeq 2^{2N} \frac{1}{\sqrt{\pi N}} \exp \left(-\frac{m^2}{N} \right)$$

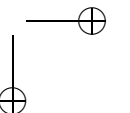
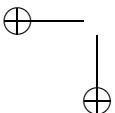
we find the asymptotic expression of the Fourier coefficient

$$\psi_m \simeq \left(\frac{2}{\pi N} \right)^{1/4} \exp \left(-\frac{m^2}{N} \right). \quad (4.18)$$

This demonstrates that the half width in angular momentum is of the order of $\sqrt{N/2}$.

If we take the duration τ of the light pulse short and the moment of inertia I is large, so that $\hbar^2 l^2 \tau / (2I)$, no propagation occurs, and the kinetic-energy term can be neglected during the interaction. This is the equivalence of the standard Raman-Nath approximation applied by Cook et al [47]. Then the final state at time 0 after the interaction is

$$\Phi(\phi, 0) = \Phi(\phi, -\tau) \exp(i\Omega\tau \cos^2 l\phi). \quad (4.19)$$



This state can be expressed as an expansion in angular-momentum eigenstates, in the form Fourier series, which is just an expansion in the angular-momentum eigenstates. This gives

$$\Phi(\phi, 0) = \frac{1}{\sqrt{2\pi}} \sum_m \zeta_m e^{im\phi}, \quad (4.20)$$

where

$$\zeta_m = \exp(i\Omega\tau/2) \sum_n i^n \psi_{m-2nl} J_n(\Omega\tau/2), \quad (4.21)$$

in terms of the ordinary Bessel functions.

States with large angular momentum $|m| > N$ are initially not populated, whereas all angular momentum states get populated after the interaction. Thus, the configuration with two LG modes leads to more efficient exchange between the light field and the atom than a single LG beam. The physical interpretation is the same as for diffraction in the field of classical counterpropagating waves: an atom picks up a photon from the light beam with one helicity and emits a photon into the opposite one.

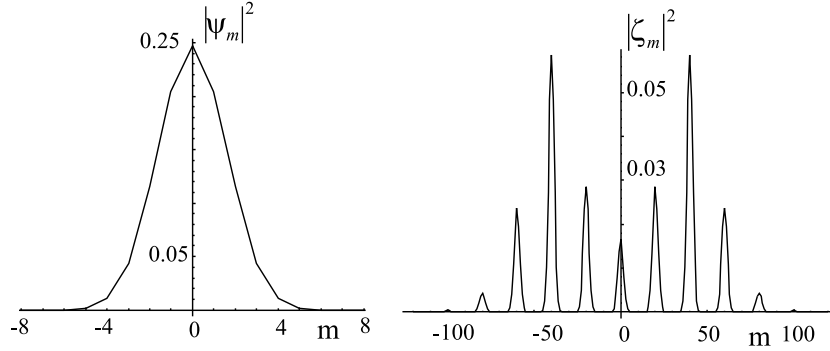


Figure 4.2: Probability distribution of angular momentum m before (left figure) and after the pulse (right figure). Here the helicity of the circular lattice is $l = 10$, the initial state is determined by $N = 10$ and the pulse duration τ is given by $\Omega\tau = 6$.

In Fig. 4.2 we present a typical diffraction pattern calculated for the case that $l > N$. More precisely, we plot the angular-momentum coefficients $|\psi_m|^2$ before the interaction, and the coefficients $|\zeta_m|^2$ after the interaction with the circular lattice, for $\Omega\tau = 6$. In the latter case, the momentum peaks correspond to different values of n . The distance between neighboring peaks is equal to $2l$. The half width of each peak is of the order of $\sqrt{N/2}$.

4.5 Free evolution on a ring

As shown above, the angular-momentum distribution of an atom after the interaction with a pair of counterrotating LG beams can be broad. However, as a result of the Raman-Nath

approximation, the angular distribution of the atom has not been modified during the interaction, so that $|\Phi(\phi, -\tau)|^2 = |\Phi(\phi, 0)|^2$. In this chapter we investigate the spatial form of the atomic distribution in the far field, i. e. after free evolution of the atom over the ring. As before, the motion along the z axis is completely free and the radial motion is restricted on a ring. The initial state of this free evolution is given by Eq. (4.19), with the expansion in angular-momentum states given by Eqs. (4.20) and (4.21). For positive times, the atomic motion is still restricted to the ring with radius ρ_0 by the confining potential $U(\rho)$, and the evolution of the angular wave function $\Phi(\phi)$ is governed by the Hamiltonian (4.12) with $\Omega = 0$. With the initial state (4.20), the time-dependent wave function is given by the expansion

$$\Phi(\phi, t) = \frac{1}{\sqrt{2\pi}} \sum_m \zeta_m \exp(im\phi - i\xi t m^2) \quad (4.22)$$

where $\xi = \hbar/(2I)$, and the coefficients ζ_m are given in Eq. (4.21). As displayed in Fig. 4.2, the distribution $|\zeta_m|^2$ typically separates in a number of peaks centered at $\bar{m} = 2nl$, where $n = 0, \pm 1, \pm 2, \dots$ which are separated by $2l$. Thus, the superposition state (4.22) can be considered as a series of elementary wave packets centered at $2nl$, in the angular-momentum space. Each of these peaks gives a separate contribution to the wave function that moves with its own angular group velocity $2\xi\bar{m} = 4\xi nl \equiv \nu_n$. The angular separation between neighboring wavepackets is given by $4\xi lt$, which is proportional to l . Since wave packets with opposite angular-momentum values will move in opposite directions, i. e. clockwise and anticlockwise, they will eventually meet again at some time $t = T$ and start to interfere.

In order to estimate the time value that interference sets in, we use the fact that for not too small arguments $\Omega\tau/2$ the Bessel function $J_n(\Omega\tau/2)$ with the maximal value is the one with $n = n_{\max} \simeq \Omega\tau/2$. Hence, the meeting time of the pair of the strongest counterpropagating packets is

$$T = \frac{\pi}{v_{\max}} = \frac{\pi}{2\xi\Omega\tau l}.$$

The exact expression for the time-dependent wave function can be expressed in an integral form by using the mathematical identity [4]

$$\exp(im\phi - i\xi t m^2) = \frac{1}{\sqrt{4\pi i\xi t}} \int_{-\infty}^{\infty} d\phi' e^{im\phi'} \exp\left[i\left(\phi - \phi'\right)^2 / 4\xi t\right], \quad (4.23)$$

which can be checked by performing the integration. When substituting this identity in the right-hand side of Eq. (4.22), and using the expansion (4.20), we arrive at the exact expression

$$\Phi(\phi, t) = \frac{1}{\sqrt{4\pi i\xi t}} \int_{-\infty}^{\infty} d\phi' \Phi(\phi', 0) \exp\left[i\left(\phi - \phi'\right)^2 / 4\xi t\right]. \quad (4.24)$$

A similar equation is well-known to describe the free evolution of a quantum particle in one dimension. In the present case it is crucial that the integration be performed over all values of ϕ' , while using that the wave function $\Phi(\phi', 0)$ is periodic. Because of this periodicity, we can express the integral in (4.24) as a sum of bounded integrals

$$\Phi(\phi, t) = \frac{1}{\sqrt{4i\pi\xi t}} \sum_{p=-\infty}^{\infty} \int_{2\pi p}^{2\pi(p+1)} d\phi' \Phi(\phi', 0) \exp \left[i(\phi - \phi')^2 / 4\xi t \right]. \quad (4.25)$$

By a shift of variables the integrations can be performed over the interval $[0, 2\pi]$, which leads to an integral expression over a single interval

$$\begin{aligned} \Phi(\phi, t) = \frac{1}{\sqrt{4i\pi\xi t}} \sum_{p=-\infty}^{\infty} \exp \left[i(\phi - 2\pi p)^2 / 4\xi t \right] \\ \int_0^{2\pi} d\phi' \tilde{\Phi}(\phi', t) \exp \left[-i(\phi - 2\pi p)\phi' / 2\xi t \right]. \end{aligned} \quad (4.26)$$

Here we introduced the modified wave function $\tilde{\Phi}$ which is just the initial wave function, modified by a phase factor, defined by

$$\tilde{\Phi}(\phi', t) = \Phi(\phi', 0) \exp \left[i\phi'^2 / 4\xi t \right]. \quad (4.27)$$

In order to emphasize its physical significance, we write Eq. (4.26) in the form

$$\Phi(\phi, t) = \frac{1}{\sqrt{2i\xi t}} \sum_{p=-\infty}^{\infty} \exp \left[i(\phi - 2\pi p)^2 / 4\xi t \right] F \left(\frac{\phi - 2\pi p}{2\xi t} \right), \quad (4.28)$$

where the function F is the Fourier transform of the modified wave function defined over a single period

$$F(x) = \frac{1}{\sqrt{2\pi}} \int_0^{2\pi} d\phi' \tilde{\Phi}(\phi', t) \exp \left[-ix\phi' \right]. \quad (4.29)$$

For a freely evolving quantum particle in one dimension, the time-dependent wave function has the same form as the term with $p = 0$ in (4.28). The other terms can be understood from the periodic nature of the dynamics on the circle, where each period of the initial wave function serves as an additional source that contributes to the wave function $\Psi(\phi, t)$ in the relevant interval $[0, 2\pi]$. Because of the finite range of the integration in Eq. (4.29), the distinction between the modified wave function and the initial wave function vanishes for times t obeying the inequality $t \gg 1/(\xi N)$, when we find in a good approximation

$$\tilde{\Phi}(\phi', t) \simeq \Phi(\phi', 0). \quad (4.30)$$

In this limit, the function F is just the Fourier transform of the initial wave function $\Phi(\phi, 0)$, and $\Phi(\phi, t)$ is simply determined by the Fourier transform F of the initial wave function $\Phi(\phi, 0)$ multiplied by a phase factor. The equation (4.28) has the flavor of the far-field picture of the time-dependent wave function. The Fourier transform of the initial state determines not only the momentum wave function, but also the asymptotic form of the coordinate wave function, scaled by a factor that varies linearly with time. Characteristic for the present case

of evolution on a circle is that each interval of length 2π serves as a separate source, each giving a contribution to $\Phi(\phi, t)$. Since the Fourier transform of the wave function determines the angular-momentum amplitudes, we may conclude that the wave function for not too small times has the same form as the initial distribution of angular momentum, scaled by the factor $2\xi t$. It is clarifying to follow the temporal evolution of $|\Phi(\phi, t)|^2$ by distinguishing two time regions, namely $0 \leq t < T$ and $t \geq T$. In the region $0 \leq t < T$, the wave function has not yet spread beyond a single period of length 2π , and only a single term in eq. (4.28) (or (4.26)) differs from zero.

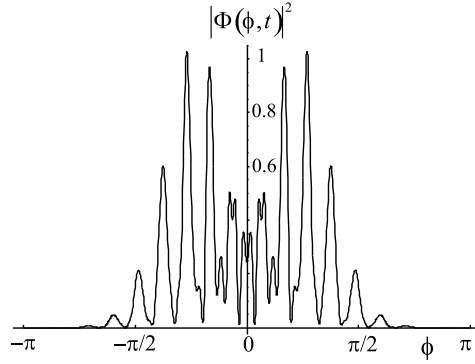


Figure 4.3: Angular distribution $|\Phi(\phi, t)|^2$ is plotted versus the azimuthal angle ϕ before the left and right rotating components cross. Here $\xi t = 3\pi \times 10^{-3}$, the value of N determining the width of the initial state, the helicity l and the pulse duration τ are the same as in Fig. 4.2.

The contribution to the wave function coming from different sources do not overlap yet, so that one can neglect the interference term between them. At later times $t \geq T$, the diffraction pattern on the interval $[0, 2\pi]$ is formed as an interference pattern between two and more terms in the superposition state (4.25). This picture is confirmed by numerical calculation of the diffraction pattern for the two time regimes. In Fig. 4.3 the angular probability distribution $|\Phi(\phi, t)|^2$ is shown for a time $t < T$. The spatial pattern resembles the angular momentum distribution shown in Fig. 4.2. Figure 4.4 displays the same probability distribution for a later time $t > T$. One notices that the counterrotating components give rise to clear interference fringes. These fringes will be quite sensitive to any perturbation in one of the arms. This suggests to use the present scheme as an atomic interferometer [4]. Usually, interferometers have two key components, namely a beam splitter and a mirror. A coherent incoming atomic beam is split into spatially separated components by the beam splitter. Two arms are getting formed, which freely propagate and may undergo different phase shifts, which are probed by recombining the two arms. The interference pattern contains the information of the phase perturbation in one of the arms. Recombination usually requires atomic mirrors. In atom optics, beam splitters and mirrors are commonly realized by using light pulses, with carefully selected duration and shape.

In the present case, only a single pulse is required that splits the initial atomic wave packet into components rotating to the left and to the right. No mirrors are employed in this scheme. Instead, one uses the radial potential $U(\rho)$, to constrain the atomic motion to a ring.

Radial potentials can be realized by hollow light beams, which are widely used in atomic interferometric schemes.

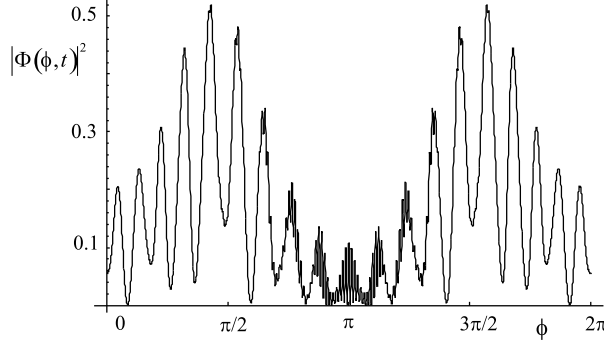


Figure 4.4: Angular distribution $|\Phi(\phi, t)|^2$ is plotted versus the azimuthal angle ϕ after the left and right rotating components cross. Here $\xi t = 6\pi \times 10^{-3}$, the value of N , the helicity l and the pulse duration τ are the same as in Fig. 4.2.

4.6 Radial dispersion

In this chapter we consider the radial dynamics of the diffracted wave function during its free evolution, after the passage of the circular lattice. We assume that the wave function at time $t = 0$, after the diffracting pulse, is factorized as

$$\Psi(\rho, \phi, 0) = Q(\rho, 0)\Phi(\phi, 0), \quad (4.31)$$

where the radial part Q of the wave function is sharply peaked at $\rho = \rho_0$, and the angular wave function is specified by Eq. (4.20). The radial function Q is normalized ($\int_0^\infty d\rho Q^2(\rho)\rho = 1$). We wish to study the possible deformation of the wave packet, when the radial dispersion is included during the stage of free evolution. We take the simplest possible trapping potential, which allows radial dispersion, and we take for the confining potential $U(\rho)$ an infinitely deep cylindrical box with radius a , as defined by

$$U(\rho) = 0 \text{ for } \rho \leq a, \text{ and } U(\rho) = \infty \text{ for } \rho > a. \quad (4.32)$$

This potential models a hollow light beam. With this potential, the normalized eigenfunctions of the Hamiltonian for the cylindrical coordinates during the free-evolution stage take the form

$$\Psi_{nm}(\rho, \phi) = R_{nm}(\rho) \frac{1}{\sqrt{2\pi}} e^{im\phi}, \quad (4.33)$$

where the radial functions R_{nm} are solutions of the equation

$$\left[-\frac{\hbar^2}{2M} \left(\frac{1}{\rho} \frac{\partial}{\partial \rho} \rho \frac{\partial}{\partial \rho} - \frac{m^2}{\rho^2} \right) + U(\rho) \right] R_{nm}(\rho) = \mathcal{E}_{nm} R_{nm}(\rho), \quad (4.34)$$

with \mathcal{E}_{nm} are the corresponding eigenenergies. The radial functions are proportional to the Bessel function of order m

$$R_{nm}(\rho) \propto J_m(\alpha_{nm}\rho/a), \quad (4.35)$$

with R_{nm} normalized in the interval $0 \leq \rho \leq a$. In order that the wave function vanishes at the edge $\rho = a$ of the cylindrical well, we have to take the numbers α_{nm} for various values of n as the subsequent zero's of the Bessel function J_m . This determines the corresponding eigenenergies as

$$\mathcal{E}_{nm} = \hbar\lambda\alpha_{nm}^2. \quad (4.36)$$

with $\lambda = \hbar/(2Ma^2)$. For each value of the angular momentum m , the set of functions $R_{nm}(\rho)$ is complete. An expansion of the initial state (4.31) in the energy eigenfunction is found when we expand the initial radial wave function $Q(\rho, 0)$ in the radial eigenfunctions (4.35), so that

$$Q(\rho, 0) = \sum_n c_{nm} R_{nm}(\rho), \quad (4.37)$$

while substituting Eq. (4.20) for the initial angular state $\Phi(\phi, 0)$. For the time-dependent state we find

$$\Psi(\rho, \phi, t) = \sum_m \frac{1}{\sqrt{2\pi}} \zeta_m e^{im\phi} Q_m(\rho, t), \quad (4.38)$$

where the m -dependent radial wave function Q_m is

$$Q_m(\rho, t) = \sum_n c_{nm} R_{nm}(\rho) \exp(-i\mathcal{E}_{nm}t/\hbar). \quad (4.39)$$

From Eq. (4.37) one notices that $Q_m(\rho, 0) = Q(\rho, 0)$, independent of the angular momentum m . It is obvious from the radial Schrödinger equation (4.34) and the initial condition (4.31) that the normalized radial wave function obeys the identity $Q_m(\rho, t) = Q_{-m}(\rho, t)$ for all m . Moreover, since the total wave function before diffraction is even in ϕ , it must remain even for all times. This implies that $\zeta_m = \zeta_{-m}$ for all m . So just as discussed in Sec. IV, the angular distribution separates in different wave packets that are counterrotating. Since the phase of $\zeta_m Q_m$ is even in m , its derivative with respect to m will be odd, and the angular group velocities of packets with opposite values of \overline{m} will be opposite. This leads to interference after the packets have traversed the entire ring. The initial radial function is taken as a narrow Gaussian

$$Q(\rho, 0) \propto \exp\left(-(\rho - \rho_0)^2 / 2L^2\right), \quad (4.40)$$

Here L is the width and ρ_0 represents the initial position of the wave packet within the box. The normalized wave function $Q_m(\rho, t)$ describes the radial dynamics for each value of the angular momentum m . As an example, we evaluate the time behavior of the average

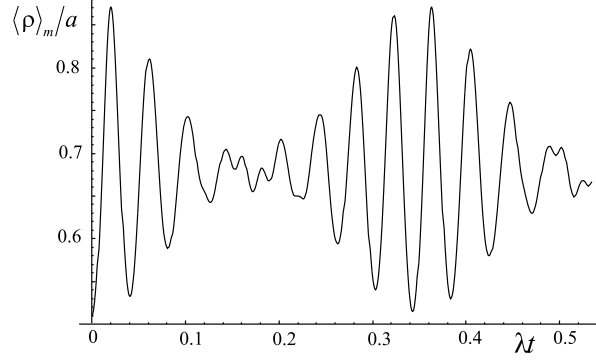


Figure 4.5: Time behavior of the average radial distance $\langle \rho(t) \rangle_m / a$ for the angular momentum $m = 10$. N is the same as in Fig. 4.2, the width of the initial Gaussian is $L = 0.01a$, and the initial average radial distance is $\rho_0 = a/2$.

radius for each angular momentum, with the given initial radial state (4.40), according to the expression

$$\langle \rho(t) \rangle_m = \int_0^\infty d\rho |Q_m(\rho, t)|^2 \rho^2.$$

The result is displayed in Fig. 4.5, in the special case that $m = 10$. The average radius displays oscillations, which can be understood as arising from the outward motion due to the centrifugal potential, followed by reflection at the hard wall of the cylinder. The oscillations display collapse, followed by a revival. These may be viewed as arising from the initial dephasing of the contribution from the radial eigenfunctions R_{nm} with different values of n , due to their energy difference. The revival of the oscillation can be understood from the discrete nature of the contributing energy eigenvalues, when the phase factors due to neighboring eigenenergies have built up a phase difference 2π . Because of the conservation of angular momentum, the probability density near the origin remains zero. The interference between the counterrotating wave packets is illustrated in Fig. 4.6, for the ring at radius $\rho = \rho_0 = a/2$. Fig. 4.6a shows the short-time separation of the angular wave packets. Fig. 4.6b displays the interference that arises as soon as overlap occurs around $\phi = \pi$ between the clockwise and the anti-clockwise rotating packets. This demonstrates that the radial wave functions $Q_m(\rho, t)$ for different values of m have sufficient overlap, so that the angular interference survives the effect of radial dispersion.

4.7 Conclusions

In this paper we describe the diffraction of an atomic wave by a circular optical lattice. Such a lattice can be formed by the superposition of two Laguerre-Gaussian beams with opposite helicity, which gives rise to a standing wave in the angular direction. Such a light field will split a single localized atom into clockwise and anticlockwise rotating components. If the system

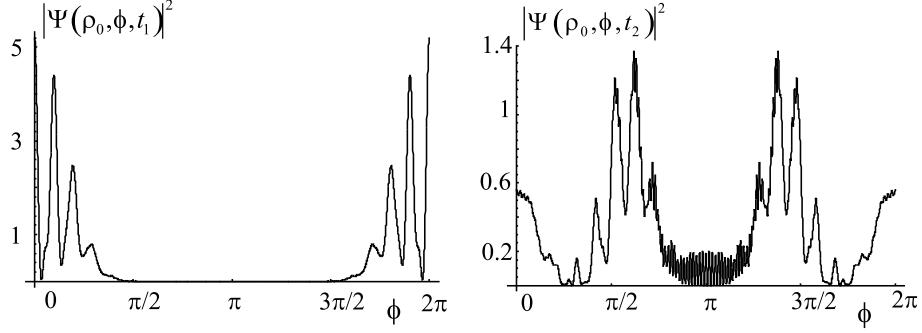
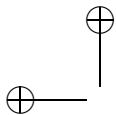
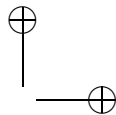


Figure 4.6: Angular distribution $|\Psi(\rho_0, \phi, t)|^2$ in the presence of radial dispersion, at the ring $\rho = \rho_0 = a/2$. The time values are determined by $\lambda t_1 = \pi \times 10^{-3}$ and $\lambda t_2 = 2\pi \times 10^{-3}$. $N, l, \Omega\tau$ are the same as in Fig. Fig. 4.2.

is in a trapping potential in the form of a ring or in a cylindrical box, these counterrotating components give rise to interference. We express the spatial pattern in the far diffraction field in terms of the Fourier transform of the near-field diffraction pattern. The periodic nature of the circular motion modifies this relation compared with the case of diffraction by a linear standing wave. The general conclusions are backed up by numerical calculations. Characteristic for the circular case is that the wave packets corresponding to opposite angular momentum will cross each other, even without applying light pulses to reverse their motion, as in more common interferometric schemes. The scheme is reasonably robust to changes in the radial confining potential.

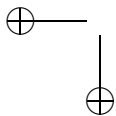


|

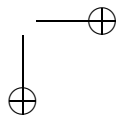


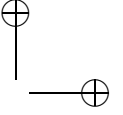
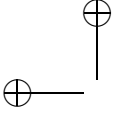
—

—



|





Chapter 5

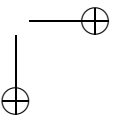
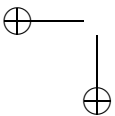
Analogy between a two-well Bose-Einstein condensate and atom diffraction

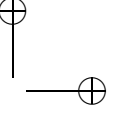
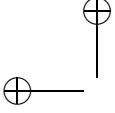
We compare the dynamics of a Bose-Einstein condensate in two coupled potential wells with atoms diffracting from a standing light wave. The corresponding Hamiltonians have an identical appearance, but with a different set of commutation rules. Well-known diffraction phenomena as Pendellösung oscillations between opposite momenta in the case of Bragg diffraction, and adiabatic transitions between momentum states are shown to have analogies in the two-well case. They represent the collective exchange of a fixed number of atoms between the wells.

5.1 Introduction

The most common approach to the description of a trapped Bose-condensed gas is based on the mean-field approximation, which yields the Gross-Pitaevski equation for the macroscopic wave function. This wave function, which depends on the number of atoms, plays the role of the mode function for the Maxwell field. This approach is reliable when the condensate is trapped in a single quantum state in a potential well. However, when the condensate is separated into two or more parts, so that more than one quantum state is populated, the mean-field approach is not evidently justified. It has been shown by Javanainen and Yoo [15] that two originally separate parts of a condensate that are initially in a Fock state and that are brought to overlap will reveal an interference pattern that varies in position from one realization to another. This effect, which has also been observed experimentally [69, 70], cannot be described by a single macroscopic wave function. A simple model for a condensate in a double potential well is defined by a field-theoretical Hamiltonian for a boson-Hubbard dimer [71, 72], which can be expressed in terms of $SU(2)$ angular-momentum-type operators with a quadratic term. This latter term represents the interaction between atoms in a well. The mean-field approximation is basically equivalent to classical equations of motion for the expectation values of the $SU(2)$ operators [73, 74]. The quantum regime has mainly been studied numerically, leading to collapse and revival [73], and to nonclassical dynamics arising from the periodic modulation of the coupling between the wells [75]. The formation of a two-well condensate by the raising of the barrier has been analyzed theoretically [76]. The situation of a Bose-Einstein condensate (BEC) in a two-well trap is also studied experimentally [77, 78].

A very similar Hamiltonian describes the situation of an atom diffracting from a standing-wave optical potential. This problem has received attention already in the early days of laser cooling [47–49, 65]. More recent work has developed the band structure of the energy





spectrum [79], and a number of regimes have been distinguished that allow an analytical description [80]. In a simple version of the model, the Hamiltonian is identical in form as in the two-well problem mentioned above. Now the quadratic term represent the kinetic energy of the atom. The only difference between the two cases is that the commutation rules for the operators in the diffraction case are slightly simplified compared to the case of SU(2) symmetry.

In this paper, we discuss the analogy and the differences between these two systems. We point that a number of analytical solutions known for the diffraction problem can be carried over to the two-well system. The physics of these cases is discussed.

5.2 BEC in a double potential well

We consider a potential consisting of two wells. When the barrier between the wells is not too low, the ground state and the first excited state $|g\rangle$ and $|e\rangle$ of a single atom are well approximated as the even and odd superposition of the lowest bound states in the two wells. Therefore, these states can be described as

$$|g\rangle = \frac{1}{\sqrt{2}}(|1\rangle + |2\rangle), \quad |e\rangle = \frac{1}{\sqrt{2}}(|1\rangle - |2\rangle), \quad (5.1)$$

with $|1\rangle$ and $|2\rangle$ the localized states in either well. When the energy separation between the excited and the ground state is indicated as $\hbar\delta$, the off-diagonal element of the one-particle Hamiltonian \hat{H}_1 between the localized states is

$$\langle 1 | \hat{H}_1 | 2 \rangle = -\hbar\delta/2.$$

At the low energies that are of interest here, the two particle interaction is well approximated by the standard contact potential $U(\vec{r}, \vec{r}') = (4\pi\hbar^2 a/m)\delta(\vec{r} - \vec{r}')$, with a the scattering length. The second-quantized field operator is now

$$\hat{\Psi}(\vec{r}) = \hat{a}_g \psi_g(\vec{r}) + \hat{a}_e \psi_e(\vec{r}) = \hat{a}_1 \psi_1(\vec{r}) + \hat{a}_2 \psi_2(\vec{r}), \quad (5.2)$$

in terms of the wave functions ψ_i and the annihilation operators \hat{a}_i of the single-particle states. The annihilation operators and the corresponding creation operators obey the standard bosonic commutation rules. The corresponding Hamiltonian is

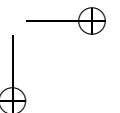
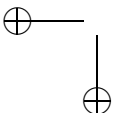
$$\hat{H} = \int d\vec{r} \hat{\Psi}^\dagger(\vec{r}) \hat{H}_1 \hat{\Psi}(\vec{r}) + \frac{1}{2} \int d\vec{r} d\vec{r}' \hat{\Psi}^\dagger(\vec{r}) \hat{\Psi}^\dagger(\vec{r}') U(\vec{r}, \vec{r}') \hat{\Psi}(\vec{r}) \hat{\Psi}(\vec{r}'). \quad (5.3)$$

The wave functions ψ_1 and ψ_2 of the localized states have the same form, and we assume that they do not overlap. Then the interaction term can be expressed exclusively in the parameter κ defined by

$$\hbar\kappa = \frac{4\pi\hbar^2 a}{m} \int d\vec{r} |\psi_1(\vec{r})|^4, \quad (5.4)$$

which measures the strength of the interatomic interaction. Performing the integrations in eq. (5.3) leads to the expression for the Hamiltonian

$$\hat{H} = -\frac{\hbar\delta}{2} (\hat{a}_1^\dagger \hat{a}_2 + \hat{a}_2^\dagger \hat{a}_1) + \frac{\hbar\kappa}{2} (\hat{a}_1^\dagger \hat{a}_1^\dagger \hat{a}_1 \hat{a}_1 + \hat{a}_2^\dagger \hat{a}_2^\dagger \hat{a}_2 \hat{a}_2), \quad (5.5)$$



where we took the zero of energy halfway the two energy levels of a single atom. This is also known as the boson-Hubbard dimer Hamiltonian [71].

The Hamiltonian (5.5) can also be expressed in terms of SU(2) operators by applying the standard Schwinger representation of two modes. This leads to the definition

$$\hat{J}_0 = \frac{1}{2} (\hat{a}_1^\dagger \hat{a}_1 - \hat{a}_2^\dagger \hat{a}_2), \quad \hat{J}_+ = \hat{a}_1^\dagger \hat{a}_2, \quad \hat{J}_- = \hat{a}_2^\dagger \hat{a}_1. \quad (5.6)$$

These operators are related to the Cartesian components of angular momentum by the standard relations $\hat{J}_\pm = \hat{J}_x \pm i\hat{J}_y$ and $\hat{J}_0 = \hat{J}_z$. They obey the commutation rules for angular momentum operators

$$[\hat{J}_0, \hat{J}_\pm] = \pm \hat{J}_\pm, \quad [\hat{J}_+, \hat{J}_-] = 2\hat{J}_0, \quad (5.7)$$

which generate the SU(2) algebra. The Hamiltonian (5.5) can be rewritten in the form

$$\hat{H} = -\frac{\hbar\delta}{2}(\hat{J}_+ + \hat{J}_-) + \hbar\kappa\hat{J}_0^2 + \frac{\hbar\kappa}{4}(\hat{N}^2 - 2\hat{N}), \quad (5.8)$$

with $\hat{N} = \hat{a}_1^\dagger \hat{a}_1 + \hat{a}_2^\dagger \hat{a}_2$ the operator for the total number of particles. Obviously, Hamiltonian (5.8) commutes with \hat{N} , and it is block diagonal in the number of particles N . For each value of N , the Hamiltonian (5.8) can be expressed as

$$\hat{H}_N + \frac{\hbar\kappa}{4}(N^2 - 2N),$$

with the N -particle Hamiltonian

$$\hat{H}_N = -\frac{\hbar\delta}{2}(\hat{J}_+ + \hat{J}_-) + \hbar\kappa\hat{J}_0^2, \quad (5.9)$$

where the operators are now restricted to the $N + 1$ Fock states $|n, N - n\rangle$ with $n = 0, 1, \dots, N$, with n particles in well 1 and $N - n$ particles in well 2. In the language of angular momentum, this manifold of states corresponds to the angular-momentum quantum number $J = N/2$, and the $2J + 1$ Fock states are eigenstates of \hat{J}_0 with eigenvalue $\mu = n - N/2$ with $\mu = -J, -J + 1, \dots, J$. Note that μ is half the difference of the particle number in the two wells. For an even number of particles, the angular-momentum quantum number J as well as the "magnetic" quantum numbers are integer, whereas these number are half integer in case of an odd number of particles. The action of the operators \hat{J}_0 and \hat{J}_\pm on the Fock states has the well-known behavior

$$\hat{J}_0 |\mu\rangle = \mu |\mu\rangle, \quad \hat{J}_+ |\mu\rangle = f_{\mu+1} |\mu + 1\rangle, \quad \hat{J}_- |\mu\rangle = f_\mu |\mu - 1\rangle, \quad (5.10)$$

with $f_\mu = \sqrt{(J + \mu)(J - \mu + 1)}$. The μ dependence of the strength of the hopping operators \hat{J}_\pm reflects the bosonic accumulation factor, which favors the arrival of an additional bosonic atom in an already occupied state.

When the quadratic term in eq. (5.9) would be replaced by a linear term, the evolution would be a uniform rotation in the $(2J + 1)$ -dimensional state space with angular frequency $\sqrt{\delta^2 + \kappa^2}$. The presence of the quadratic term makes the dynamics considerably more complex. Therefore, we compare this dynamics with another well-known case in which a similar quadratic term appears.

5.3 Standing-wave diffraction of atoms

The translational motion of a two-level atom in a far detuned standing-wave light field is described by the effective Hamiltonian

$$\hat{H}_d = -\frac{\hbar^2}{2m} \frac{\partial^2}{\partial z^2} - \frac{\hbar\omega_R^2}{\Delta} \cos^2 kz, \quad (5.11)$$

with $\Delta = \omega_0 - \omega$ is the difference of the resonance frequency and the optical frequency, and ω_R is the Rabi frequency of each of the traveling waves that make up the standing wave. The Hamiltonian takes a particularly simple form in momentum representation, since the kinetic-energy term is diagonal in momentum and the potential energy changes the momentum by $\pm 2\hbar k$. Therefore, we introduce momentum eigenstates $|\mu\rangle$ which have the momentum $2\mu\hbar k$. Then apart from an irrelevant constant, Hamiltonian (5.11) can be represented in the algebraic form

$$\hat{H}_d = -\frac{\hbar\delta}{2} (\hat{B}_+ + \hat{B}_-) + \hbar\kappa\hat{B}_0^2, \quad (5.12)$$

where $\kappa = 2\hbar k^2/m$ determines the kinetic energy term and $\delta = \omega_R^2/2\Delta$ the atom-field coupling. The operators occurring on the right-hand side are defined by the relations

$$\hat{B}_0|\mu\rangle = \mu|\mu\rangle, \quad \hat{B}_\pm|\mu\rangle = |\mu \pm 1\rangle. \quad (5.13)$$

They differ from the corresponding relations (5.10) in that now the strength of the hopping operators is uniform.

This Hamiltonian (5.12) has the same form as eq. (5.9), even though they describe completely different physical situations. The difference is mathematically characterized by the commutation relations. The SU(2) relations (5.7) are replaced by the simpler set

$$[\hat{B}_0, \hat{B}_\pm] = \pm \hat{B}_\pm, \quad [\hat{B}_+, \hat{B}_-] = 0, \quad (5.14)$$

which is easily found from their explicit expressions (5.13). The two operators \hat{B}_\pm are found to commute. A result of this difference is that the state space in the two-well case has a finite dimension $2J + 1 = N + 1$, whereas the momentum space has an infinite number of dimensions.

A mathematically identical set of operators occurs in the description of the dynamics of the Wannier-Stark system, consisting of a particle in a periodic potential with an additional uniform force (Chapter 2). In that case, the eigenstates of \hat{B}_0 represent the spatially localized Wannier states, rather than the momentum states.

We recall three approximate solutions of the evolution governed by Hamiltonian (5.12), which are valid in different situations, and which allow analytical solutions.

The Raman-Nath regime is valid for interaction times that are so short that the atom has no time to propagate. Then the quadratic term in eq. (5.12) can be neglected, and the evolution is determined by the atom-field coupling $\delta(t)$. The evolution operator is simply $\hat{U} = \exp[i\phi(\hat{B}_+ + \hat{B}_-)/2]$, where $\phi = \int dt\delta(t)$ is the integral of the coupling constant over the evolution period. The matrix elements of the resulting evolution operator for the pulse can be found by operator algebra in the form (Chapter 2)

$$\langle\mu'|\hat{U}|\mu\rangle = i^{\mu'-\mu} J_{\mu'-\mu}(\phi), \quad (5.15)$$

in terms of Bessel functions. For an initial state $|\mu\rangle$ with a well-determined momentum, the time-dependent state following the pulse can be expressed as

$$|\Psi(t)\rangle \simeq \sum_{\mu'} e^{-i\kappa t \mu'^2} |\mu'\rangle \langle \mu' | \hat{U} | \mu \rangle. \quad (5.16)$$

This leads to explicit analytical expressions for diffraction experiments [47–49, 65]. The probability of transfer of n units of momentum is proportional to $|J_n(\phi)|^2$.

The Bragg regime is valid when the coupling δ between neighboring momentum states is small compared to the kinetic-energy separation $\approx 2\hbar\kappa\mu$ of the initial state $|\mu\rangle$ from its neighboring states $|\mu+1\rangle$. This initial state leads to an oscillating time-dependent state between the two states $|\mu\rangle$ and $|\mu-1\rangle$ with the same kinetic energy

$$|\Psi(t)\rangle = \cos \frac{\Omega_\mu t}{2} |\mu\rangle + i \sin \frac{\Omega_\mu t}{2} |\mu-1\rangle, \quad (5.17)$$

apart from an overall phase factor. This can only occur when the momentum transfer 2μ (in units of $2\hbar k$) is an integer, which corresponds precisely to the Bragg condition. The *Pendellösung* frequency is given by $\Omega_\mu = \delta(\delta/2\kappa)^{2\mu-1} / [(2\mu-1)!]^2$ [80]. This expression is fully analogous to the effective Rabi frequency for a resonant multiphoton transition, with nonresonant intermediate states [81, 82].

The regime of adiabatic coupling arises for a time-dependent atom-field coupling $\delta(t)$ that varies sufficiently slowly, so that an initial energy eigenstate remains an eigenstate. The adiabaticity condition in the present case reads

$$\frac{d\delta}{dt} \ll \kappa\delta. \quad (5.18)$$

When an atom passes a standing wave with a sufficiently smooth variation of the intensity, and the Bragg condition is fulfilled, the presence of two initially degenerate eigenstates $|\pm\mu\rangle$ leads to interference after the passage, which produces two outgoing beams. Because of the similarity between the two Hamiltonians (5.9) and (5.12), these well-known diffraction cases can be expected to have analogies in the dynamics of the two-well problem.

5.4 Symmetry considerations of generic Hamiltonian

The Hamiltonians (5.9) and (5.12) can be represented in the generic form

$$\hat{H} = -\hbar\delta\hat{L}_x + \hbar\kappa\hat{L}_z^2, \quad (5.19)$$

with $\hat{L}_x = (\hat{L}_+ + \hat{L}_-)/2$, $\hat{L}_z = \hat{L}_0$, where the operators \hat{L}_i represent \hat{J}_i or \hat{B}_i , depending on the commutation rules and the corresponding algebra that they obey. In the two-well case, the eigenstates $|\mu\rangle$ of the operator \hat{L}_z represent number states in the two-well case, with the eigenvalue μ half the number difference between the wells. In the diffraction case, the states $|\mu\rangle$ are momentum eigenstates. In this latter case, the coupling between neighboring momentum states is independent of μ [eq. (5.13)], whereas in the two-well case the μ dependence of

the hopping operator indicated in eq. (5.10) reflects the bosonic accumulation effect. A consequence of this is also that the Hamiltonian in the diffraction case couples an infinite number of states $|\mu\rangle$, whereas in the two-well case the number of coupled states has the finite value $N + 1$. In the diffraction case, we restrict ourselves to the situation that the Bragg condition is respected. Therefore, both in the diffraction case and in the two-well case μ attains either integer or half-integer values. The action of \hat{L}_z is the same in both cases.

Hamiltonian (5.19) is invariant for inversion of μ . In order to demonstrate this, we introduce the inversion operator \hat{P} , defined by the relation $\hat{P}|\mu\rangle = |-\mu\rangle$. In the diffraction case, the operator \hat{P} corresponds to inversion of momentum, which does not change the kinetic energy. In the two-well case, the operator \hat{P} represents interchanging the particle numbers in the two wells, which has no effect on the interparticle interaction. The commutation rules of the inversion operator with the operators \hat{L}_i are specified by $\hat{P}\hat{L}_z\hat{P} = -\hat{L}_z$, $\hat{P}\hat{L}_\pm\hat{P} = \hat{L}_\mp$, so that \hat{P} inverts \hat{L}_y and \hat{L}_z , and commutes with \hat{L}_x . It follows that Hamiltonian (5.19) commutes with \hat{P} , so that it is invariant for inversion of μ . Therefore, Hamiltonian has vanishing matrix elements between the even and the odd subspaces, which are the eigenspaces of \hat{P} with eigenvalue 1 and -1 , respectively. For half-integer μ values, these spaces are spanned by the states

$$|\mu\rangle_+ \equiv \frac{|\mu\rangle + |-\mu\rangle}{\sqrt{2}}; \quad |\mu\rangle_- \equiv \frac{|\mu\rangle - |-\mu\rangle}{\sqrt{2}}; \quad (5.20)$$

for positive values of μ . In the case of integer μ values, the state $|\mu = 0\rangle$ also belongs to the even subspace. The even and odd subspace evolve independently from one another. This symmetry property of H depends on the fact that it is quadratic in the operator \hat{L}_z .

The action of the quadratic term in Hamiltonian (5.19) on the new basis is simply given by the relation $\hat{L}_z^2|\mu\rangle_\pm = \mu^2|\mu\rangle_\pm$. The action of the coupling term in the Hamiltonian can be expressed in a general form by introducing coefficients F_μ for non-negative values of μ . In the case of the SU(2) algebra, we define $F_\mu = f_\mu$, whereas in the diffraction case we simply have $F_\mu = 1$. The matrix elements of \hat{L}_x can be fully expressed in terms of the coefficients F_μ for positive μ . Within the even or the odd subspace, the operator \hat{L}_x has off-diagonal matrix elements only between two states for which the values of μ differ by one, and we find

$$\pm \langle \mu + 1 | \hat{L}_x | \mu \rangle_\pm = \frac{1}{2} F_{\mu+1}, \quad (5.21)$$

provided that the value of μ is positive. These matrix elements coincide with those on the basis of the states $|\mu\rangle$. For the state $|\mu = 0\rangle$, which belongs to the even subspace of a manifold of states with integer μ values, the matrix element is

$$+ \langle 1 | \hat{L}_x | 0 \rangle = F_1 / \sqrt{2}. \quad (5.22)$$

On the other hand, in a manifold of states with half-integer μ values, \hat{L}_x has a single nonzero diagonal element for $\mu = 1/2$, that is given by

$$\pm \langle 1/2 | \hat{L}_x | 1/2 \rangle_\pm = \pm F_{1/2}. \quad (5.23)$$

Hence, in the case of half-integer μ values, the Hamiltonian projected on the even and the odd subspace differ exclusively in the diagonal matrix element for $\mu = \frac{1}{2}$, for which we find

$${}_{\pm} \langle 1/2 | \hat{H} | 1/2 \rangle_{\pm} = \frac{\hbar\kappa}{4} \mp \frac{1}{2} \hbar\delta F_{1/2}. \quad (5.24)$$

For integer values of μ , the Hamiltonian for the odd subspace is identical to the Hamiltonian for the even subspace with $\mu \gtrsim 1$. The only difference is that the even subspace also contains the state $|0\rangle$, which is coupled to the other states by the matrix element

$${}_+ \langle 1 | \hat{H} | 0 \rangle = \langle 0 | \hat{H} | 1 \rangle_+ = -\hbar\delta F_1 / \sqrt{2}. \quad (5.25)$$

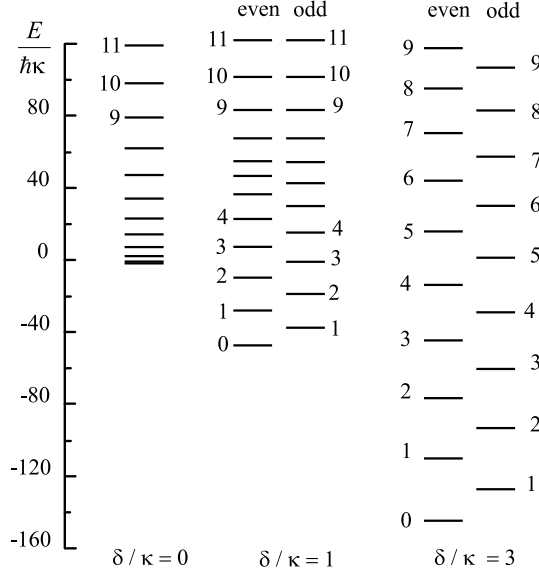
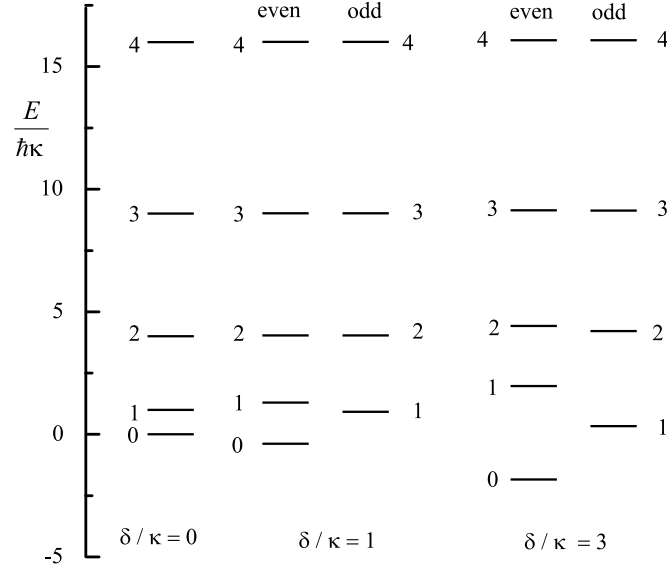


Figure 5.1: Energy levels in units of $\hbar\kappa$ for the double well with $N = 100$ particles, for various values of δ/κ . The levels are labeled by the quantum number μ .

In both cases, the difference between the Hamiltonian parts on the even and odd subspaces are proportional to δ . These differences are responsible for the energy splitting between the even and the odd energy eigenstates. Moreover, since these differences in the Hamiltonian parts occur for low values of μ , we expect that for a fixed value of δ/κ , the even-odd energy splittings decrease for increasing μ values. This is confirmed by numerical calculations. In Figs. 5.1 and 5.2, we display the energy levels of the Hamiltonian, for a few values of δ/κ , both for the double-well case (with $N = 100$), and for the diffraction case.

The energy levels are found to be alternatingly even and odd, with increasing energy. In the two-well case, the energy shifts and splittings due to the coupling are larger for the same value of δ/κ and the same value of μ . This arises from the factor F_μ , which is unity in the diffraction case, whereas in the two-well case it decreases from $\sim J = N/2$ at $\mu = 0$ to zero

Figure 5.2: Energy levels in units of $\hbar\kappa$ for the diffraction case, for various values of δ/κ .

at $\mu = J$. In fact, the condition for weak coupling is that matrix elements coupling the states $|\mu\rangle$ and $|\mu - 1\rangle$ are small compared with their unperturbed energy separation. This condition can be expressed as

$$\lambda_\mu = \frac{\delta}{2\kappa} \frac{F_\mu}{2\mu - 1} < 1. \quad (5.26)$$

This confirms that for a given value of δ/κ , the region of weakest coupling occurs for the highest values of μ . In the two-well case, the lowest-energy states start out to be nearly equidistant for low μ values as long as λ_μ is large.

5.5 Pendellösung oscillations

The energy splittings between the even and the odd eigenstates give rise to time-dependent states that oscillate between the states $|\pm\mu\rangle$. In the diffraction case, they correspond to the well-known Pendellösung oscillations in the Bragg regime. Here we show that similar oscillations can occur for the two-well problem, and we give an analytical estimation of the oscillation frequencies. For the generic Hamiltonian given by eq. (5.19), the Bragg condition is fulfilled when inequality (5.26) holds.

The energy differences between the even and odd states to lowest order in λ_μ can be found from the effective Hamiltonian for two degenerate states that are coupled via a number of nonresonant intermediate states. This situation occurs for the states $|\pm\mu\rangle$, with their $2\mu - 1$ intermediate states. In this case, the intermediate states can be eliminated adiabatically, as

demonstrated in Sec. 18.7 of ref. [81]. The resulting effective Hamiltonian for these two states $|\pm\mu\rangle$ has an off-diagonal element that is the ratio between two products. The numerator contains the product of the successive 2μ matrix elements $-\hbar\delta F_{\mu'}/2$ of the Hamiltonian coupling neighboring states, and the denominator is the product of the $2\mu - 1$ unperturbed energy differences of the degenerate states $|\pm\mu\rangle$ with the successive intermediate states. In the diffraction case, this result coincides with the calculation given in ref. [79], which was obtained by diagonalizing a tridiagonal matrix and keeping only the lowest order in δ/κ .

Generalizing this result to the present case of the two states $|\pm\mu\rangle$, we find that the effective Hamiltonian has the diagonal element

$$\langle \pm\mu | \hat{H}_{eff} | \pm\mu \rangle = \hbar\kappa\mu^2, \quad (5.27)$$

and the off-diagonal element

$$\langle \mp\mu | \hat{H}_{eff} | \pm\mu \rangle = -\hbar\Omega_\mu/2, \quad (5.28)$$

with Ω_μ an effective oscillation frequency given by

$$\Omega_\mu = (-1)^{2\mu+1} \frac{1}{2^{2\mu-1}} \frac{\delta^{2\mu}}{\kappa^{2\mu-1}} \frac{1}{[(2\mu-1)!]^2} F. \quad (5.29)$$

The factor F is just the product of the coefficients F_μ successively coupling the states intermediate between $|\mu\rangle$ and $|- \mu\rangle$. In the diffraction case, we simply have $F = 1$, whereas in the case of SU(2) symmetry, applying to the double well, we find

$$F = \frac{(J + \mu)!}{(J - \mu)!}. \quad (5.30)$$

These expressions are valid both for integer and half-integer values of μ . The eigenstates of the effective Hamiltonian are the even and odd states, and the eigenvalue equations are $\hat{H}_{eff} |\mu\rangle_\pm = (\hbar\kappa\mu^2 \mp \hbar\Omega_\mu/2) |\mu\rangle_\pm$. For integer values of μ , the frequency Ω_μ is negative, so that the even states $|\mu\rangle_+$ are shifted upwards and the odd states are shifted downwards in energy. The opposite is true for half-integer values of μ . In both cases, the ground state is even, and the energy eigenstates for increasing energy are alternatingly even and odd. In view of the results of the numerical calculation mentioned above, one may expect that this alternating behavior of the even and odd eigenstates is valid for all finite values of the ratio δ/κ . It is interesting to notice that in the special case that $\mu = J \equiv N/2$, eq. (5.29) for the two-well case coincides with the ground-state energy splitting of two coupled quantum anharmonic oscillators, which model two coupled vibrational degrees of freedom in a molecule [83].

For an initial state $|\mu\rangle$, the effective Hamiltonian \hat{H}_{eff} leads to a time-dependent state that is given by eq. (5.17), apart from an irrelevant overall phase factor. This shows that the oscillating solution (5.17) corresponding to the Bragg regime of diffraction can be generalized to the case of a condensate in a double well. The same expression (5.17) remains valid, while the oscillation frequency Ω_μ is determined by eqs. (5.29) and (5.30). This describes a state of the condensate atoms in the double well in the weak-coupling limit. In this case, the state oscillates between the Fock states $|n_1, n_2\rangle = |N/2 + \mu, N/2 - \mu\rangle$ and $|n_1, n_2\rangle = |N/2 - \mu, N/2 + \mu\rangle$.

Obviously, when the initial state is given by $|\mu\rangle_{\pm}$, the system is in a stationary state, and no oscillations occur. In this case, Pendellösung oscillations can still be induced by including in the Hamiltonian a term that is linear in \hat{L}_z . In the diffraction case, there is no obvious physical realization of such a term. For the Wannier-Stark system, where the quadratic term in \hat{L}_z^2 is absent, the linear term can be realized by imposing a uniform force, which gives rise to Bloch oscillations [25, 26] and Chapter 2. In the case of the BEC in a double well, a term $\hbar\xi\hat{L}_z$ in the Hamiltonian can be realized by imposing an energy difference $\hbar\xi$ between the single-particle ground states in the two wells. When this term is periodically varying, it can be used for coherent control of the condensate [84]. The additional term couples the even and odd subspaces, thereby breaking the symmetry of the Hamiltonian. On the basis of the states $|\mu\rangle_{\pm}$, the effective Hamiltonian attains the off-diagonal element

$$\pm \langle \mu | \hat{H}_{eff} | \mu \rangle_{\mp} = \hbar\xi\mu/2. \quad (5.31)$$

When we assume that both δ and ξ are small compared with the splitting due to the inter-particle interaction κ , so that we remain in the Bragg regime, the two states $|\pm\mu\rangle$ remain decoupled from the other number states, and we have an effective two-state system. In practice, the parameter ξ can be easily controlled, so that many effects of two-state atoms [45] can also be realized for these two states. For example, in analogy to the excitation of ground-state by an adiabatic sweep across the resonance, one could create an effective transfer from the state $|\mu\rangle$ to the state $|- \mu\rangle$ by varying the parameter ξ adiabatically from a positive to a negative value that is large compared to Ω_{μ} . This gives an effective collective transfer of $n = 2\mu$ atoms from one well to the other one.

5.6 Time-dependent coupling

When the coupling $\delta(t)$ varies with time, the time-dependent eigenstates of the Hamiltonian are coupled to each other. The eigenstate that correlates in the limit $\delta \rightarrow 0$ to the state $|\mu\rangle_{\pm}$ is denoted as $|\varphi_{\mu}^{\pm}\rangle$. Note that even eigenstates are only coupled to other even eigenstates, and odd eigenstates to odd eigenstates. The coupling results from the time dependence of the eigenstates. In fact, the term in the Schrödinger equation coupling $|\varphi_{\mu}^{\pm}\rangle$ to $|\varphi_{\nu}^{\pm}\rangle$ is proportional to

$$\langle \varphi_{\nu}^{\pm} | (t) | \frac{d}{dt} | \varphi_{\mu}^{\pm}(t) \rangle = - \langle \varphi_{\nu}^{\pm} | (t) | \hat{L}_x | \varphi_{\mu}^{\pm}(t) \rangle \frac{\hbar \dot{\delta}(t)}{E_{\nu}^{\pm} - E_{\mu}^{\pm}}; \mu \neq \nu. \quad (5.32)$$

This coupling is ineffective in the case that the r.h.s. of eq. (5.32) is small compared with $(E_{\nu}^{\pm} - E_{\mu}^{\pm})/\hbar$. In this case, an initial eigenstate remains an eigenstate at all times. This is the standard case of adiabatic following, which has been discussed in the diffraction case [80]. Since within the even or the odd subspace there are no degeneracies, the dynamics of adiabatic following is particularly simple. When the coupling coefficient δ is smoothly switched on, with the system initially in the state $|\mu\rangle = (|\mu\rangle_{+} + |\mu\rangle_{-})/\sqrt{2}$, the time-dependent state is obviously

$$|\Psi(t)\rangle = e^{-i\vartheta(t)} \left(|\varphi_{\mu}^{+}\rangle e^{-i\eta(t)/2} + |\varphi_{\mu}^{-}\rangle e^{i\eta(t)/2} \right) / \sqrt{2}, \quad (5.33)$$

with $\vartheta(t) = \int^t dt' (E_\mu^+(t') + E_\mu^-(t')) / 2\hbar$ the average phase and

$$\eta(t) = \int^t dt' [E_\mu^+(t') - E_\mu^-(t')] / \hbar, \quad (5.34)$$

the accumulated phase difference of the two eigenstates.

In a time interval that the coupling δ is constant, the phase difference $\eta(t)$ increases linearly with time, and state (5.33) gives rise to expectation values oscillating at the single frequency $[E_\mu^+(t') - E_\mu^-(t')] / \hbar$. When the coupling is switched off again, the phase difference approaches a constant limiting value $\bar{\eta} = \eta(\infty)$.

State (5.33) at later times corresponds to a linear superposition of the states $|\pm\mu\rangle$ proportional to $|\mu\rangle \cos(\bar{\eta}/2) + |-\mu\rangle \sin(\bar{\eta}/2)$. Again, as we see, this effect that is known in the diffraction case also has a counterpart for the double-well problem, where adiabatic switching of the coupling between the wells leads to a linear superposition of the Fock states $|n_1, n_2\rangle = |N/2 + \mu, N/2 - \mu\rangle$ and $|n_1, n_2\rangle = |N/2 - \mu, N/2 + \mu\rangle$. By proper tailoring of the pulse, the final state can be made to coincide with either one of these Fock states, with the even state $|\mu\rangle_+$ or with the odd state $|\mu\rangle_-$, depending on the precise value of the accumulated phase difference $\bar{\eta}$, which in turn is determined by the energy difference $E_\mu^+ - E_\mu^-$ between the even and the odd eigenstate. In Fig. 5.3, we plot this energy difference in the two-well case, for $N = 100$, and for a few values of δ/κ . This shows that these splittings decrease monotonously for increasing quantum number μ . When δ/κ is not small, the decrease starts out to be slow, and then falls rapidly to zero.

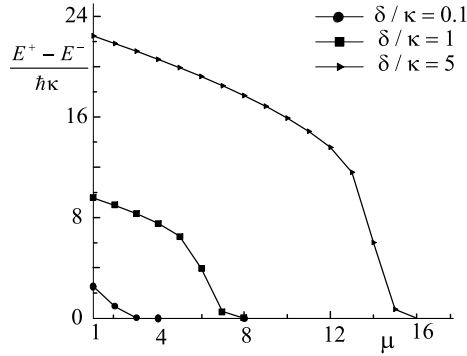


Figure 5.3: Even-odd energy splittings for the double well as a function of the quantum number μ , for various values of δ/κ and for $N = 100$ particles.

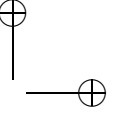
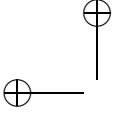
In contrast, when the coupling term $\delta(t)$ has the form of a short pulse around time zero, such that the action of the quadratic term can be neglected during the pulse, the initial state $|\mu\rangle$ couples to all other states $|\mu'\rangle$. The state vector has exactly the same form (5.16) as for diffraction in the Raman-Nath regime. For the two-well problem, the evolution operator takes the form $\hat{U} = \exp(i\phi\hat{L}_x)$ with $\phi = \int dt\delta(t)$, which has matrix elements that can be expressed in the Wigner rotation matrices [85] by

$$\langle\mu'|\hat{U}|\mu\rangle = i^{\mu'-\mu} d_{\mu'\mu}^J(\phi), \quad (5.35)$$

with $J = N/2$. A comparison with Eq. (5.15) shows that for the two-well-problem, the Wigner functions play the same role as the Bessel functions in the diffraction case.

5.7 Conclusions

In this paper, we have analyzed both the similarity and the difference between the dynamical behavior of atom diffraction from a standing wave and a Bose-Einstein condensate in a double-well potential. In both cases, the Hamiltonian is given by the generic form (5.19), the only difference being in the commutation rules for the operators \hat{L}_i with $i = x, y, z$. Well-known diffraction phenomena as *Pendellösung* oscillations between opposite momenta in the case of Bragg diffraction, and the result of adiabatic transitions between momentum states have counterparts in the behavior of the atom distribution over the two wells, in the case that the coupling between the wells is weak compared to the interatomic interaction or slowly varying with time. A common underlying reason for these effects is the symmetry of the Hamiltonian for inversion $\mu \leftrightarrow -\mu$, and the energy splitting between even and odd states arising from the coupling term. In these cases, effective coupling occurs between the states $|n_1, n_2\rangle$ and $|n_2, n_1\rangle$ with opposite imbalance between the particle numbers in the two wells. These states are coupled without population of the intermediate states, so that a number of $n_1 - n_2$ particles oscillate collectively between the two wells. The interparticle interaction is essential for this effect to occur. A simple analytical expression is obtained for the *Pendellösung* frequency. An initial state $|n_1, n_2\rangle$ with a well-determined number of atoms in each well can be transferred to a linear superposition of $|n_1, n_2\rangle$ and $|n_2, n_1\rangle$, which is a highly entangled state of the two wells. A similar analogy is obtained to diffraction in the Raman-Nath regime. For the double-well problem this requires that the coupling is sufficiently short to ignore dynamical effect of the atomic interaction during the coupling. The well-known diffraction pattern in terms of the Bessel function is replaced by elements of the Wigner rotation matrix for the double well. These effects do not show up in the mean-field approximation, where the Gross-Pitaevski equation holds.



Chapter 6

Resonances for coupled Bose-Einstein Condensates

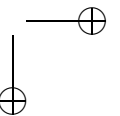
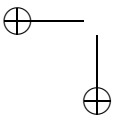
We study some effects arising from periodic modulation of the asymmetry and the barrier height of a two-well potential containing a Bose-Einstein condensate. At certain modulation frequencies the system exhibits resonances, which may lead to enhancement of the tunneling rate between the wells and which can be used to control the particle distribution among the wells. Some of the effects predicted for a two-well system can be carried over to the case of a Bose-Einstein condensate in an optical lattice.

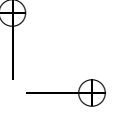
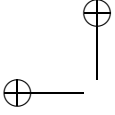
6.1 Introduction

Since the experimental realization of Bose-Einstein condensates (BEC) one has considered the possibility of extending one-mode models to two or more modes [69, 70]. This raises the issue of the relative phase between modes. As indicated by several authors [74, 86], a two-well BEC may exhibit features that are not covered by the semiclassical description in terms of the Gross-Pitaevski equation. These features are significant at low particle numbers and for strong interactions. In previous work, we discussed some aspects of the dynamics of a two-well BEC in the strong-interaction regime Chapter 5. This is close to the experimental situation for a BEC in a double-well trap, designed in Ref. [78].

A sensitive way to probe the properties of a BEC in a double-well potential with strong interatomic interactions is to look for resonant behavior when a parameter of the system is periodically modulated. The response of the system may be expected to be very sensitive to the value of the modulation frequency in the neighborhood of a resonance. A periodic perturbation can be implemented in various ways. One example would be periodically modulating the trapping potential. Salmond et al [75] study a numerical model of a double-well potential with periodically modulated coupling between the wells. This semiclassical analysis reveals the existence of uncoupled regions with chaotic and regular motion. The inclusion of the quantum nature of the evolution leads to transitions between these regions. Another type of periodic perturbation can be imposed by periodically modulating the energy difference between the ground states in the two wells.

Periodic modulations are known to give rise to dynamical localization in some cases. This effect has been widely discussed in the literature in the case a particle in a periodic potential, such as an electron in a crystal or an atom in an optical lattice [87] and Chapter 2. When the particle also feels a uniform force in addition to the lattice potential (a tilted optical lattice), it





is found to have an infinite discrete set of equidistant energy levels, with a level separation that is determined by the strength of the uniform force Chapter 2. A variation of the magnitude of the uniform force affects the phase of the state. So, when this magnitude is periodically modulated, resonances may be expected. The population in one well is described by adding the amplitudes for arriving at this well from various other wells, each one with a different phase shift. In the long time limit, when the time of observation is long compared to the period of the modulation, this gives rise to destructive interference, leading to a suppression of the net tunneling rate. Hence, the asymptotic distribution over the wells coincides with the initial one, and dynamical localization has been realized.

Another example of dynamical localization arises for a single two-level atom in a driving field with a periodically modulated detuning [88]. For certain ratios of the modulation frequency and the strength of the field, the atom is localized in its ground state. The time scale is restricted by the modulation frequency.

In the present case of a BEC in a two-well potential with a fixed total number of atoms, the state space is finite dimensional. In the $SU(2)$ representation of the operator algebra, the Hamiltonian has a quadratic term due to the interatomic interactions. So, in this sense the system is quite different from that of an atom in a tilted lattice, with its infinite number of states and a Hamiltonian that is linear in the $SU(2)$ operators. Still, there are some obvious similarities: the discrete structure of the energy and the presence of interatomic interactions and tunneling between wells as competing processes. Therefore, we expect interesting effects also in the two-well case when the energy difference or the hopping between wells is periodically modulated. From a formal point of view, the analysis in the present paper may be regarded as a generalization of the process of dynamical localization for the Hamiltonian with a quadratic term. Specifically, this paper considers the possibilities of coherent control of a BEC in a double-well potential by using any kind of time-periodic perturbation.

6.2 BEC in a double potential well

We describe a BEC in a double potential well in terms of a one-particle Hamiltonian $H^{(1)}$ and a two-particle interaction $U(\vec{r}, \vec{r}')$. The states $|1\rangle$ and $|2\rangle$ are the localized ground states in either well, with wave functions $\psi_1(\vec{r})$ and $\psi_2(\vec{r})$. On the basis of the states $|1\rangle$ and $|2\rangle$, the one-particle Hamiltonian has the matrix elements

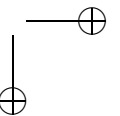
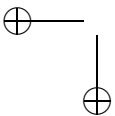
$$\langle 1 | H^{(1)} | 1 \rangle = -\langle 2 | H^{(1)} | 2 \rangle = \hbar\varepsilon/2, \quad \langle 1 | H^{(1)} | 2 \rangle = \langle 2 | H^{(1)} | 1 \rangle = -\hbar\delta/2. \quad (6.1)$$

In the case that $\varepsilon = 0$, the coupling between the wells lifts their degeneracy, and creates an energy splitting $\hbar\delta$ between the even ground state $|g\rangle$ and the odd excited state $|e\rangle$, defined by

$$|g\rangle = \frac{1}{\sqrt{2}}(|1\rangle + |2\rangle); \quad |e\rangle = \frac{1}{\sqrt{2}}(|1\rangle - |2\rangle). \quad (6.2)$$

When we restrict ourselves to these two states, the field operator in second quantization has the standard form

$$\hat{\Psi}(\vec{r}) = \hat{a}_1\psi_1(\vec{r}) + \hat{a}_2\psi_2(\vec{r}), \quad (6.3)$$



with \hat{a}_i the one-particle annihilation operator in the two states, which together with the corresponding creation operators obey the bosonic commutation rules. When we substitute this expression in the formal expression

$$\hat{H} = \int d\vec{r} \hat{\Psi}^\dagger(\vec{r}) H^{(1)} \hat{\Psi}(\vec{r}) + \frac{1}{2} \int d\vec{r} d\vec{r}' \hat{\Psi}^\dagger(\vec{r}) \hat{\Psi}^\dagger(\vec{r}') U(\vec{r}, \vec{r}') \hat{\Psi}(\vec{r}) \hat{\Psi}(\vec{r}'). \quad (6.4)$$

for the second-quantized Hamiltonian, we find

$$\hat{H} = \sum_{i,k} \hbar \langle i | H^{(1)} | k \rangle \hat{a}_i^\dagger \hat{a}_k + \frac{1}{2} \sum_{i,k,l,m} \hbar \langle i, k | U | l, m \rangle \kappa_{i,k,l,m} \hat{a}_i^\dagger \hat{a}_k^\dagger \hat{a}_l \hat{a}_m, \quad (6.5)$$

where the indices $i, j, k, l = 1$ or 2 , and the matrix elements are taken between the states ψ_1 and ψ_2 .

At sufficiently low energy, the two particle interaction is well approximated by the contact potential $U(\vec{r}, \vec{r}') = (4\pi\hbar^2 a/m)\delta(\vec{r} - \vec{r}')$, with a the scattering length. The function ψ_1 and ψ_2 states have the same form, and we assume that they do not overlap. So we obtain the following expression for the Hamiltonian

$$\hat{H} = \frac{\hbar\varepsilon}{2} (\hat{a}_1^\dagger \hat{a}_1 - \hat{a}_2^\dagger \hat{a}_2) - \frac{\hbar\delta}{2} (\hat{a}_1^\dagger \hat{a}_2 + \hat{a}_2^\dagger \hat{a}_1) + \frac{\hbar\kappa}{2} (\hat{a}_1^\dagger \hat{a}_1^\dagger \hat{a}_1 \hat{a}_1 + \hat{a}_2^\dagger \hat{a}_2^\dagger \hat{a}_2 \hat{a}_2). \quad (6.6)$$

where the parameter κ defined by

$$\hbar\kappa = \frac{4\pi\hbar^2 a}{m} \int d\vec{r} |\psi_1(\vec{r})|^4 \quad (6.7)$$

measures the strength of the interatomic interaction.

For convenience we express the Hamiltonian (6.6) in terms of SU(2) operators by applying the standard Schwinger representation of two modes. This leads to the definition

$$\hat{J}_z = \frac{1}{2} (\hat{a}_1^\dagger \hat{a}_1 - \hat{a}_2^\dagger \hat{a}_2), \quad \hat{J}_+ = \hat{a}_1^\dagger \hat{a}_2, \quad \hat{J}_- = \hat{a}_2^\dagger \hat{a}_1. \quad (6.8)$$

These operators are related to the Cartesian components of a fictitious angular momentum by the standard relations $\hat{J}_\pm = \hat{J}_x \pm i\hat{J}_y$. They obey the commutation rules for angular momentum operators

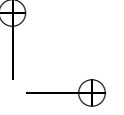
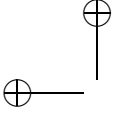
$$[\hat{J}_z, \hat{J}_\pm] = \pm \hat{J}_\pm, \quad [\hat{J}_+, \hat{J}_-] = 2\hat{J}_z, \quad (6.9)$$

which generate the SU(2) algebra. These operators commute with the operator for the total number of particles $\hat{N} = \hat{a}_1^\dagger \hat{a}_1 + \hat{a}_2^\dagger \hat{a}_2$. The Hamiltonian (6.6) can be rewritten in the form

$$\hat{H} = \hat{H}_N + \frac{\hbar\kappa}{4} (\hat{N}^2 - 2\hat{N}), \quad (6.10)$$

where the N -particle Hamiltonian \hat{H}_N is defined by

$$\hat{H}_N = \hbar\varepsilon \hat{J}_z - \hbar\delta \hat{J}_x + \hbar\kappa \hat{J}_z^2. \quad (6.11)$$



For a given number of particles N , the last term in Eq. (6.10) is a constant, and it suffices to consider the dynamics of the subspace of the $N + 1$ number states $|n, N - n\rangle$, with $n = 0, 1, \dots, N$, with n particles in well 1, and $N - n$ particles in well 2. This subspace has the structure of the angular momentum states, with $J = N/2$, and the $2J + 1$ magnetic quantum numbers $\mu = n - N/2$, with $\mu = -J, -J + 1, \dots, J$. Note that μ is half the difference of the particle number in two wells. For a given particle number N we represent the number states by the quantum number μ , so that $|\mu\rangle \equiv |n, N - n\rangle$. The action of the operators \hat{J}_0 and \hat{J}_\pm on the Fock states has the well-known behavior

$$\hat{J}_z |\mu\rangle = \mu |\mu\rangle, \quad \hat{J}_\pm |\mu\rangle = \sqrt{(J \mp \mu)(J \pm \mu + 1)} |\mu \pm 1\rangle. \quad (6.12)$$

This also determines the action of the Cartesian operators \hat{J}_x and \hat{J}_y .

6.3 Quantum states in two wells

The Schwinger representation of the operators occurring in the Hamiltonian suggests in a natural way various possible choices of states of N atoms in the two wells. Arecchi et al [89] introduced the spin coherent states (SCS) [90], in analogy to the Glauber coherent state of a mode of the quantum radiation field. The SCS follow from applying an arbitrary rotation to the state $|\mu\rangle$ with $\mu = J$. As rotation operator we take

$$\hat{R}(\theta, \phi) = \exp(-i\phi\hat{J}_z) \exp(-i\theta\hat{J}_y) \exp(i\phi\hat{J}_z) = \exp[-i\theta(\hat{J}_y \cos \phi - \hat{J}_x \sin \phi)], \quad (6.13)$$

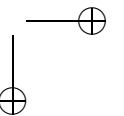
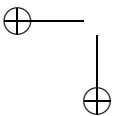
which represents a rotation over an angle θ , around an axis in the xy -plane, specified by the angle ϕ with the y -axis. The SCS $|\theta, \phi; J\rangle$ is

$$|\theta, \phi; J\rangle = \hat{R}(\theta, \phi) |J\rangle \quad (6.14)$$

which is also the eigenstate with eigenvalue J of the component $\vec{u} \cdot \hat{\vec{J}}$ of the angular-momentum vector in the direction \vec{u} specified by the polar angle θ and the azimuthal angle ϕ . Just as the Glauber coherent states of a mode with annihilation operator \hat{c} can be obtained by acting with a displacement operator $\hat{D}(\zeta) = \exp(\zeta\hat{c}^\dagger - \zeta^*\hat{c})$ on the vacuum state, the SCS follows by a rotation $\hat{R}(\theta, \phi) = \exp(\zeta\hat{J}_- - \zeta^*\hat{J}_+)$ with $\zeta = (\theta/2) \exp(i\phi)$, acting on the state $|J\rangle$. When we view this state $|J\rangle$ as the ground state, the operator \hat{J}_+ is analogous to the annihilation operator, since $\hat{J}_+ |J\rangle = 0$. An essential difference between the two cases is, of course, that the state space of a radiation mode has infinite dimensions, while the dimension of the angular-momentum state space is $2J + 1$.

In our case, the analogy is carried one step further, since the SCS defined by (6.14) do not represent angular-momentum states, but refer to the states of N atoms, distributed over two potential wells. The ground state $|J\rangle$ represents the state with all particles in the first well. When we substitute the identity $|J\rangle = (\hat{a}_1^\dagger)^N |vac\rangle / \sqrt{N!}$ with $N = 2J$ into the right-hand side of (6.14), we obtain an expression for the SCS in the language of the two wells, in the form

$$|\theta, \phi; J\rangle = \frac{1}{\sqrt{N!}} \left(\cos \frac{\theta}{2} \hat{a}_1^\dagger + e^{i\phi} \sin \frac{\theta}{2} \hat{a}_2^\dagger \right)^N |vac\rangle. \quad (6.15)$$



We can interpret (6.15) as a state with N atoms in the one-particle superposition state

$$\cos \frac{\theta}{2} |1\rangle + e^{i\phi} \sin \frac{\theta}{2} |2\rangle$$

of the two wells. A special case arises for $\theta = \pi/2$, when the average populations of the two wells are the same. Then the state (6.15) describes a collective mode from two interfering sources of equal intensity, and its expansion in number states is given by

$$|\pi/2, \phi; J\rangle = \frac{1}{2^{N/2}} \sum_{n=0}^N \binom{N}{n}^{1/2} e^{i(N-n)\phi} |n, N-n\rangle \quad (6.16)$$

Such a state can be considered as a state with a well-defined phase difference ϕ . The atom distribution over the two wells is binomial, and they have been termed phase states (PS) of a two-mode boson system in Ref. [91]. For simplicity, we suppress the value $\pi/2$ in this case, and we simply denote the PS as $|\phi; J\rangle$. Upon rotation around the z -axis, a PS transforms as

$$\exp(-i\alpha \hat{J}_z) |\phi; J\rangle = \exp(-i\alpha J) |\phi + \alpha; J\rangle \quad (6.17)$$

The concept of Glauber coherent states of a radiation mode has been generalized by de Oliveira et al [92], who introduced so called displaced coherent states defining them as a displaced number state, rather than a displaced vacuum state. The corresponding generalization of a SCS is found when the rotation operator (6.13) acts on a number state $|\mu\rangle$. The resulting displaced spin coherent states (DSCS) are

$$|\theta, \phi; \mu\rangle = \hat{R}(\theta, \phi) |\mu\rangle. \quad (6.18)$$

They are the eigenstates of the angular-momentum component $\vec{u} \cdot \hat{\vec{J}}$ with eigenvalue μ . In the special case that $\theta = \pi/2$ and $\phi = 0$, we find that $\hat{R}(\theta, \phi) = \exp(-i\pi \hat{J}_y/2)$, and this component is simply \hat{J}_x . Its eigenstates are denoted as

$$|\pi/2, 0; \mu\rangle = |\mu\rangle_x.$$

and they obey the eigenvalue relation $\hat{J}_x |\mu\rangle_x = \mu |\mu\rangle_x$. The state $|\mu\rangle_x$ describes a state with $J + \mu$ atoms in the even state $|g\rangle$, and $J - \mu$ atoms in the odd state $|e\rangle$. These states are coupled by the ladder operators

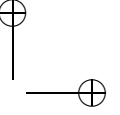
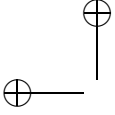
$$\hat{J}_x^\pm \equiv \exp(-i\pi \hat{J}_y/2) \hat{J}_\pm \exp(i\pi \hat{J}_y/2) = -\hat{J}_z \pm i\hat{J}_y, \quad (6.19)$$

according to the relations

$$\hat{J}_x^\pm |\mu\rangle_x = \sqrt{(J \mp \mu)(J \pm \mu + 1)} |\mu \pm 1\rangle_x.$$

When $\theta = \pi/2$ and $\phi = \pi/2$, the DSCS are indicated as

$$|\pi/2, \pi/2; \mu\rangle = |\mu\rangle_y,$$



which are eigenstates of $\vec{u} \cdot \hat{\vec{J}} = \hat{J}_y$, as specified by the relation $\hat{J}_y |\mu\rangle_y = \mu |\mu\rangle_y$. The corresponding ladder operators are

$$\hat{J}_y^\pm \equiv \exp(i\pi \hat{J}_x/2) \hat{J}_\pm \exp(-i\pi \hat{J}_x/2) = \hat{J}_x \mp i\hat{J}_z. \quad (6.20)$$

In the special case that $\mu = J$, the DSCS $|\mu\rangle_x$ and $|\mu\rangle_y$ become the SCS $|J\rangle_x$ and $|J\rangle_y$, which are also the PS with $\phi = 0$ and $\phi = \pi/2$, respectively.

6.4 Evolution in limiting cases

For a given number N of atoms, the evolution is characterized by an evolution operator that is governed by the Hamiltonian (6.11), and that obeys the Schrödinger equation

$$i\hbar \frac{d\hat{U}}{dt} = \hat{H}_N \hat{U}. \quad (6.21)$$

In order to get an intuitive insight into the evolution, we first consider two extreme cases, which are simple to understand. We assume that the two wells have equal energy, so that $\varepsilon = 0$. If the interatomic interactions are negligible, the quadratic term in (6.11) can be skipped. For a possibly time-dependent coupling strength δ , the evolution operator is

$$\hat{U}(t) = \exp\left(i\eta(t) \hat{J}_x\right), \quad (6.22)$$

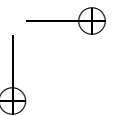
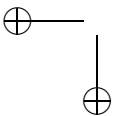
with $\eta(t) = \int_0^t \delta(t') dt'$ the area of the coupling pulse. In the language of angular momentum, \hat{U} represent a rotation over an angle $-\eta$ around the x -axis. In this case, the states $|\mu\rangle_x$ are eigenstates of the evolution operator, so that these states acquire only a phase factor $\exp(i\eta(t)\mu)$. An initial state in the form of a single number state $|\mu\rangle$ state gets rotated by the operator (6.22) and evolves into a superposition of number states. At the instant that $\eta(t) = \pi/2$ an initial number state has evolved into an eigenstate of the operator \hat{J}_y .

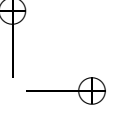
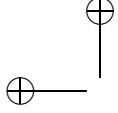
Conversely, when the interatomic interactions are strong enough on the scale of tunneling, the hopping between the wells can get suppressed Chapter 5. Now, a single number state $|\mu\rangle$ only acquires a phase factor $\exp(-i\kappa\mu^2 t)$. The evolution operator takes the form

$$\hat{U}(t) = e^{-i\kappa \hat{J}_z^2 t}, \quad (6.23)$$

which cannot be conceived as a rotation in the angular-momentum space. Since the eigenvalues of \hat{J}_z^2 are discrete, the evolution (6.23) has revivals. First we consider the situation that the number of particles N is even, so that the eigenvalues μ of \hat{J}_z are integer. Then the eigenvalues of \hat{U} are $\exp(-i\kappa\mu^2 t) = 1$ when $t = mT$, with m an integer, and $T = 2\pi/\kappa$. At these times the initial state is reproduced, which proves that the evolution of any initial state is time periodic, with period T . For a time $t = T/2$, which is half the period, the eigenvalues of $\hat{U}(T/2)$ are $\exp(-i\pi\mu^2) = (-1)^\mu$, which proves that the evolution operator at this instant is equal to

$$\hat{U}(T/2) = \exp(-i\pi \hat{J}_z).$$





For an initial PS $|\Psi(0)\rangle = |\phi; J\rangle$, we find that the state at the time $t = T/2$ is

$$|\Psi(T/2)\rangle = \exp(-i\pi J) |\phi + \pi; J\rangle,$$

which is just the opposite PS. At other instants of time, that are a simple rational fraction of T , an initial PS can be transformed into a linear combination of a few PS. For $t = T/4$, the relevant eigenvalues of \hat{U} can be rewritten as

$$\exp(-i\pi\mu^2/2) = \frac{1}{\sqrt{2}} \left(e^{-i\pi/4} + \exp(-i\pi\hat{J}_z) e^{i\pi/4} \right).$$

The corresponding expression for the evolution operator is then

$$\hat{U}(T/4) = \frac{1}{\sqrt{2}} \left[e^{-i\pi/4} + e^{i\pi/4} \exp(-i\pi\hat{J}_z) \right].$$

For the same initial state $|\Psi(0)\rangle = |\phi; J\rangle$, we apply Eq. (6.17), and arrive at the result for the state at $t = T/4$

$$|\Psi(T/4)\rangle = \frac{1}{\sqrt{2}} \left[e^{-i\pi/4} |\phi; J\rangle + e^{i\pi/4} e^{-i\pi J} |\phi + \pi; J\rangle \right], \quad (6.24)$$

which is the linear superposition of two PS's. For times t that are equal to other simple rational fractions of the period T ($t = T/3, T/5, \dots$) a superposition of more PS's is found. One may use the fact that the eigenvalues $\exp(-i\kappa\mu^2 t)$ of \hat{U} are periodic in μ with some integer period p . Therefore these eigenvalues can be expressed as a finite Fourier series in powers of $\exp(2\pi i\mu/p)$, which is equivalent to expressing the evolution operator $\hat{U}(t)$ as a finite sum of rotations around the z -axis.

When the number N of particles is odd, so that the values of J and μ are half-integer, full revival of the initial state is again found after one period $t = T$. In fact, since 2μ is an odd number, $(4\mu^2 - 1)/4$ is always an even integer, and it follows that both at time T and $T/2$, the evolution operator is just a phase factor

$$\hat{U}(T) = \exp(-i\pi/2), \hat{U}(T/2) = \exp(-i\pi/4).$$

Hence, apart from a phase factor, full revival is found already at half the time T . In order to obtain the evolution operator at the time $t = T/4$, it is convenient to use the identity for half integer values of μ

$$\exp(-i\pi\mu^2/2) = \frac{1}{\sqrt{2}} e^{-i\pi/8} \left(e^{i\pi\mu/2} + e^{-i\pi\mu/2} \right).$$

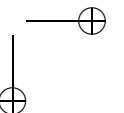
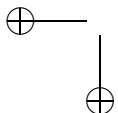
For the evolution operator this gives the expression

$$\hat{U}(T/4) = \frac{1}{\sqrt{2}} e^{-i\pi/8} \left[\exp(i\pi\hat{J}_z/2) + \exp(-i\pi\hat{J}_z/2) \right].$$

For the initial PS $|\Psi(0)\rangle = |\phi; J\rangle$, we obtain for the state vector at time $T/4$

$$|\Psi(T/4)\rangle = \frac{1}{\sqrt{2}} e^{-i\pi/8} \left[e^{i\pi J/2} |\phi - \pi/2; J\rangle + e^{-i\pi J/2} |\phi + \pi/2; J\rangle \right].$$

Revivals of the state of a BEC have been observed in an optical lattice [16].



6.5 Periodic modulation of energy difference

A simple example of a periodic modulation of the two-well system is to include a time-varying energy difference between the two wells. This is realized by substituting in the N -particle Hamiltonian (6.11) the harmonically varying parameter $\varepsilon(t) = \varepsilon_1 \cos \omega t$, while δ and κ remain constant. It is convenient to describe the evolution in an interaction picture that removes the diagonal terms in the Hamiltonian. We introduce the transformed state vector $|\Psi'(t)\rangle$ by the relation

$$|\Psi(t)\rangle = \hat{T}(t) |\Psi'(t)\rangle, \quad (6.25)$$

where the state vector $|\Psi(t)\rangle$ obeys the Schrödinger equation with the Hamiltonian (6.11), and the transformation operator $\hat{T}(t)$ is defined by

$$\hat{T}(t) = \exp \left[-i\theta(t) \hat{J}_z - i\kappa t \hat{J}_z^2 \right], \quad (6.26)$$

with $\theta(t) = \int_0^t dt' \varepsilon(t') = \varepsilon_1 (\sin \omega t) / \omega$. Notice that the transformed state $|\Psi'(t)\rangle$ has the same distribution over the number states $|\mu\rangle$ as the actual state $|\Psi(t)\rangle$. The transformed Schrödinger equation has the standard form

$$i\hbar \frac{d}{dt} |\Psi'(t)\rangle = \hat{H}'(t) |\Psi'(t)\rangle. \quad (6.27)$$

An explicit form of the transformed Hamiltonian

$$\hat{H}'(t) = -\hbar\delta \hat{T}^\dagger(t) \hat{J}_x \hat{T}(t) \quad (6.28)$$

follows from the general transformation rule [93]

$$f(\hat{J}_z) \hat{J}_+ = \hat{J}_+ f(\hat{J}_z + 1). \quad (6.29)$$

This relation (6.29) holds for any analytical function f of the operator \hat{J}_z . After substituting (6.29) into (6.28), we arrive at the result

$$\hat{H}'(t) = -\frac{\hbar\delta}{2} \left[\hat{J}_+ e^{i\theta(t) + i\kappa t(2\hat{J}_z + 1)} + \text{H.c.} \right].$$

After a Fourier expansion of the exponentials, we find

$$\hat{H}'(t) = -\frac{\hbar\delta}{2} \sum_{n=-\infty}^{\infty} J_n(\varepsilon_1/\omega) \left(\hat{J}_+ e^{it[\kappa(2\hat{J}_z + 1) + n\omega]} + \text{H.c.} \right). \quad (6.30)$$

The form (6.30) of the operator $\hat{H}'(t)$ allows a clear physical interpretation. The oscillating energy difference $\varepsilon(t)$ is equivalent to a series of harmonic couplings between the wells with equally spaced driving frequencies $n\omega$. The amplitude for each harmonic is proportional to

the Bessel function of the corresponding order. So the effective coupling between the number states $|\mu\rangle$ depends strongly on the frequency.

The Hamiltonian $\hat{H}'(t)$ contains only non-vanishing elements coupling neighboring number states $|\mu\rangle$ and $|\mu + 1\rangle$. A resonance occurs for the n th harmonic when

$$n\omega + \kappa(2\mu + 1) = 0, \quad (6.31)$$

which requires that $\kappa(2\mu + 1)/\omega$ is an integer.

The strength of this coupling is $-\Omega_\mu J_n(\varepsilon_1/e\omega)/2$, with

$$\Omega_\mu = \delta \sqrt{(J - \mu)(J + \mu + 1)}. \quad (6.32)$$

The effective coupling by the n th harmonic is measured by the parameter

$$U_\mu^n = \frac{\Omega_\mu}{n\omega + \kappa(2\mu + 1)} J_n\left(\frac{\varepsilon_1}{\omega}\right), \quad (6.33)$$

which is the ratio of the coupling strength and the detuning from resonance for the transition. Whenever $|U_\mu^n| \ll 1$, the coupling is weak.

When the oscillation frequency ω is large compared with the maximal diagonal frequency splitting $\kappa(2J + 1)$, all the time-dependent couplings are weak, and the dominant coupling term is the static one with $n = 0$. The effect of the modulated energy difference is then that the coupling term is reduced by the factor $J_0(\varepsilon_1/\omega)$. In the high-frequency limit $\omega \gg \varepsilon_1$, this factor is one, and we recover the case of a static and symmetric double-well potential with $\varepsilon_1 = 0$.

A simple isolated resonance between two number states can occur involving the states $|\mu\rangle$ with $\mu = -J$ or $\mu = J$, since these can be coupled to only one other state. Suppose that at $t = 0$ all atoms are in one of the two wells, so that

$$|\Psi(t = 0)\rangle = |-J\rangle. \quad (6.34)$$

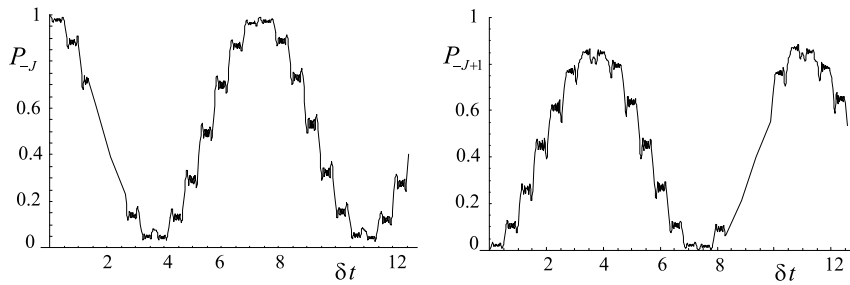


Figure 6.1: Time dependence of the populations P_μ for the state $|\mu\rangle = |-J\rangle$ and $|\mu\rangle = |-J + 1\rangle$. The parameters are taken as $\delta/\kappa = 0.25$, $\varepsilon_1/\kappa = 14$, $\omega/\kappa = 3$, $N = 2J = 16$.

If one chooses the frequency ω such that the resonance condition (6.31) holds at certain integer n_0 , the corresponding harmonic can be made dominant. Indeed, provided that

$|U_\mu^n| \ll 1$ for $\mu = -J + 1$, for all n , coupling to other states is weak, and we have an effective two-level system. This is possible provided that at resonance ω is large compared with κ , which in turn is large compared with the coupling parameter δ . This is demonstrated in Fig. 6.1, where oscillations between the states $|-J\rangle$ and $|-J + 1\rangle$ are displayed for the initial state (6.34). This means that a single atom out of N atoms resonantly oscillates between the wells. Upon decreasing the coupling between the wells, the rate of off-resonant coupling is decreasing, so one approaches ideal Rabi oscillations between resonant levels. Weaker coupling implies a larger oscillation period. The two-level behavior can only occur for a system with a nonlinear term \hat{J}_z^2 , since for a linear system the various transitions are simultaneously in resonance [87] and Chapter 2.

In the case that the modulation frequency ω is of the same order as κ , resonances on the different transitions can coincide, and the initial state (6.34) can spread out over many number states. For example, in the simple case that $\omega = \kappa$, the resonance condition (6.31) shows that for each value of μ , there is a harmonic $n = -(2\mu + 1)$ that is resonant, and the population spreads out over all number states.

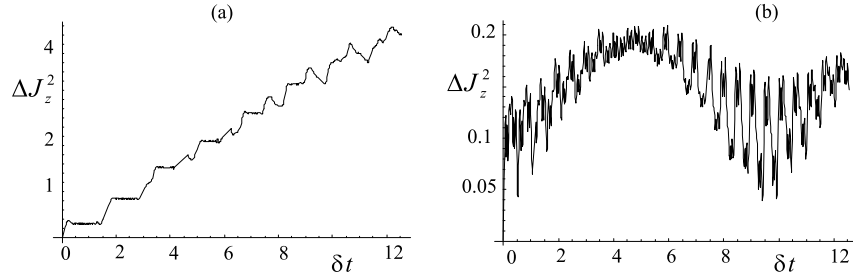


Figure 6.2: Time dependence of the fluctuation $\langle \hat{J}_z \rangle^2$ of operator \hat{J}_z at resonance (a) $\omega = \kappa$ and out of resonance (b) $\omega = 6\kappa$. The other parameters are taken the same as in the previous figure.

The difference with the high-frequency case is demonstrated in Fig. 6.2, where we plot the fluctuations ΔJ_z^2 of \hat{J}_z as a function of time, for the initial condition (6.34), for $\omega = \kappa$ (a) and $\omega = 6\kappa$ (b). In the first case, a resonance occurs on each transition, and ΔJ_z^2 continues to increase. In the second case, the fluctuations remain limited. Even for a very small coupling between wells, resonances designed in such a way can lead to enhancement in the tunneling rate. This is close to the experimental situation for the double-well trap presented in Ref. [78]. Again, this situation is specific for a system with a non-linear term \hat{J}_z^2 in the Hamiltonian, since for a linear system various transitions have the same effective coupling. Since the coupling is proportional to $J_n(\varepsilon_1/\omega)$, a resonant transition can be turned off by setting the ratio ε_1/ω equal to a zero of the Bessel function.

This can be used to restrict the evolution to a limited number of states, thereby locating a desired number of particles in one of the wells. We demonstrate this idea in Fig. 6.3. There we start from the same initial condition (6.34) and see that 11 atoms out of 16 are localized in the left well if one chooses the ratio ε_1/ω such that $J_7(\varepsilon_1/\omega) = 0$ (Fig. 6.3a). Then, taking $J_{11}(\varepsilon_1/\omega) = 0$, or $J_{15}(\varepsilon_1/\omega) = 0$, one can localize 13 or 16 particles in one of the wells, as

demonstrated on fig. 6.3b and 6.3c).

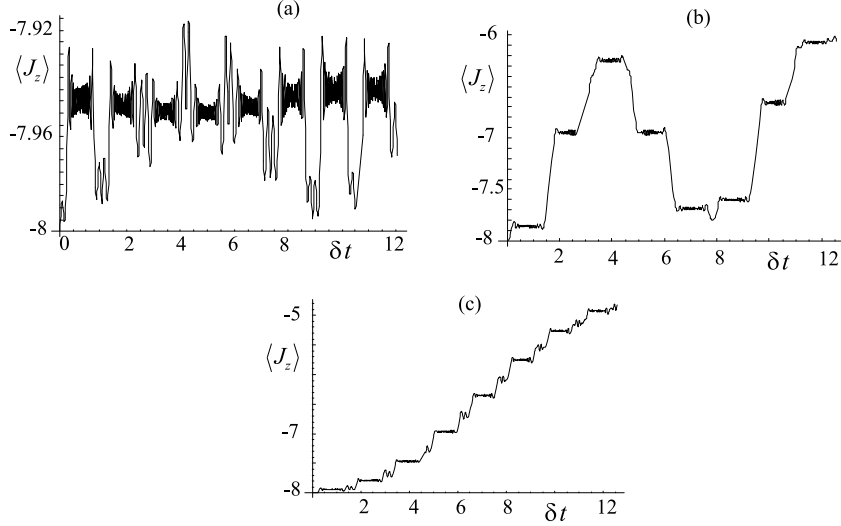


Figure 6.3: Time dependence of the expectation value of \hat{J}_z operator is plotted at resonance $\omega = \kappa$. The ratio ε_1/ω is chosen such that (a) $\varepsilon_1/\omega = 24.26918$ ($J_{13}(\varepsilon_1/\omega) = 0$), (b) $\varepsilon_1/\omega = 23.2759$ ($J_{11}(\varepsilon_1/\omega) = 0$) (c) $\varepsilon_1/\omega = 24.93493$ ($J_7(\varepsilon_1/\omega) = 0$). The total number of particles is chosen $N = 16$.

6.6 Generalization to an optical lattice

The discussion of the previous section for two wells with an energy difference can be generalized to the case of a multimode system, consisting of a chain of potential wells. As a model, we take a BEC in a tilted optical lattice Chapter 2. As usual, we neglect the higher bands in the lattice, and we consider only a BEC trapped in the lowest energy band, that roughly speaking is composed of the ground states in all the wells [12, 94–96]. If one takes the Wannier states $|l\rangle$ with $l = \dots -2, -1, 0, 1, 2, \dots$ as the basis of one-particle states, the Hamiltonian in second quantization is a direct generalization of Eq. (6.6) for two wells, and it takes the form

$$\hat{H}_{BH} = -\frac{\hbar\delta}{2} \sum_l \left(\hat{a}_{l+1}^\dagger \hat{a}_l + \hat{a}_l^\dagger \hat{a}_{l+1} \right) + \frac{\hbar\kappa}{2} \sum_l \hat{a}_l^\dagger \hat{a}_l^\dagger \hat{a}_l \hat{a}_l + \hbar\varepsilon(t) \sum_l l \hat{a}_l^\dagger \hat{a}_l, \quad (6.35)$$

where \hat{a}_l (\hat{a}_l^\dagger) are bosonic annihilation (creation) operators in a single Wannier state, δ and κ are the obvious multimode generalizations of two-mode definitions for the nearest neighbor coupling and interaction constant (6.1, 6.7), ε is the energy difference in frequency units between neighboring Wannier states, which determines the uniform force. This Hamiltonian defines the so-called Bose-Hubbard model.

The time evolution in a lattice is governed by the time-dependent Schrödinger equation

$$i\hbar \frac{d|\Psi(t)\rangle}{dt} = \hat{H}_{BH} |\Psi(t)\rangle. \quad (6.36)$$

The uniform force and the interatomic interaction can be eliminated by the substitution

$$|\Psi_{BH}(t)\rangle = \hat{T}_{BH}(t) |\Psi'_{BH}(t)\rangle,$$

with

$$\hat{T}_{BH}(t) = \exp \left(-i\theta(t) \sum_l \hat{a}_l^\dagger \hat{a}_l - \frac{i\kappa t}{2} \sum_l \hat{a}_l^\dagger \hat{a}_l^\dagger \hat{a}_l \hat{a}_l \right)$$

and $\theta(t) = \int_0^t dt' \varepsilon(t')$ is the area of pulse. The Schrödinger equation for the transformed state $|\Psi'_{BH}(t)\rangle$ follows by using the transformation properties of the annihilation operator

$$\hat{T}_{BH}^\dagger(t) \hat{a}_l \hat{T}_{BH}(t) = \hat{a}_l \exp \left(-i\theta(t) - i\kappa t \left(\hat{a}_l^\dagger \hat{a}_l - 1 \right) \right) = \exp \left(-i\theta(t) - i\kappa t \hat{a}_l^\dagger \hat{a}_l \right) \hat{a}_l,$$

which leads to the identity

$$\hat{T}_{BH}^\dagger(t) \hat{a}_{l+1}^\dagger \hat{a}_l \hat{T}_{BH}(t) = \hat{a}_{l+1}^\dagger \hat{a}_l \exp \left[i\theta(t) + i\kappa t \left(\hat{a}_{l+1}^\dagger \hat{a}_{l+1} - \hat{a}_l^\dagger \hat{a}_l + 1 \right) \right].$$

We obtain the evolution equation

$$i\hbar \frac{d|\Psi'_{BH}(t)\rangle}{dt} = \hat{H}'_{BH} |\Psi'_{BH}(t)\rangle, \quad (6.37)$$

with the effective Hamiltonian

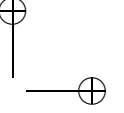
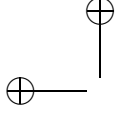
$$\hat{H}'_{BH} = -\frac{\hbar\delta}{2} \sum_l \left(\hat{a}_{l+1}^\dagger \hat{a}_l \exp \left[i\theta(t) + i\kappa t \left(\hat{a}_{l+1}^\dagger \hat{a}_{l+1} - \hat{a}_l^\dagger \hat{a}_l + 1 \right) \right] + \text{H.c.} \right). \quad (6.38)$$

For the case of a periodically modulated uniform force, described by $\varepsilon(t) = \varepsilon_1 \cos \omega t$, this Hamiltonian can be put in the form

$$\hat{H}'_{BH} = -\frac{\hbar\delta}{2} \sum_l \sum_n J_n \left(\frac{\varepsilon_1}{\omega} \right) \left(\hat{a}_{l+1}^\dagger \hat{a}_l \exp \left[in\omega t + i\kappa t \left(\hat{a}_{l+1}^\dagger \hat{a}_{l+1} - \hat{a}_l^\dagger \hat{a}_l + 1 \right) \right] + \text{H.c.} \right). \quad (6.39)$$

This Hamiltonian couples collective number states $|\vec{N}\rangle = |\dots, N_{-1}, N_0, N_1, \dots\rangle$ where two neighboring wells l and $l+1$ have exchanged one particle. The coupling between states with $N_l = p$, $N_{l+1} = q$ and $N_l = p-1$, $N_{l+1} = q+1$ is resonant for a harmonic n when

$$n\omega + \kappa(q-p+1) = 0, \quad (6.40)$$



which is analogous to the resonance condition (6.31). At small tunneling rate we can exclude non-resonant coupling terms while assuming that their effective coupling rate is negligible. When the uniform force also contains a constant term, so that $\varepsilon(t) = \varepsilon_0 + \varepsilon_1 \cos \omega t$, we have to add a term $\varepsilon_0 t$ to $\theta(t)$, and the resonance condition is modified into

$$n\omega + \varepsilon_0 + \kappa(q - p + 1) = 0. \quad (6.41)$$

When $p - q = 1$, this condition is independent of κ , and a resonant oscillation can occur between states with $N_l - N_{l+1} = \pm 1$.

Another interesting case is a Mott insulator state, with the same number of particles N_0 in each well. Such a state has been predicted in [12] and has been recently experimentally realized in ([14]), where one (two) atoms have been put in a single lattice site. So, $|\Psi(t=0)\rangle = |\dots, N_0, N_0, N_0, \dots\rangle$. This state is directly coupled to the collective Fock state which arises if a boson escapes to a neighbouring well, so it has $N_0 + 1$ atoms in one lattice site, and $N_0 - 1$ in the neighboring one. Then the resonant condition is $n\omega + \varepsilon_0 + \kappa = 0$.

Just as in the case of two wells, resonances coincide when ω is of the same order as κ . When $\omega = \kappa$, there is always a harmonic that resonantly couples neighboring wells. In the absence of the constant term ε_0 , the resonance condition takes the universal form $n + q - p + 1 = 0$. So, if in the Mott insulator phase the number fluctuations are suppressed between wells, we obtain their increase at resonances.

6.7 Periodic modulation of coupling

In this Section we consider the effects of a periodic modulation of the coupling coefficient $\delta(t)$ between the wells. As a simple model, we assume that δ contains a harmonic component, so that

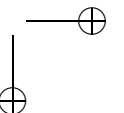
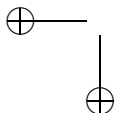
$$\delta(t) = \delta_0 + \delta_1 \cos \omega t. \quad (6.42)$$

In order that the even state $|g\rangle = (|1\rangle + |2\rangle)/\sqrt{2}$ is the ground state, we keep $\delta(t)$ positive at all times, and we choose δ_1 to be smaller than δ_0 . Hence we assume that $\delta_0 \geq \delta_1 \geq 0$. Moreover, we take the energy of the two wells to be equal, so that $\varepsilon = 0$. The Hamiltonian in the form of (6.11) with the coupling coefficient (6.42) can be easily implemented in practice. It describes a BEC in a two-well configuration with a periodically modulated barrier height. Precise calculations of the coupling coefficient are given in [75].

Since in the Hamiltonian (6.11) the term proportional to \hat{J}_x is periodically modulated, we expect that the basis of states $|\mu\rangle_x$, which are eigenstates of the operator \hat{J}_x , is the natural basis to describe the evolution. Then it is convenient to describe the Hamiltonian in terms of the operators \hat{J}_x and \hat{J}_x^\pm , which are defined in Eq. (6.19). By using the identities $\hat{J}_z = -(\hat{J}_x^+ + \hat{J}_x^-)/2$ and $\hat{J}_x^+ \hat{J}_x^- + \hat{J}_x^- \hat{J}_x^+ = 2[J(J+1) - \hat{J}_x^2]$, we rewrite the N -particle Hamiltonian (6.11) in the form

$$\hat{H}_N = -\hbar\delta(t)\hat{J}_x + \frac{\hbar\kappa}{2} \left(J(J+1) - \hat{J}_x^2 \right) + \frac{\hbar\kappa}{4} \left(\hat{J}_x^{+2} + \hat{J}_x^{-2} \right). \quad (6.43)$$

This expression demonstrates that a state $|\mu\rangle_x$ is coupled only to its next nearest neighbors



$|\mu \pm 2\rangle_x$. The coupling strength is measured by the matrix element

$$\Omega_\mu^x = \frac{\kappa}{4} \langle \mu + 2 | \hat{J}_x^{+2} | \mu \rangle_x = \frac{\kappa}{4} \sqrt{(J + \mu + 1)(J + \mu + 2)(J - \mu - 1)(J - \mu)}, \quad (6.44)$$

which depends on the interparticle interaction coefficient κ and the particle number $N = 2J$.

In order to get a closer insight to the role of periodic modulation and its resonances, we again eliminate the diagonal part of the Hamiltonian, now with respect to the basis of states $|\mu\rangle_x$. The time-dependent state is expressed

$$|\Psi(t)\rangle = \hat{S}(t) |\Psi''(t)\rangle, \quad (6.45)$$

with

$$\hat{S}(t) = \exp \left[i\eta(t) \hat{J}_x - \frac{1}{2} i\kappa t (J(J+1) - \hat{J}_x^2) \right], \quad (6.46)$$

and $\eta(t) = \int_0^t dt' \delta(t')$ is the integrated coupling coefficient. In order to obtain the Schrödinger equation for the transformed state $|\Psi''(t)\rangle$, we need the transformation property of the off-diagonal operators \hat{J}_x^{+2} and \hat{J}_x^{-2} . The transformed state $|\Psi''(t)\rangle$ obeys the Schrödinger equation with the effective Hamiltonian

$$\hat{H}''(t) = \frac{\hbar\kappa}{4} \hat{S}^\dagger(t) (\hat{J}_x^{+2} + \hat{J}_x^{-2}) \hat{S}(t).$$

In analogy to Eq. (6.29), we now apply the general transformation rule

$$g(\hat{J}_x) \hat{J}_x^{+2} = \hat{J}_x^{+2} g(\hat{J}_x + 2), \quad (6.47)$$

for an arbitrary analytical function g of \hat{J}_x . After making a Fourier expansion we obtain for $\hat{H}''(t)$ the explicit expression

$$\hat{H}''(t) = \frac{\hbar\kappa}{4} \sum_{n=-\infty}^{\infty} J_n \left(\frac{2\delta_1}{\omega} \right) \left[\hat{J}_x^{+2} e^{-it(\delta_0 + 2\kappa(\hat{J}_x + 1) + n\omega)} + \text{H.c.} \right] \quad (6.48)$$

The form of the Hamiltonian $\hat{H}''(t)$ resembles the Hamiltonian $\hat{H}'(t)$, as specified in Eq. (6.30). In the present case, the basis states are the states $|\mu\rangle_x$, which are now coupled by the square of the corresponding ladder operator $\hat{J}_x^{\pm 2}$. As in (6.30), the coupling term is a series of harmonics with equidistant frequencies $n\omega$, with an amplitude proportional to the Bessel function of the corresponding order.

In the high-frequency limit, when the modulation frequency ω is large compared with the diagonal frequency splittings of the Hamiltonian (6.43), the effect of the static term proportional to $J_0(2\delta_1/\omega)$ in Eq. (6.48) will be dominant, and the Hamiltonian will be effectively constant. Just as in previous sections, the physical reason is that a rapidly modulated field, which has a negligible average pulse area, also has a negligible influence.

On the other hand, Eq. (6.48) immediately shows that the coupling between the state $|\mu\rangle_x$ and $|\mu + 2\rangle_x$ of the n th harmonic is resonant when

$$n\omega + 2\kappa(\mu + 1) + \delta_0 = 0. \quad (6.49)$$

The other coupling terms are negligible when the coupling strength is small compared with the oscillation frequency, which leads to the weak-coupling criterion

$$\left| \frac{\Omega_\mu^x}{n\omega + 2\kappa(\mu + 1) + \delta_0} J_n \left(\frac{2\delta_1}{\omega} \right) \right| \ll 1. \quad (6.50)$$

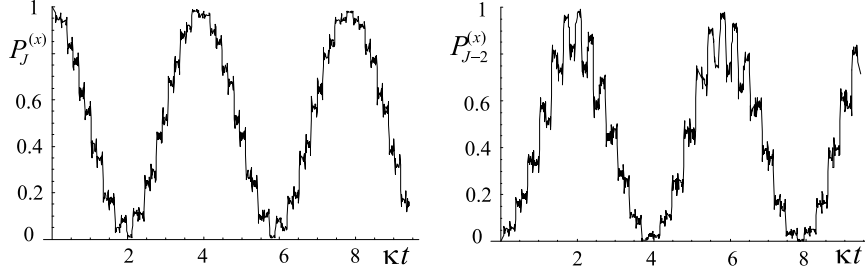
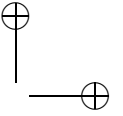
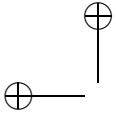


Figure 6.4: Time dependence of the populations $P_\mu^{(x)}$ of the state $|\mu\rangle_x$ with $\mu = J$ and $\mu = J - 2$. The other parameters are taken as $\delta_1/\kappa = 14$, $\delta_0/\kappa = 16$, $\omega/\kappa = 20$, $N = 14$.

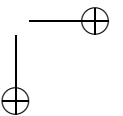
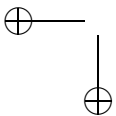
So, if the initial state $|\Psi(0)\rangle = |J\rangle_x$ is resonantly coupled to $|J - 2\rangle_x$, while further couplings of this alter state are negligible, we have an effective two-level system. This is demonstrated on the figure 6.4, where besides the resonant oscillations, one obtains non-resonant escape of population to the rest of manifold. Upon decreasing the coupling between the state $|\mu\rangle_x$, only the resonant states are involved and they exhibit clear Rabi oscillations. This shows how resonances lead to an escape of population from the initial state to the other states in the manifold of states $|\mu\rangle_x$. The similarity with the response to the periodic modulation in the form of a periodically modulated energy difference between the wells. Recall that the state $|J\rangle_x$ is the state in which all particles are in the even state $|g\rangle = (|1\rangle + |2\rangle)/\sqrt{2}$, which is the one-particle ground state. In the state $|J - 2\rangle_x$, two particles have been transferred to the odd excited state.

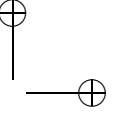
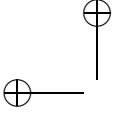
6.8 Conclusions

A BEC trapped in a two-well potential can be expected to be very sensitive to the frequency of any applied periodic perturbation. We test this idea by periodically modulating the asymmetry or the barrier height of such a configuration. Compared with the analogous situation of a single atom trapped in a light field with a periodic modulation, the many-particle nature of the BEC gives rise to some new effects. For both types of modulation, two-state resonances may be observed, where a single atom out of the BEC oscillates between the wells. It is also possible to enter a regime of parameters where more than two states are resonantly coupled, with more than one particle oscillating between the wells. Using such resonances, one can manipulate the average number of particles in the wells by varying the relevant parameters, such as the magnitude and the modulation frequency of the energy difference. This effect can be considered also as a means to resonantly enhance the tunnelling rate between wells. We generalize the basic ideas developed for two-wells to a multiwell system, such as a BEC



in an optical lattice. Whereas the periodic modulation of the energy difference is related to coupling between number states in the two wells, the periodic modulation of the height of the barrier leads to coupling between number states in superposition states of the two wells with specific values of the relative phase.





Chapter 7

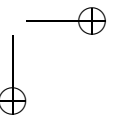
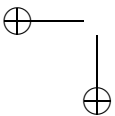
Phase dynamics of a multimode Bose condensate controlled by decay

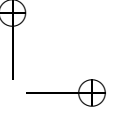
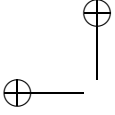
The relative phase between two uncoupled Bose-Einstein condensates tends to attain a specific value when the phase is measured. This can be done by observing their decay products in interference. We discuss exactly solvable models for this process in cases where competing observation channels drive the phases to different sets of values. We treat the case of two modes which both emit into the input ports of two beam splitters and a linear or circular chain of modes. In these latter cases, the transitivity of relative phase becomes an issue.

7.1 Introduction

Since the first observation of Bose-Einstein condensation, the formation and the nature of the relative phase between two condensates has been a central issue of many theoretical and experimental studies. It has been predicted by Javanainen and Yoo [15] and observed by Andrews et al. [69] that two interfering Bose-Einstein condensates exhibit a clear spatial interference pattern. This shows that in a single run of an interference experiment, they manifest themselves as being coherent. Furthermore, it was predicted in [15] that two cases should be distinguished. When a cold cloud of atoms is first split into two modes, which are separately cooled further into two condensates ("cut then cool"), two independent condensates arise. Alternatively, two correlated condensates arise when a single condensate is split into two parts ("cool then cut") [69, 70]. The interference pattern from two independent condensates can be different for each realization of interference experiment, while correlated condensates show the same interference pattern for each run. Cirac et al [97] showed by analytical arguments that a system consisting of two independent Bose-Einstein condensates evolves into a state with a fixed relative phase if one detects the emitted bosonic atoms while observing their spatial interference pattern.

A number of authors have studied the possible manipulation of phase coherence and entanglement between two or more Bose-Einstein condensates, with tunneling interaction as the key mechanism [98–100]. A scheme has been proposed to use an interferometric scheme including an atomic beam splitter to recombine two modes in order to reconstruct the state of a two-mode condensate [101]. The buildup of a relative phase between two independent condensates has also been investigated in the situation that the atoms emitted from the two condensates are mixed in a 50% – 50% beam splitter [91, 102]. Two initially independent bosonic modes, described by a factorized state, have a uniform distribution over the relative





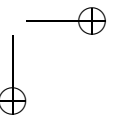
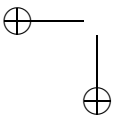
phase. Hence all values of this phase are equally probable as the outcome of a phase measurement. After a large number of detections in the output ports of the beam splitter the system evolves into an entangled state of the two modes. An exactly solvable analytical model has been discussed [102] which allows one to get closed expression for the particle detection statistics over two output channels of the beam splitter for a fixed total number of detections. It is remarkable that even though both detection channels are identical, in a typical detection history the detections are unevenly distributed over the two output ports. This is obviously connected to the bosonic nature of the particles, for which boson accumulation applies. After the first few emissions, the subsequent particles have a tendency to choose the same port as the majority of their predecessors, and the relative phase of the modes converges to one of the phases imposed by the beam splitter. This can also be viewed as an example of spontaneous symmetry breaking [103]. The role of interparticle interaction is also discussed, and it has been shown that it leads to collapse and revival of the relative phase distribution, thereby reflecting the discrete nature of the states of the system [91].

We recalled that in the presence of a single beam splitter, after a large number of detections, the relative phase converges to a single value. It is interesting to consider cases where more detection channels are present which tend to project the relative phase on different values, so that a detection from one beam splitter favors phase values that are incompatible with the setting of another one. In the present paper we consider a number of model cases where such a conflicting tendency arises. This raises the question whether in the end the system simply settles down in one of the possible phase values or whether it continues to shift between values, without ever coming to a final decision. We consider cases where the detection statistics can be solved analytically. Also we study the effect of a direct Hamiltonian coupling between the condensates on both the detection statistics and the corresponding behavior of the relative phase. Examples of such couplings are tunneling between condensates in two spatially separated potential wells or stimulated Raman coupling between two condensates corresponding to two different internal states [104]. We treat the condensates just as modes of bosonic particles, so that most of the considerations hold just as well for photons in cavities.

7.2 Quantum states of two boson modes

It will be convenient to express the states of two boson modes in terms of spin-coherent states (SCS's), which is normally defined for the $(2J + 1)$ -dimensional manifold of states with angular momentum J [89]. The spin-coherent state $|\theta, \phi\rangle$ is the eigenstate of the component $\vec{u} \cdot \hat{\vec{J}}$ of the angular momentum vector with the maximal eigenvalue J , where $\vec{u} \equiv \hat{x} \cos \phi \sin \theta + \hat{y} \sin \phi \sin \theta + \hat{z} \cos \theta$ is the unit vector in the direction specified by the spherical angles θ and ϕ . This state is obtained from the eigenstate of J_z with eigenvalue J after performing the appropriate rotation. In the context of two boson modes (or two harmonic oscillators), an $SU(2)$ representation arises by introducing the fictitious angular-momentum operators

$$\hat{J}_x = \frac{1}{2} (\hat{a}^\dagger \hat{b} + \hat{b}^\dagger \hat{a}), \quad \hat{J}_y = \frac{1}{2i} (\hat{a}^\dagger \hat{b} - \hat{b}^\dagger \hat{a}), \quad \hat{J}_z = \frac{1}{2} (\hat{a}^\dagger \hat{a} - \hat{b}^\dagger \hat{b}), \quad (7.1)$$



where \hat{a} and \hat{b} are the annihilation operators for modes A and B . This is the well-known Schwinger representation. These operators obey the standard commutation rules of angular momentum ($[\hat{J}_x, \hat{J}_y] = i\hat{J}_z$, etc.), so that the matrix form of the operators (7.1) on the eigenvectors of \hat{J}_z and \hat{J}^2 attains the shape that is well known from angular-momentum algebra. Notice that $\hat{J}^2 = (\hat{N}/2)(\hat{N}/2 + 1)$, with $\hat{N} = \hat{a}^\dagger \hat{a} + \hat{b}^\dagger \hat{b}$ the number operator. The eigenvectors of \hat{J}_z and \hat{J}^2 are just the double Fock states $|n_a, n_b\rangle$. A given number of particles, N , corresponds to the value $J = N/2$. The eigenstate of \hat{J}_z with this same eigenvalue is the Fock state $|N, 0\rangle$, so that the SCS with direction \vec{u} can be defined by the rotation

$$|\theta, \phi\rangle_N = \hat{R}(\theta, \phi) |N, 0\rangle, \quad (7.2)$$

with the rotation operator

$$\hat{R}(\theta, \phi) = \exp(-i\phi\hat{J}_z) \exp(-i\theta\hat{J}_y) \exp(i\phi\hat{J}_z) = \exp[-i\theta(\hat{J}_y \cos \phi - \hat{J}_x \sin \phi)]. \quad (7.3)$$

The SCS can be represented as a point on a sphere of radius J , specified by the polar angle θ and the azimuthal angle ϕ . This sphere generalizes the Bloch sphere, describing the state of a spin 1/2, or the Poincaré sphere which describes the polarization state of a light beam or a photon. In the present case, the radius specifies the number of particles, $N = 2J$. An explicit expansion of the SCS (7.2) in the Fock states follows then from the transformation of the creation operators:

$$\hat{R}(\theta, \phi) \hat{a}^\dagger \hat{R}^\dagger(\theta, \phi) = \hat{a}^\dagger \cos \frac{\theta}{2} + \hat{b}^\dagger \sin \frac{\theta}{2} e^{i\phi} \equiv \hat{c}^\dagger(\theta, \phi). \quad (7.4)$$

The SCS (7.2) is found after operating N times with the operator $\hat{c}^\dagger(\theta, \phi)$ on the vacuum state, which leads to the explicit result

$$|\theta, \phi\rangle_N = \sum_{n=0}^N \binom{N}{n}^{1/2} \cos^n \frac{\theta}{2} \sin^{N-n} \frac{\theta}{2} e^{i(N-n)\phi} |n, N-n\rangle. \quad (7.5)$$

This demonstrates that the SCS $|\theta, \phi\rangle_N$ can be viewed as a number state in the mode that is a linear combination of the modes A and B and for which the operator $\hat{c}^\dagger(\theta, \phi)$, defined in eq. (7.4), is the creation operator. In the SCS, the distribution of the N particles over the two modes is binomial, and the angle θ specifies the average partition by $\langle n_a \rangle = N \cos^2(\theta/2)$ and $\langle n_b \rangle = N \sin^2(\theta/2)$. The azimuthal angle ϕ represents the relative phase between the modes. This quantity is complementary to the number difference $\hat{a}^\dagger \hat{a} - \hat{b}^\dagger \hat{b}$. Number states with all particles in the mode A are represented by the north pole of the Bloch sphere ($\theta = 0$), while the south pole represents the SCS with all N particles in mode B . Points on the equator ($\theta = \pi/2$) stand for states with equal population of the modes. Since the state (7.2) [or (7.5)] is eigenstate of \hat{N} , the absolute phase is fully undetermined.

The relation between the SCS and the more common Glauber coherent states (GCS) is easily found by representing the latter ones in the form

$$|r_a e^{-i\phi_a}, r_b e^{-i\phi_b}\rangle = e^{-(r_a^2 + r_b^2)/2} \sum_N \frac{1}{N!} (r_a e^{-i\phi_a} \hat{a}^\dagger + r_b e^{-i\phi_b} \hat{b}^\dagger)^N |vac\rangle. \quad (7.6)$$

These states are eigenstates of \hat{a} and \hat{b} , and they are obviously factorized, so that they carry no entanglement between the modes. It is easy to check that they are related to the SCS by the expansion [97]

$$|r_a e^{-i\phi_a}, r_b e^{-i\phi_b}\rangle = e^{-R^2/2} \sum_N \frac{1}{\sqrt{N!}} R^N e^{-iN\phi_a} |\theta, \phi\rangle_N, \quad (7.7)$$

with the parameters R , θ and ϕ determined by $R^2 = r_a^2 + r_b^2$, $\tan(\theta/2) = r_b/r_a$, and $\phi = \phi_a - \phi_b$. This indicates that the GCS has a Poissonian distribution of the total particle number N , with average value $\langle N \rangle = R^2$, while the absolute phases ϕ_a and ϕ_b of both modes are well specified. For bosonic atoms, states with a different total number of particles do not superpose, according to the superselection rule, so that we have to restrict ourselves to density matrices that are diagonal in N . Since the particle number is conjugate to the overall phase, we introduce the density matrix

$$\hat{\rho}(R, \theta, \phi) = \frac{1}{2\pi} \int_0^{2\pi} d\phi_a |r_a e^{-i\phi_a}, r_b e^{-i(\phi_a - \phi)}\rangle \langle r_a e^{-i\phi_a}, r_b e^{-i(\phi_a - \phi)}| \quad (7.8)$$

as the uniform mixture of the GCS (7.6) over the overall phase ϕ_a , for a given value of the relative phase $\phi = \phi_a - \phi_b$. Applying eq. (7.7) leads to an expansion of this same density matrix in the SCS in the form

$$\hat{\rho}(R, \theta, \phi) = e^{-R^2} \sum_N \frac{1}{N!} R^{2N} |\theta, \phi\rangle_N \langle \theta, \phi|. \quad (7.9)$$

The density matrix $\hat{\rho}(R, \theta, \phi)$ is therefore diagonal in the particle number N .

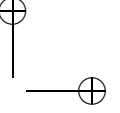
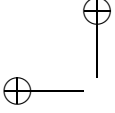
In this paper we shall use density matrices that can be represented as a superposition of the states (7.9) for a single value of the strength parameter R in the form

$$\int d\Omega f(\theta, \phi) \hat{\rho}(R, \theta, \phi), \quad (7.10)$$

where we use the abbreviation $\int d\Omega = \int_0^{2\pi} d\phi \int_0^\pi d\theta \sin \theta$ for the integration over the Bloch sphere. When we express $\hat{\rho}(R, \theta, \phi)$ as in eq. (7.8), it becomes clear that eq. (7.10) is just the two-mode version of the Glauber-Sudarshan diagonal coherent-state representation of the initial density matrix [106], where the P distribution is uniform in ϕ_A , and is nonzero only for a single value of R . This state is normalized as soon as the distribution f is, which we shall assume. Another special case arises when the function f is nonzero only for a single value of θ and uniform in ϕ . Then the density matrix (7.10) can be written as

$$\int d\phi \hat{\rho}(R, \theta, \phi) / 2\pi. \quad (7.11)$$

It follows from the coherent-state representation (7.8) that in this case the density matrix factorizes into a product of separate density matrices for the two modes, implying that the state (7.11) is not entangled. The phase of both modes is uniformly distributed, and the state is diagonal in both particle numbers n_a and n_b .



7.3 Decay and detection statistics of two boson modes

7.3.1 Master equation and detection histories

We assume that particles are leaking out of the two boson modes A and B at a total loss rate Γ . The emitted particles are detected after passing through a beam splitter. For simplicity, we assume perfect detection efficiency and lossless beam splitters. Moreover, the mode evolution is governed by a Hamiltonian \hat{H} that is supposed to commute with the number operator \hat{N} and which describes the energy per particle and possibly tunneling between the modes. Since the two modes form an open system, their evolution can be described by a quantum master equation [105, 106] for the two-mode density matrix $\hat{\rho}$, which we formally express as

$$\frac{d\hat{\rho}}{dt} \equiv (\mathcal{L}_0 + \mathcal{L}_1) \hat{\rho}. \quad (7.12)$$

Here \mathcal{L}_0 describes the coherent evolution of the system, which is determined by the Hamiltonian evolution, and the loss of the probability of states due to the emission of particles. Its explicit form is given by its action on a density matrix

$$\mathcal{L}_0 \hat{\rho} = -\frac{i}{\hbar} [\hat{H}, \hat{\rho}] - \frac{1}{2} \Gamma (\hat{N} \hat{\rho} + \hat{\rho} \hat{N}), \quad (7.13)$$

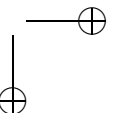
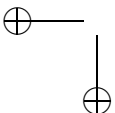
while the compensating probability gain is accounted for by

$$\mathcal{L}_1 \hat{\rho} = \Gamma (\hat{a} \hat{\rho} \hat{a}^\dagger + \hat{b} \hat{\rho} \hat{b}^\dagger). \quad (7.14)$$

For simplicity the loss rate of the two modes is taken to be the same. The solution of eq. (7.12) describes the evolution of the system averaged over all possible detection histories. In fact, we are interested in the conditional evolution for specific histories, where the arrival times for particles at each detector are specified. Depending on the specific setup, we have to separate the total gain term (7.14) in terms corresponding to each detector separately, in accordance with the method of quantum trajectories [91, 97, 102]. For instance, when a detector is directly coupled to each mode, the term $\hat{a} \hat{\rho} \hat{a}^\dagger$ describes the effect of the detection of a particle from mode A , which corresponds to the annihilation of a particle from this mode. Now we consider the setup sketched in Fig. 7.1, where each mode emits particles into the input port of two different beam splitters.

Detections in the two output ports of beam splitter I correspond to the detection operators $\hat{c}_\pm = (\hat{a} \pm \hat{b})/\sqrt{2}$, and detections in the output ports of beam splitter II correspond to the detection operators $\hat{d}_\pm = (\hat{a} \pm e^{-i\xi} \hat{b})/\sqrt{2}$. The relative phases can be set either by using dephasers or by differences in the path lengths of the channels. Notice that the detection operators are annihilation operators corresponding to a spin-coherent state that is represented by points on the equator of the Bloch sphere. For this setup the gain operator \mathcal{L}_1 can be separated into four terms corresponding to the four detectors as

$$\mathcal{L}_1 \hat{\rho} = \frac{\Gamma}{2} (\hat{c}_+ \hat{\rho} \hat{c}_+^\dagger + \hat{c}_- \hat{\rho} \hat{c}_-^\dagger + \hat{d}_+ \hat{\rho} \hat{d}_+^\dagger + \hat{d}_- \hat{\rho} \hat{d}_-^\dagger) \equiv \frac{\Gamma}{2} \sum_{s=1}^4 \hat{c}_s \hat{\rho} \hat{c}_s^\dagger = \sum_{s=1}^4 \mathcal{L}_{1s} \hat{\rho}. \quad (7.15)$$



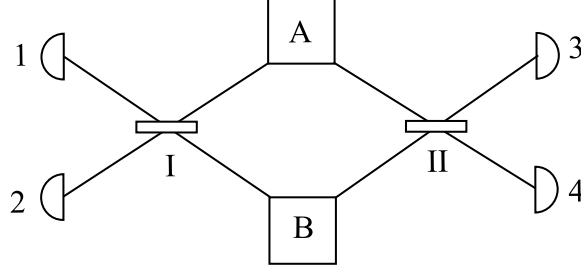


Figure 7.1: Sketch of setup with two decaying boson modes A and B. Each mode emits particles into the input port of two beam splitters I and II. Output ports are coupled to particle detectors 1-4.

The integral form of the master equation (7.12)

$$\hat{\rho}(T) = e^{\mathcal{L}_0 T} \hat{\rho}(0) + \sum_i \int_0^T dt e^{\mathcal{L}_0(T-t)} \mathcal{L}_{1i} \hat{\rho}(t) \quad (7.16)$$

allows us after iteration to express the density matrix as a summation and integration over detection histories. The contribution to $\hat{\rho}(T)$ from the history with detections at the successive time instants $t_1 \leq t_2 \leq \dots \leq t_L$ by the detectors s_1, s_2, \dots, s_L in the time interval $[0, T]$ is described by the operator

$$\hat{\rho}_L(\{t_i, s_i\}, T) = e^{\mathcal{L}_0(T-t_{L-1})} \mathcal{L}_{1s_L} e^{\mathcal{L}_0(t_L-t_{L-1})} \dots \mathcal{L}_{1s_1} e^{\mathcal{L}_0 t_1} \hat{\rho}(0). \quad (7.17)$$

The effect of the detection operators \mathcal{L}_{1i} is a sudden change in the density matrix, which indicates the quantum-jump nature of a detection.

Since eqs. (7.14) and (7.15) are different representations of the same gain operator, the unitarity of the evolution is guaranteed. The separated form (7.15) represents the physical situation that the emitted particles from each mode can go into two different input channels, with equal rate constants $\Gamma/2$.

7.3.2 Detection statistics and phase distribution

As the initial state $\hat{\rho}(0)$ of the system we take a density matrix of the form (7.10), so that

$$\hat{\rho}(0) = \int d\Omega f(\theta, \phi) \hat{\rho}(R, \theta, \phi). \quad (7.18)$$

When the Hamiltonian only attributes a fixed energy per particle, its form is $\hat{H} = \hbar\omega \hat{N}$. Since all density matrices that we shall encounter are diagonal in the total number of particles, the Hamiltonian has no effect and can be ignored. The coherent evolution of the density matrix is easily obtained from the identity $\mathcal{L}_0 |\phi, \theta\rangle_{NN} \langle\theta, \phi| = -\Gamma N |\phi, \theta\rangle_{NN} \langle\theta, \phi|$, which when substituted into eq. (7.9) gives the result

$$e^{\mathcal{L}_0 T} \hat{\rho}(R, \theta, \phi) = \exp[-R^2(1 - e^{-\Gamma T})] \hat{\rho}(R e^{-\Gamma T/2}, \theta, \phi). \quad (7.19)$$

This shows that the evolution of the density matrix during a detection-free period of time only gives a damping of the strength parameter R , without changing the distribution over the Bloch sphere. The action of the detection operators on the density matrix is most easily obtained by using eq. (7.8). The action of the annihilation operators on the SCS is found to be given by

$$\hat{a}|\theta, \phi\rangle_N = \sqrt{N} \cos \frac{\theta}{2} |\theta, \phi\rangle_{N-1}, \quad \hat{b}|\theta, \phi\rangle_N = \sqrt{N} \sin \frac{\theta}{2} e^{i\phi} |\theta, \phi\rangle_{N-1} \quad (7.20)$$

We observe that to each pair of spherical angles θ and ϕ or equivalently, to each real Cartesian unit vector \vec{u} corresponds a density matrix $\hat{\rho}(R, \theta, \phi)$ given in eq. (7.9) and an annihilation operator $\hat{c}(\theta, \phi)$ as defined in eq. (7.4). Now consider the annihilation operator $\hat{c}(\theta_0, \phi_0)$, corresponding to the unit vector \vec{u}_0 . Then a direct calculation shows that

$$\hat{c}(\theta_0, \phi_0) \hat{\rho}(R, \theta, \phi) \hat{c}^\dagger(\theta_0, \phi_0) = \frac{1}{2} R^2 (1 + \vec{u} \cdot \vec{u}_0) \hat{\rho}(R, \theta, \phi). \quad (7.21)$$

The unit vectors \vec{u} and \vec{u}_0 in eq. (7.21) are defined to point in the directions specified by the angles (θ, ϕ) and (θ_0, ϕ_0) respectively. This indicates that for these operators $\hat{c} \hat{\rho} \hat{c}^\dagger$ is proportional to $\hat{\rho}$. The proportionality factor takes the maximal value R^2 when the two directions \vec{u}_0 and \vec{u} coincide, and it is zero when the directions are opposite. It is noteworthy that this factor depends only on the inner product of the two unit vectors and thereby on the distance between the two points on the unit sphere. This indicates that the effect of a detection on the density matrix is determined by the relative geometry on the Bloch sphere.

Application of eq. (7.21) leads to the expression

$$\mathcal{L}_{1s} \hat{\rho}(R, \theta, \phi) = \Gamma R^2 g_s(\theta, \phi) \hat{\rho}(R, \theta, \phi), \quad (7.22)$$

where the functions g_i for the detectors 1 and 2 are given by

$$g_1(\theta, \phi) = \frac{1}{4} (1 + \sin \theta \cos \phi), \quad g_2(\theta, \phi) = \frac{1}{4} (1 - \sin \theta \cos \phi), \quad (7.23)$$

and for the detectors 3 and 4 by

$$g_3(\theta, \phi) = \frac{1}{4} [1 + \sin \theta \cos(\phi - \xi)], \quad g_4(\theta, \phi) = \frac{1}{4} [1 - \sin \theta \cos(\phi - \xi)]. \quad (7.24)$$

The functions are determined by the inner product of the unit vector \vec{u} , indicated by θ and ϕ , and the unit vectors \vec{u}_0 corresponding to the detection operators \hat{c}_s . These four unit vectors are all defined by $\theta_0 = \pi/2$, whereas $\phi_0 = 0$ and π for $s = 1$ and 2 and $\phi_0 = \xi$ and $\xi + \pi$ for $s = 3$ and 4 . The functions g_s add up to 1, so that the total gain operator \mathcal{L}_1 when acting on $\hat{\rho}(R, \theta, \phi)$ just gives the factor ΓR^2 , as it should. According to eq. (7.22), the effect of the i th detection at time t_i by detector s_i is that the distribution over the Bloch sphere is multiplied by the factor g_{s_i} , while an overall factor $\Gamma R^2 \exp(-\Gamma t_i)$ has to be added. In brief, the detection-free periods produce a damping of R and the detection modifies the distribution over the Bloch sphere by a multiplication with a function g_{s_i} . For a given value of the ratio $\langle n_a \rangle / \langle n_b \rangle$, as specified by the angle θ , the factors g_s modify the distribution

over the relative phase ϕ , with a contrast that is maximal when both modes contain the same number of particles ($\theta = \pi/2$).

The equations (7.19)-(7.24) allow one to evaluate explicitly the density matrix (7.17) corresponding to a given detection history, with the initial state determined by eq. (7.18). The contribution (7.17) to the density matrix is then found as

$$\begin{aligned} \hat{\rho}_L(\{t_i, s_i\}, T) = & \exp[-R^2(1 - e^{-\Gamma T})] \prod_{i=1}^L (\Gamma R^2 e^{-\Gamma t_i}) \\ & \times \int d\Omega f(\theta, \phi) \left[\prod_{s=1}^4 g_s^{n_s}(\theta, \phi) \right] \hat{\rho}(Re^{-\Gamma T/2}, \theta, \phi), \end{aligned} \quad (7.25)$$

with n_s the total number of detections in channel s (with $\sum n_s = L$). This contribution (7.25) does not depend on the specific order of the detections in the various channels. The trace of eq. (7.25) specifies the probability distribution of the detection history $\{t_i, s_i\}$ in the factorized form

$$w_L(\{t_i, s_i\}, T) = F(\{n_s\}) \exp[-R^2(1 - e^{-\Gamma T})] \prod_{i=1}^L (\Gamma R^2 e^{-\Gamma t_i}), \quad (7.26)$$

with

$$F(\{n_s\}) = \int d\Omega f(\theta, \phi) \prod_{s=1}^4 g_s^{n_s}(\theta, \phi) \quad (7.27)$$

the probability that L successive detections occur in the specific order (s_1, s_2, \dots, s_L) . This factor F only depends on the number of detections n_s for each channel, not on the time ordering of the detections. The remaining time-dependent factor in eq. (7.26) is the probability density for detections at the specified instants of time, irrespective of the detection channel. The conditional density of the system, given the detection history $\{t_i, s_i\}$, is equal to $\hat{\rho}_L(\{t_i, s_i\}, T) / w_L(\{t_i, s_i\}, T)$, which is the normalized version of eq. (7.25). From the expression (7.26) of the probability density one obtains the probability $p(\{n_s\}, T)$ that in the time interval $[0, T]$ there were n_s detections in channel s , ($s = 1, \dots, 4$), irrespective of the order of the detections. This requires an integration over the ordered detection times and a multiplication with the number of possible orderings of the L detections over the four detectors, given the partition $\{n_s\}$. The result can be expressed as

$$p(\{n_s\}, T) = P_L(T) p_L(\{n_s\}), \quad (7.28)$$

where $P_L(T)$ gives the probability that precisely L detections occurred in the time interval $[0, T]$, irrespective of the detection channel. This distribution is Poissonian with average $R^2(1 - e^{-\Gamma T})$. The factor $p_L(\{n_s\})$ is the probability that the L detections are distributed over the four detectors by the partition $\{n_s\}$ and takes the form

$$p_L(\{n_s\}) = \frac{L!}{n_1! n_2! n_3! n_4!} F(\{n_s\}). \quad (7.29)$$

This distribution is independent of the strength factor R , the detection time T and the decay rate Γ . Notice that both the distribution $P_L(T)$ over the total number L of detections and the distribution $p_L(\{n_s\})$ of the L detections over the partitions are normalized.

In summary, we notice that the decay process only has the effect that the strength factor R is damped. The effect of a detection is that the distribution over the Bloch sphere is multiplied by one of the factors g_s , which changes both the distribution over the relative phase and the probability distribution for subsequent detections. The probability distribution of L detections over the four detection channels is given by (eq. 7.29). After a detection series given by the partition $\{n_s\}$, the normalized distribution function over the Bloch sphere is given by $f(\theta, \phi) \prod_s g_s^{n_s}(\theta, \phi) / F(\{n_s\})$. The detection statistics is invariant when both the distribution function f and the detection functions g_s are changed by the same rotation over the Bloch sphere.

7.3.3 Special cases

When the detections in channels 3 and 4 are ignored and M detections have occurred in channels 1 and 2, the distribution of these detections over the two channels can be evaluated in the same fashion. The result is

$$p_M(n_1, n_2) = 2^M \binom{M}{n_1} \int d\Omega f(\theta, \phi) g_1^{n_1}(\theta, \phi) g_2^{n_2}(\theta, \phi), \quad (7.30)$$

with $n_1 + n_2 = M$. The factor 2^M is needed to ensure normalization, since $g_1 + g_2 = 1/2$ in this case. This expression is a simple generalization of the result of [102] for the case of two decaying modes observed through a single beam splitter. The generalization consists in the fact that the populations of the two modes need not be the same in eq. (7.30). Intuitively it is obvious that the partial statistics of detections in channels 1 and 2 is not affected when for some reason the detections in channels 3 and 4 are simply added without distinguishing them. This situation is equivalent to the case that beam splitter II is missing and a single detector is just collecting particles in both of its input channels.

We have noticed that the effect of detections on the phase distribution is strongest when the average number of particles is the same in both modes, so we consider the case that the polar angle is $\theta = \pi/2$ or $r_a = r_b = R/\sqrt{2} \equiv r$. For this situation, the two-channel distribution (7.30) has been evaluated in ref. [102]. When the relative phase ϕ has a well-defined value ϕ_0 , the two-channel distribution is binomial:

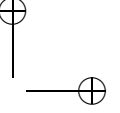
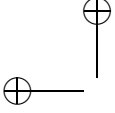
$$p_M(n_1, n_2) = \binom{M}{n_1} \cos^{2n_1} \frac{\phi_0}{2} \sin^{2n_2} \frac{\phi_0}{2}, \quad (7.31)$$

where the most probable detection history has the values

$$n_1 = M \cos^2(\phi_0/2), \quad n_2 = M \sin^2(\phi_0/2). \quad (7.32)$$

When the phase distribution is uniform, the two-channel distribution was found as [102]

$$p_M(n_1, n_2) = \frac{1}{2^{2M}} \binom{2n_1}{n_1} \binom{2n_2}{n_2}. \quad (7.33)$$



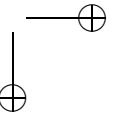
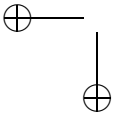
This displays boson accumulation, and in a typical detection history the numbers n_1 and n_2 of detections in the two channels are quite different. In fact, the most probable history is specified by $(n_1, n_2) = (M, 0)$ or $(0, M)$. After such a history, the relative-phase distribution is proportional to $\cos^{2M}(\phi/2)$ or $\sin^{2M}(\phi/2)$, which peaks at the positions corresponding to the output channels of the beam splitter I . The width of this distribution is significant, so that for large detection numbers M the probability of these most probable histories is quite small in absolute terms. Nevertheless, they do characterize typical detection histories as being in their neighborhood.

Now we turn to the detection statistics over the four channels when the initial density matrix is specified by eq. (7.11), with equal population of the two modes and initial uniform relative phase. Then the initial density matrix is equivalent to the factorized form $\hat{\rho}(0) = \hat{\rho}_a \otimes \hat{\rho}_b$, with

$$\hat{\rho}_a = \frac{1}{2\pi} \int d\phi_a |re^{-i\phi_a}\rangle \langle re^{-i\phi_a}|, \quad (7.34)$$

and a similar expression for $\hat{\rho}_b$. Both modes have a density matrix that is diagonal in the number state, with a Poissonian distribution. In order to characterize the statistics, we look for the detection histories with the largest probabilities. A typical detection history can be expected to be in the neighborhood of these maxima. First we notice that the emission probability onto both beam splitters I and II is the same, so that for a total of L detections a most probable history must have $n_1 + n_2 = n_3 + n_4 = L/2$. (We assume that L is even for simplicity.) If nothing is specified on the distribution of the $L/2$ detections in channels 3 and 4, the distribution over the two channels 1 and 2 is given by eq. (7.33) with $M = L/2$, with the most probable partitions $(n_1, n_2) = (L/2, 0)$ or $(0, L/2)$. The relative phase has then converged to the value $\phi = 0$ or $\phi = \pi$, which makes the distribution over the $L/2$ detections in channels 3 and 4 binomial. For example, for the partition $(n_1, n_2) = (L/2, 0)$, the partition over the two other detectors has maximal probability for $(n_3, n_4) = (L/2)(\cos^2(\xi/2), \sin^2(\xi/2))$. Since the pair of detectors 1 and 2 is fully equivalent to the pair 3 and 4, another history with the same maximal probability occurs for the partition $(n_3, n_4) = (L/2, 0)$, with $(n_1, n_2) = (L/2)(\cos^2(\xi/2), \sin^2(\xi/2))$. This corresponds to a relative phase converging to the value $\phi = \xi$. In summary, we expect four most probable histories for L detections. The partitions over the four detectors attain the values $(n_1, n_2, n_3, n_4) = (L/2)(1, 0, \cos^2(\xi/2), \sin^2(\xi/2))$, $(L/2)(0, 1, \sin^2(\xi/2), \cos^2(\xi/2))$, $(L/2)(\cos^2(\xi/2), \sin^2(\xi/2), 1, 0)$ and $(L/2)(\sin^2(\xi/2), \cos^2(\xi/2), 0, 1)$, while the phase has converged in these cases to the values $\phi = 0, \pi, \xi$ and $\xi + \pi$, respectively. These considerations are backed up by a numerical calculation of the probability distribution $p_L(\{n_s\})$, for $L = 40$, equal population of the two wells ($\theta = \pi/2$), and uniform distribution over the relative phase ϕ , while the setting of the two beam splitters is maximally different ($\xi = \pi/2$). The distribution for equal number of detections through both beam splitters is plotted in Fig. 7.2.

The most probable histories are marked. The gradual transition between the two distributions (7.31) and (7.33) is noticed along the axis n_1 , when n_3 varies from 0 (binomial distribution over n_1 and $n_2 = L/2 - n_1$) and $L/2$ [bunching distribution (7.33)].



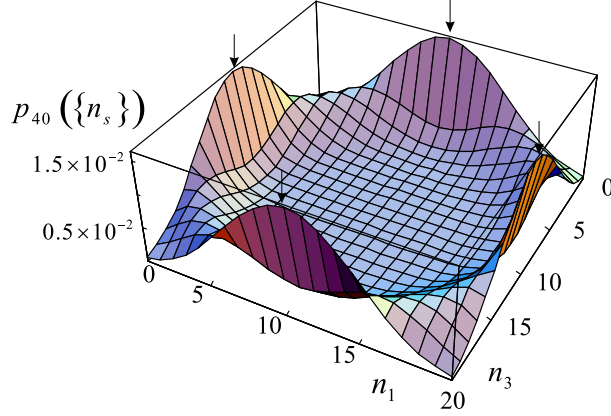


Figure 7.2: The probability distribution $p_L(\{n_s\})$ as a function of n_1 and n_3 , for equal particle numbers in the modes. The total detection number is $L = 40$, with 20 particles going into each beam splitter. The phase difference between the beam splitters is equal to $\xi = \pi/2$. The most probable detection histories are marked.

7.4 Detection statistics of two coupled boson modes

7.4.1 Pulsed coupling between modes

In this section, we consider the case that the particles emitted by the two boson modes A and B are detected directly, without the use of beam splitters, as sketched in Fig. 7.3(a). Therefore we separate the gain operator in the master equation (7.12) as $\mathcal{L}_1 = \mathcal{L}_{1a} + \mathcal{L}_{1b}$, corresponding to the two terms in eq. (7.14). The coherent-evolution operator \mathcal{L}_0 is given by eq. (7.13), where the Hamiltonian \hat{H} describes coupling between the two modes by tunneling, in the form

$$\hat{H} = -\frac{\hbar\delta}{2} (\hat{a}^\dagger \hat{b} + \hat{a} \hat{b}^\dagger) = -\hbar\delta \hat{J}_x. \quad (7.35)$$

In realistic cases we can imagine that the coupling can be switched on during a time interval τ , which is sufficiently small so that decay during the coupling is negligible. This means that the initial state for the decay process is found by applying the pulse evolution operator

$$\hat{U}_0 = \exp(-i\hat{H}\tau/\hbar) = \exp(i\delta\tau \hat{J}_x). \quad (7.36)$$

In the picture of the Bloch sphere, this is a rotation about the x axis in a negative direction over an angle $\delta\tau$. When the initial state before the coupling is given by eq. (7.10), the state after switching off the coupling at the beginning of the detection period is

$$\hat{\rho}(0) = \int d\Omega f(\theta, \phi) \hat{U}_0 \hat{\rho}(R, \theta, \phi) \hat{U}_0^\dagger. \quad (7.37)$$

The contribution to the density matrix from a given detection history $\{t_i, s_i\}$ is expressed by eq. (7.17), where now the indices s of the jump operators \mathcal{L}_{1s} can take the values a or b and

where eq. (7.37) specifies the initial density matrix. The evolution during the detection-free periods is given in eq. (7.19). The effect of the jump operators on the rotated density matrix can be expressed using the identity

$$\mathcal{L}_{1a}\hat{U}_0\hat{\rho}\hat{U}_0^\dagger = \Gamma\hat{U}_0\hat{c}_a\hat{\rho}\hat{c}_a^\dagger\hat{U}_0^\dagger$$

and a similar expression for \mathcal{L}_{1b} , where we introduced the counterrotated operators $\hat{c}_a \equiv \hat{U}_0^\dagger\hat{a}\hat{U}_0$ and $\hat{c}_b \equiv \hat{U}_0^\dagger\hat{b}\hat{U}_0$. Their explicit expressions are then

$$\hat{c}_a = \hat{a} \cos \frac{\delta\tau}{2} + i\hat{b} \sin \frac{\delta\tau}{2}, \hat{c}_b = i\hat{a} \sin \frac{\delta\tau}{2} + \hat{b} \cos \frac{\delta\tau}{2}.$$

They correspond in the sense of eq. (7.4) to the two unit vectors $\vec{u}_a = -\hat{y} \sin \delta\tau + \hat{z} \cos \delta\tau$ and $\vec{u}_b = \hat{y} \sin \delta\tau - \hat{z} \cos \delta\tau$, which arise when the opposite rotation is applied to $\pm\hat{z}$. By using eq. (7.21), the action of the jump operators \mathcal{L}_{1a} and \mathcal{L}_{1b} in a detection history is given by the relation

$$\begin{aligned} \mathcal{L}_{1a}\hat{U}_0\hat{\rho}(R, \theta, \phi)\hat{U}_0^\dagger &= \Gamma R^2 g_a(\theta, \phi)\hat{U}_0\hat{\rho}(R, \theta, \phi)\hat{U}_0^\dagger, \\ \mathcal{L}_{1b}\hat{U}_0\hat{\rho}(R, \theta, \phi)\hat{U}_0^\dagger &= \Gamma R^2 g_b(\theta, \phi)\hat{U}_0\hat{\rho}(R, \theta, \phi)\hat{U}_0^\dagger, \end{aligned} \quad (7.38)$$

with

$$g_a(\theta, \phi) = \frac{1}{2}(1 + \vec{u} \cdot \vec{u}_a), \quad g_b(\theta, \phi) = \frac{1}{2}(1 + \vec{u} \cdot \vec{u}_b). \quad (7.39)$$

Notice that these factors add up to ΓR^2 . The contribution to the density matrix arising from the history $\{t_i, s_i\}$ is now easily found in the form

$$\begin{aligned} \hat{\rho}_L(\{t_i, s_i\}, T) &= \exp[-R^2(1 - e^{-\Gamma T})] \prod_{i=1}^L (\Gamma R^2 e^{-\Gamma t_i}) \\ &\times \int d\Omega f(\theta, \phi) g_a^{n_a}(\theta, \phi) g_b^{n_b}(\theta, \phi) \hat{U}_0\hat{\rho}(R e^{-\Gamma T/2}, \theta, \phi)\hat{U}_0^\dagger, \end{aligned} \quad (7.40)$$

which looks quite similar as eq. (7.25). The probability distribution for detection histories is given by the trace of eq. (7.40), and the detection statistics can be obtained in the same way as above. In analogy to eq. (7.28), the probability $p(n_a, n_b, T)$ that in the time interval $[0, T]$ there were n_a detections in channel a and n_b in channel b , irrespective of their order, is now

$$p(n_a, n_b, T) = P_L(T) p_L(n_a, n_b),$$

where, as before, $P_L(T)$ is the Poissonian distribution of the total number $L = n_a + n_b$ of detections in the interval $[0, T]$. The factor $p_L(n_a, n_b)$, which represents the probability that the L detections are partitioned over the two detectors as (n_a, n_b) , is

$$p_L(n_a, n_b) = \binom{L}{n_a} F(n_a, n_b), \quad (7.41)$$

with

$$F(n_a, n_b) = \int d\Omega f(\theta, \phi) g_a^{n_a}(\theta, \phi) g_b^{n_b}(\theta, \phi). \quad (7.42)$$

As an example, we consider the case that before the coupling period the two modes are fully decoupled, with equal population, so that the function f is uniform over the equator of the sphere. The density matrix before coupling has then the form (7.11), with $\theta = \pi/2$. When moreover the pulse duration is chosen such that $\delta\tau = \pi/2$, we find $\vec{u}_a = -\hat{y}$, $\vec{u}_b = \hat{y}$, and the functions g_a and g_b at the equator are found as $g_a(\phi) = (1 - \sin \phi)/2$ and $g_b(\phi) = (1 + \sin \phi)/2$. The distribution $p_L(n_a, n_b)$ is now exactly the same as in the case of an initially uniform phase distribution, with detectors placed in the output channel of a single 50% – 50% beam splitter [102]. We recover the bunching distribution

$$p_L(n_a, n_b) = \frac{1}{2^{2L}} \binom{2n_a}{n_a} \binom{2n_b}{n_b},$$

with $(n_a, n_b) = (L, 0)$ or $(0, L)$ the most probable histories of L detections. The identity of the distribution in these two cases may be surprising in view of the quite different physical situations. It is the merit of the description of states and detections as distributions on the Bloch sphere that it clarifies this identity, since the two cases have the same relative geometry on the Bloch sphere.

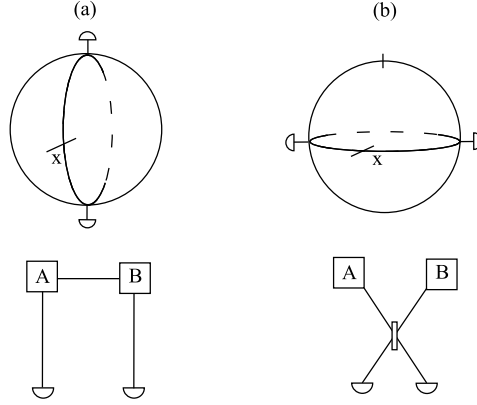


Figure 7.3: Comparison of the geometry on the Bloch sphere for two cases. (a) particles emitted by modes A and B are detected directly, without the use of a beam splitter; (b) emitted particles are detected through a beam splitter. For each case, the position of the detectors on the Bloch sphere are indicated in both cases. The large circles on the sphere indicate the distribution f that determines the initial state just before the detections.

This is illustrated by Fig. 7.3. The situation that the pulse duration deviates slightly from the identity $\delta\tau = \pi/2$ implies that the detector positions do not lie precisely on the large

circle that describes the initial distribution. Then it follows from the general expressions (7.39) that the contrast of the functions g_a and g_b on the large circle is diminished, so that convergence to a single phase value is slowed down. Accordingly, the distribution $p_L(n_a, n_b)$ will have a diminished bunching.

For the initially coupled modes and the detections without the beam splitter, the relative phase is initially rather well determined around $\phi = 0$ and $\phi = \pi$. A typical detection series now projects the state of the system onto the state with most particles either in mode A or in mode B , with an undetermined relative phase. If at the end of the detection series a second pulsed coupling is applied as described by the operator \hat{U}_0 , the final state after this pulse has a well-determined relative phase. The final state after the entire scheme of pulsed coupling, detection series and second pulse is the same as the result of just a detection series through the beam splitter. In this sense, the pulsed coupling can be viewed as a replacement of the beam splitter. This scheme with pulsed coupling offers a simple possibility of realizing the bunching distribution (7.33) of bosons, without the use of a beam splitter.

7.4.2 Continuous coupling between modes

The situation is different when the coupling between the modes is present continuously. Then in expression (7.13) for the coherent-evolution operator, the Hamiltonian is given by eq. (7.35). Since the Hamiltonian commutes with the number operator \hat{N} , the decay terms are not affected the Hamiltonian evolution, and eq. (7.19) is replaced by the modified form

$$e^{\mathcal{L}_0 T} \hat{\rho}(R, \theta, \phi) = \exp[-R^2(1 - e^{-\Gamma T})] \hat{U}(T) \hat{\rho}(R e^{-\Gamma T/2}, \theta, \phi) \hat{U}^\dagger(T) \quad (7.43)$$

with $\hat{U}(T) = \exp(-i\hat{H}T/\hbar) = \exp(i\delta T \hat{J}_x)$. The effect of the Hamiltonian on the density matrix for a detection history $\{t_i, s_i\}$ can be expressed in the Heisenberg picture, with the time-dependent detection operators

$$\hat{c}_s(t_s) = \hat{U}^\dagger(T) \hat{c}_s \hat{U}(T). \quad (7.44)$$

Their action on the density matrix follows from eq. (7.21) when one uses that $\hat{c}_a(t)$ corresponds to the direction $\vec{u}_a(t) = -\hat{y} \sin \delta t + \hat{z} \cos \delta t$ and $\hat{c}_b(t)$ to the opposite direction $\vec{u}_b(t) = \hat{y} \sin \delta t - \hat{z} \cos \delta t$. This gives

$$\hat{c}_s(t_s) \hat{\rho}(R, \theta, \phi) \hat{c}_s^\dagger(t_s) = R^2 g_s(\theta, \phi, t_s) \hat{\rho}(R, \theta, \phi), \quad (7.45)$$

with $g_s(\theta, \phi, t) = [1 + \vec{u} \cdot \vec{u}_s(t)]/2$. The general expression (7.17) for the contribution to the density matrix from a detection history $\{t_i, s_i\}$ with the initial state (7.18) is found as

$$\begin{aligned} \hat{\rho}_L(\{t_i, s_i\}, T) &= \exp[-R^2(1 - e^{-\Gamma T})] \prod_{i=1}^L (\Gamma R^2 e^{-\Gamma t_i}) \\ &\times \int d\Omega f(\theta, \phi) \prod_{i=1}^L [g_{s_i}(\theta, \phi, t_i)] \hat{U}(T) \hat{\rho}(R e^{-\Gamma T/2}, \theta, \phi) \hat{U}^\dagger(T). \end{aligned} \quad (7.46)$$

Each detection s leads to a multiplication of the distribution function over the Bloch sphere by a factor $g_s(\theta, \phi, t)$ that now depends on the detection time. This time dependence corresponds to a rotation of the direction \vec{u}_s in the yz plane.

For the initial state of two decoupled modes, with a uniform distribution of the phase, the function f is uniform over the equator of the Bloch sphere. A detection at time t of a particle emitted by mode A or B then multiplies the distribution over the relative phase ϕ by the factor $g_a(\phi) = (1 - \sin \delta t \sin \phi)/2$ or $g_b(\phi) = (1 + \sin \delta t \sin \phi)/2$. These functions have their maximum value for $\phi = 3\pi/2$ or $\phi = \pi/2$. Strictly speaking, this distribution describes the state of the system in the Heisenberg picture, where it is not affected by continuous evolution, but only by the quantum jumps that describe the effect of detections. The evolution of the phase distribution during a typical detection history is conceptually simple. The total decay rate, summed over both detectors, is autonomous and has the time dependent rate $\Gamma R^2 \exp(-\Gamma t)$. The branching over the two detectors a and b is determined by the expectation value of $g_a(\phi)$ and $g_b(\phi)$, which has a contrast that oscillates in time at the coupling frequency δ , as a result of the mode coupling. The effect of a detection on the phase distribution is a multiplication with the same factor $(1 \mp \sin \delta t \sin \phi)/2$ for detectors a and b . This will eventually lead to a convergence of the phase distribution to a single peak at a value where either one of the factors g_s is maximal; hence, $\phi = \pi/2$ or $\phi = 3\pi/2$. The convergence to these peaked distributions is slower than in the case of a detections through a single beam splitter, as a result of the oscillations of the contrast in the functions $g_s(t)$.

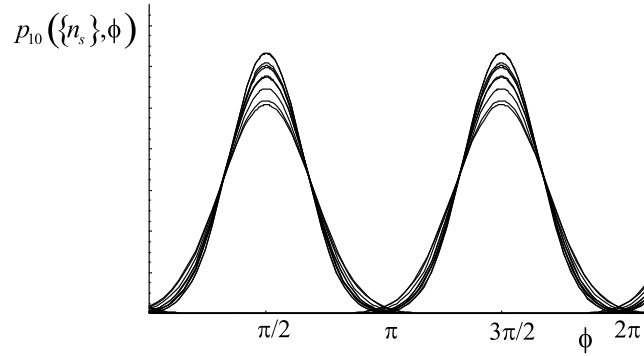


Figure 7.4: Relative phase distributions for two coupled modes after $L = 10$ detections. The sets of ten detections times are selected randomly, and for each set the most probable pair of detection histories is determined numerically. Each curve is the final phase distribution after such a detection history.

In Fig. 7.4 we plot the phase distributions for a set of typical detection histories consisting of $L = 10$ detections. These curves are numerically calculated in the following way. First we randomly select the ten time instants. Then the most probable set of ten detection channels at those instants is chosen. For each set of time instants, there are two complementary sets of detection channels, which are related by interchanging detectors a and b . The different curves in Fig. 7.4 correspond to a different selection of the time instants of detection. As seen in Fig. 7.4, after each such history, the distribution over ϕ is a peak centered either at $\pi/2$ or at $3\pi/2$.

7.4.3 Coupling and energy shift

An energy difference $\hbar\varepsilon$ between the two modes in addition to the effect of tunneling is described by the Hamiltonian

$$\hat{H} = -\hbar\delta\hat{J}_x + \hbar\varepsilon\hat{J}_z, \quad (7.47)$$

which replaces eq. (7.35). The angular momentum operators are defined in eq. (7.1). We consider the same detection scheme used in the preceding subsection. The energy difference modifies the detection statistics and the phase distribution following a representative detection history. On the Bloch sphere, the modified evolution operator $\hat{U}(t)$ is represented by a rotation in the positive direction around the axis $\varepsilon\hat{z} - \delta\hat{x}$, over an angle Ωt , with $\Omega = \sqrt{\varepsilon^2 + \delta^2}$. Equations (7.43) for the density matrix after a detection history and (7.44) for the detection operators in the Heisenberg representation $\hat{c}_s(t)$ remain valid. The detection operators are represented by points \vec{u}_s on the sphere that are reached from the poles when the opposite rotation is applied. Since the rotation axis does not lie in the equator plane, the azimuthal angle varies continuously with time, and the relative phase is no longer projected preferentially onto the same value. These unit vectors are found in the form

$$\vec{u}_a(t) = -\vec{u}_b(t) = \frac{\varepsilon\delta}{\Omega^2}(\cos\Omega t - 1)\hat{x} - \frac{\delta}{\Omega}\sin\Omega t\hat{y} + \left(\frac{\delta^2}{\Omega^2}\cos\Omega t + \frac{\varepsilon^2}{\Omega^2}\right)\hat{z}.$$

They determine the factors $g_s(\theta, \phi, t) = [1 + \vec{u} \cdot \vec{u}_s(t)]/2$ that multiply the distribution over the sphere when a particle emitted by mode A or B is detected.

As above, we consider the case of an initially factorized state, which is represented by a uniform distribution over the equator of the Bloch sphere. When a particle from mode A or B is detected, the distribution over ϕ is multiplied by

$$g_a(\phi) = \frac{1}{2} \left(1 + \frac{\varepsilon\delta}{\Omega^2} \cos\phi(\cos\Omega t - 1) - \frac{\delta}{\Omega} \sin\phi \sin\Omega t \right),$$

$$g_b(\phi) = \frac{1}{2} \left(1 - \frac{\varepsilon\delta}{\Omega^2} \cos\phi(\cos\Omega t - 1) + \frac{\delta}{\Omega} \sin\phi \sin\Omega t \right).$$

The maximum of these functions no longer coincides with the maximum of $\pm \sin\phi$, as is the case when $\varepsilon = 0$.

In Fig. 7.5 the resulting phase distributions are shown after a number of most probable detection histories, each consisting of ten detections, for $\varepsilon/\delta = 1/4$. The various curves differ in the selection of the detection times. The prescription of the calculation is the same as used in Fig. 7.4. Now not only the width of the peak, but also their position varies for different selections of the detection times. This can be explained from the time variation in the position where the maximum of $g_s(\phi, t)$ occurs.

7.5 Linear and circular chains of modes

The dynamics of a coupled chain of condensates in an optical lattice has been explored, with emphasis on the difference between a linear and a circular chain [66]. The coupling

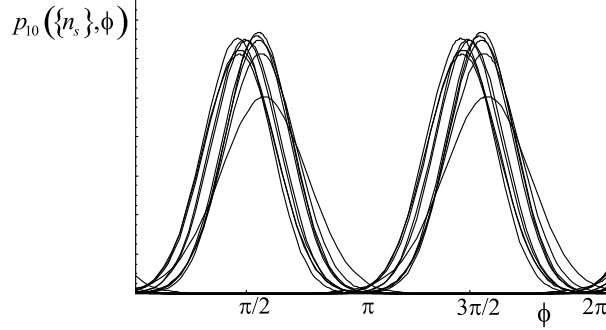


Figure 7.5: Same as Fig. 7.4, but now for coupled modes at different energies. The ratio of the energy splitting and the coupling strength is $\varepsilon/\delta = 1/4$.

was due to tunneling between neighboring modes. One expects analogous differences in the situation considered in this paper, where the phase relation between neighboring modes arises by spontaneous symmetry breaking from the observation of emitted bosons interfering through a beam splitter. This raises the question of the transitivity of the relative phase. When the relative phase between two modes A and B is well determined and the same holds for the relative phase between two modes B and C , then one expects the phase between C and A should also be fixed. On the other hand, when this latter phase is also selected by direct interaction, one may expect different dynamics depending on whether the two paths of phase determination converge to the same result or not. In the present section we compare the phase dynamics on a linear and a circular chain of modes.

7.5.1 Linear chain of modes

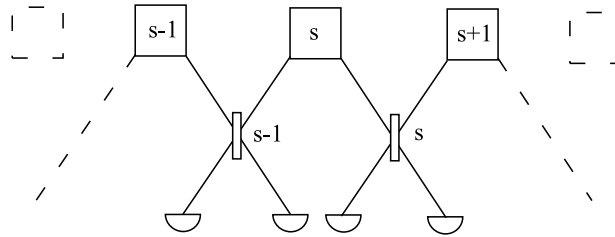
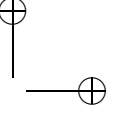
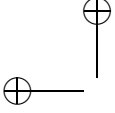


Figure 7.6: Setup with a linear chain of boson modes $\dots, s-1, s, s+1, \dots$. Neighboring modes emit particles in the input port of a beam splitter, and detectors monitor the particles in the output ports.

We consider a linear chain of modes, as sketched in Fig. 7.6. As initial state we take the uncorrelated state given by the factorized density matrix

$$\hat{\rho}(0) = \prod_s \hat{\rho}_s = \dots \hat{\rho}_{s-1} \otimes \hat{\rho}_s \otimes \hat{\rho}_{s+1} \dots, \quad (7.48)$$



where the density matrix $\hat{\rho}_s$ of each mode s has the form (7.34) with a uniform phase ϕ_s . Beam splitters are mixing the bosons emitted from neighboring modes s and $s + 1$, with orthogonal detection operators in the output channels

$$\hat{d}_{s\pm} = \frac{1}{\sqrt{2}}(\hat{a}_s \pm e^{-i\xi_s} \hat{a}_{s+1}) \quad (7.49)$$

with \hat{a}_i the annihilation operator of mode i . The evolution is described by the master equation (7.12), with

$$\mathcal{L}_0 \hat{\rho} = - \sum_s \frac{\Gamma}{2} (\hat{a}_s^\dagger \hat{a}_s \hat{\rho} + \hat{\rho} \hat{a}_s^\dagger \hat{a}_s), \quad \mathcal{L}_1 = \sum_s (\mathcal{L}_{1s+} + \mathcal{L}_{1s-}), \quad (7.50)$$

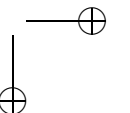
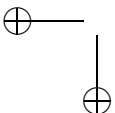
where the contribution to \mathcal{L}_1 corresponding to the detection channels s_{\pm} is specified by

$$\mathcal{L}_{1s\pm} = \frac{\Gamma}{2} \hat{d}_{s\pm} \hat{\rho} \hat{d}_{s\pm}^\dagger. \quad (7.51)$$

Physically it is obvious that the detection statistics over the output channels of each beam splitter is identical to the statistics for each of the two beam splitters in Sec. III, since each mode emits into two input channels with equal rate. The density matrix corresponding to a given detection history with n_s detections in channel s_+ and m_s detections in the channel s_- is easily written down by using the fact that a detection in channel s_+ gives a factor $\cos^2[(\Phi_s - \xi_s)/2]$ and a detection in channel s_- a factor $\sin^2[(\Phi_s - \xi_s)/2]$. After each detection history, the distribution over the phases ϕ_s of all modes factorizes into a product of distributions for each relative phase $\Phi_s \equiv \phi_s - \phi_{s+1}$ between neighbors. After n_s detections in channel s_+ and m_s detections in the channel s_- , the distribution over the relative phase $\phi_s - \phi_{s+1}$ is proportional to $\cos^{2n_s}[(\Phi_s - \xi_s)/2] \sin^{2m_s}[(\Phi_s - \xi_s)/2]$, and the distribution over the phases is proportional to the product

$$\prod_s \left[\cos^{2n_s} \left(\frac{\Phi_s - \xi_s}{2} \right) \sin^{2m_s} \left(\frac{\Phi_s - \xi_s}{2} \right) \right]. \quad (7.52)$$

Because of this factorization, the detection statistics for the pair of output channels of each beam splitter is uncorrelated to the other detections. The total number M_s of detections in the time interval $[0, T]$ on the two output channels of a single beam splitter is Poissonian with average value $r^2[1 - \exp(-\Gamma T)]$, and the probability distribution of the M_s detections over the two detectors is identical to the distribution (7.33) [102]. Therefore, the most probable histories with M_s detections on this s th beam splitter are given as $(n_s, m_s) = (M_s, 0)$ and $(0, M_s)$. The relative phase Φ_s between modes s and $s + 1$ converges to a single peak located at ξ_s or $\xi_s + \pi$, for each value of s . This also determines in a unique and unambiguous way the relative phase between any pair of modes. Hence for a linear chain of modes, the relative phase between two neighbors converges to one out of two possible values, in precisely the same way as it occurs for two modes and a single beam splitter. Spontaneous symmetry breaking occurs independently for each neighboring pair.



7.5.2 Circular chain of modes

Now we consider a series of K modes, coupled by beam splitters and arranged into a circular chain. For $K = 3$, the scheme is presented in Fig. 7.7. Equations (7.48)-(7.50) still hold, with the index s running from 1 to K . The relative phases Φ_s and the detection operators $\hat{d}_{s\pm}$ are defined as above for $s = 1, 2, \dots, K-1$, while we denote $\Phi_K = \phi_K - \phi_1$ and $\hat{d}_{K\pm} = (\hat{a}_K \pm e^{-i\xi_K} \hat{a}_1)/\sqrt{2}$. The number of beam splitters is now equal to the number of modes. On the other hand, since

$$\sum_{s=1}^K \Phi_s = 0, \quad (7.53)$$

the K modes have only $K-1$ independent relative phases Φ_s , which makes the detection system overdetermined. This is the main difference with the case of the linear chain. Detections on the s th beam splitter tend to drive the relative phase Φ_s to the value ξ_s or $\xi_s + \pi$. However, these values are consistent only when the values of all ξ_s add up to a multiple of π . The probability $p(\{n_s, m_s\}, T)$ of a specified number of detections by each detector in the time interval $[0, T]$ factorizes as in eq. (7.28) in a Poisson distribution for the total number L of detections, with the mean value $Kr^2(1 - e^{-\Gamma T})$ and the probability $p_L(\{n_s, m_s\})$ that the L detections are distributed over the detectors according to the indicated partition. This latter distribution can be specified in analogy to eq. (7.29) by

$$p_L(\{n_s, m_s\}) = \frac{L!}{\prod_s (n_s! m_s!)} F(\{n_s, m_s\}), \quad (7.54)$$

with

$$F(\{n_s, m_s\}) = \left(\frac{1}{2\pi}\right)^K \int d\phi_1 d\phi_2 \dots d\phi_K \prod_{s=1}^K \left[\cos^{2n_s} \left(\frac{\Phi_s - \xi_s}{2} \right) \sin^{2m_s} \left(\frac{\Phi_s - \xi_s}{2} \right) \right]. \quad (7.55)$$

After a detection history with n_s detections in channel s_+ and m_s detections in channel s_- , the distribution over the relative phase is still proportional to eq. (7.52). However, because of the relation (7.53), the relative phases are no longer independent, and the detection statistics of the output channels of the different beam splitters become correlated.

The most probable histories can now be found by similar considerations as we used above in Sec. 7.3.3. For a total number of $L = K \times M$ detections, the distribution for the total number of particles reaching the K beam splitters must be multinomial, with the average value M . For a most probable history the number of particles that passed each beam splitter is equal to M for each one of them. One might expect that these M particles display bosonic bunching into one output channel, with the most probable partition $(n_s, m_s) = (M, 0)$ or $(0, M)$ for all of the K beam splitters. This would indicate that the corresponding relative phases probed by these beam splitters will have converged to the value ξ_s or $\xi_s = \pi$. However, in general this can only be true for all relative phases except one, because of the phase relation (7.53). Assume that this excepted relative phase has the index s_0 . As a result of this relation, the value of the last relative phase Φ_{s_0} is thereby also fixed. The distribution over the two

output channels s_{0+} and s_{0-} will then be binomial, and the most probable partition is given by $(n_{s_0}, m_{s_0}) = (M \cos^2[(\Phi_{s_0} - \xi_{s_0})/2], M \sin^2[(\Phi_{s_0} - \xi_{s_0})/2])$. For symmetry reasons, each beam splitter has the same probability to end up in such a binomial distribution rather than a bunching one. The situation can be summarized by stating that in addition to the local spontaneous symmetry breaking for each beam splitter, also a global symmetry breaking occurs, by which the relative phase between two neighbors is not determined by the setting of their own shared beam splitter, but by the settings of all the other ones. Again, a typical detection history may be expected to be in the neighborhood of a most probable history, even though for large detection numbers, the absolute probability of a most probable history will be small.

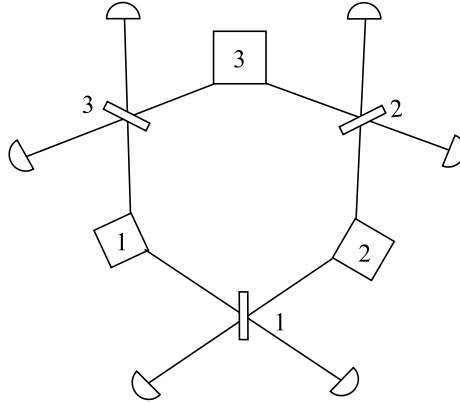


Figure 7.7: Setup of a circular chain of three boson modes 1, 2 and 3, with decay channels that are pairwise coupled by beam splitters 1, 2 and 3.

As an example, consider the case $K = 3$, as sketched in Fig. 7.7. The settings of the beam splitters are given by $\xi_1 = \xi_2 = 0$ and $\xi_3 = \pi/2$. After 30 detections, one of the partitions with the highest probability was found to be $(n_1, m_1) = (5, 5)$, $(n_2, m_2) = (10, 0)$, and $(n_3, m_3) = (10, 0)$. As one would expect from symmetry considerations, other partitions with the same maximal probability are found by swapping n_s and m_s for each beam splitter s and also by a permutation of the three indices 1, 2 and 3. This result is confirmed by a numerical calculation based on a direct evaluation of the probability distribution (7.54).

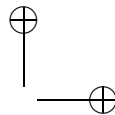
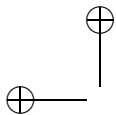
7.6 Discussion and conclusions

The absolute phase of a single-mode or multimode bosonic system is fully undetermined when the state of the system is diagonal in the total particle number. For bosonic atoms, this must be the case, since states with different particle numbers do not superpose. For a two-mode system we use the Schwinger representation with fictitious angular momentum operators to take advantage of the underlying $SU(2)$ symmetry of the state space. This allows us to represent the density matrix of the two-mode system with an undetermined absolute phase and a Poissonian distribution of the total number of particles as an integral over the

Bloch sphere of the fictitious angular momentum. The representation is given in eq. (7.10), where $f(\theta, \phi)$ is the distribution function over the sphere. It may be viewed as the Glauber-Sudarshan P function restricted to the sphere. The azimuthal angle ϕ is the relative phase, whereas the polar angle θ measures the ratio of the average number of particles in A and B , with equal populations represented by points on the equator and the poles representing states with all particles in one mode. The merit of these states with Poissonian distribution of the total particle number is that the overall decay of the modes factors out, and the detection statistics is the product of time-dependent probabilities for the total number of detections and time-independent distributions for the partitions over the various detection channels. The effect of a detection is described by the action of an annihilation operator, which also corresponds to a point on the sphere. This is equivalent to the multiplication of the distribution function $f(\theta, \phi)$ by a factor that depends only on the distance over the sphere between the points (θ, ϕ) and the detection point. This allows exact expressions, both for the detection statistics and for the conditional density matrix of the system for a given detection history. It also implies that identical detection statistics arises for different choices of the distribution f and the detection points on the Bloch sphere, provided that the setup has the same relative geometry on the sphere. This can correspond to quite different experimental setups, since the effect of detection through a beam splitter can be produced by a pulsed tunneling coupling between the modes.

In the case that the modes are constantly coupled by tunneling and in the presence of an energy difference between the modes, the phase distribution still becomes nonuniform by the detecting particles emitted by the two modes. However, since the preferred phase imposed by the detections is not the same for all detections in this case, the maximum in the phase distribution will continue to vary in position even after many detections. The convergence of the phase is expected to be perturbed more strongly when interparticle interactions are important during a detection history [107].

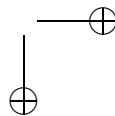
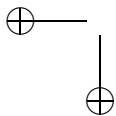
We treat explicitly the case of two modes which both emit particles in an input channel of two different beam splitters. When the settings of the beam splitters are different, they can drive the relative phase of the modes to values which are conflicting. Such a situation of conflicting phase values occurs for any number of modes which are coupled by beam splitters and arranged in a circular chain. Our model shows that in these cases the most probable detection histories lead for each pair of neighboring modes to a relative phase converging with equal probability to one of the conflicting values. The partition of the detection over the channels is a signature of the location of the peak in the phase distribution. Such a conflict does not arise for a linear chain of modes coupled by a beam splitter. A common feature of these various cases is that an initially factorized state of several modes builds up a specific value of all relative phases by only detecting their decay products in interference. In principle, this means that the modes become entangled, even though they have never been in direct contact.



|

—

—



|

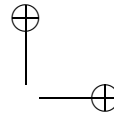
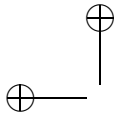
BIBLIOGRAPHY

- [1] W. D. Phillips, Rev. Mod. Phys. **70**, 721 (1998).
- [2] C. N. Cohen-Tannoudji, Rev. Mod. Phys. **70**, 707 (1998).
- [3] S. Chu, Rev. Mod. Phys. **70**, 685 (1998).
- [4] P. R. Berman, ed., *Atom Interferometry*, (Academic Press, San Diego, 1997).
- [5] C. E. Wieman, D. E. Pritchard, and D. J. Wineland, Rev. Mod. Phys. **71**, S253 (1999).
- [6] O. Mandel, M. Greiner, A. Widera, T. Rom, T. W. Hänsch, I. Bloch, Nature 425, **937** (2003).
- [7] C. Monroe, Nature **416**, 238 (2002).
- [8] K. B. Davis, M. -O. Mewes, M. R. Andrews, N. J. van Druten, D. S. Durfee, D. M. Kurn, and W. Ketterle, Phys. Rev. Lett. **75**, 3969 (1995).
- [9] M. H. Anderson, J. R. Ensher, M. R. Matthews, C. E. Wieman, and E. A. Cornell, Science 269, 198 (1995).
- [10] M. R. Matthews, B. P. Anderson, P. C. Haljan, D. S. Hall, C. E. Wieman, and E. A. Cornell, Phys. Rev. Lett. **83**, 2498 (1999).
- [11] K. W. Madison, F. Chevy, W. Wohlleben, and J. Dalibard, Phys. Rev. Lett. **84**, 806 (2000).
- [12] D. Jaksch, C. Bruder, J. I. Cirac, C. W. Gardiner and P. Zoller Phys. Rev. Lett. **81**, 3108 (1998).
- [13] C. Orzel, A. K. Tuchman, M. L. Fenselau, M. Yasuda, and M. A. Kasevich, Science **291**, 2386 (2001).
- [14] M. Greiner, O. Mandel, T. Esslinger, T. W. Hänsch and I. Bloch, Nature **415**, 39 (2002).
- [15] J. Javanainen and S. M. Yoo, Phys. Rev. Lett. **76**, 161 (1996).
- [16] M. Greiner, O. Mandel, T. W. Hänsch and I. Bloch, Nature **419**, 51 (2002).
- [17] F. Bloch, Z. Phys. **52**, 555 (1929).
- [18] L. D. Landau, Phys. Z. Sowjetunion **1**, 46 (1932).
- [19] G. Zener, Proc. R. Soc. London Ser. A **137**, 523(1934).
- [20] G. H. Wannier, Phys. Rev. **117**, 432 (1960).
- [21] P. Verkerk, B. Lounis, C. Salomon, C. Cohen-Tannoudji, J.-Y. Courtois and G. Grynberg, Phys. Rev. Lett. **68**, 3861 (1992).
- [22] P. Jessen, C. Gerz, P. D. Lett, W. D. Phillips, S. L. Rolston, R. J. C. Spreeuw and C. I. Westbrook, Phys. Rev. Lett. **69**, 49 (1992).
- [23] A. Hemmerich and T. W. Hänsch, Phys. Rev. Lett. **70**, 410 (1993).
- [24] P. S. Jessen and I. H. Deutsch, Adv. At. Mol. Opt. Phys. **37**, 95 (1996).
- [25] M. Ben Dahan, E. Peik, J. Reichel, Y. Castin, and C. Salomon, Phys. Rev. Lett. **76**, 4508 (1996).
- [26] E. Peik, M. Ben Dahan, I. Bouchoule, Y. Castin, and C. Salomon, Phys. Rev. A **55**, 2989 (1997).

- [27] S. R. Wilkinson, C. F. Bharucha, K. W. Madison, Q. Niu, and M. G. Raizen, Phys. Rev. Lett. **76**, 4512 (1996).
- [28] K. W. Madison, C. F. Bharucha, P. R. Morrow, S. R. Wilkinson, Q. Niu, B. Sundaram, and M. G. Raizen, Appl. Phys. B: Lasers Opt. **65**, 693 (1997).
- [29] M. C. Fischer, K. W. Madison, Q. Niu, and M. G. Raizen, Phys. Rev. A **58**, 2648 (1998).
- [30] M. Glück, M. Hankel, A.R. Kolovsky, and H. J. Korsch, J. Opt. B: Quantum Semiclass. Opt. **2**, 612 (2000);
- [31] M. Glück, A. R. Kolovsky, and H. J. Korsch, Phys. Rev. Lett. **82**, 1534 (1999).
- [32] T. Pertsch, P. Dannberg, W. Elflein, A. Bräuer, and F. Lederer, Phys. Rev. Lett. **83**, 4752 (1999).
- [33] D. H. Dunlap and V. M. Kenkre, Phys. Rev. B **34**, 3625 (1986).
- [34] V. M. Kenkre and S. Rhagavan, J. Opt. B: Quantum Semiclass. Opt. **2**, 686 (2000).
- [35] C. F. Bharucha, J. C. Robinson, F. L. Moore, B. Sundaram, Q. Niu, and M. G. Raizen, Phys. Rev. E **60**, 3881 (1999).
- [36] K. Drese and M. Holthaus, Phys. Rev. Lett. **78**, 2932 (1997).
- [37] M. Luban, J. Math. Phys. **26**, 2386 (1985).
- [38] G. Dattoli, J. C. Gallardo, and A. Torre, J. Math. Phys. **28**, 404 (1987).
- [39] A. M. Ishkanyan, Phys. Rev. A **61**, 063611 (2000).
- [40] P. M. Visser and G. Nienhuis, Phys. Rev. A **56**, 3950 (1997).
- [41] G. S. Agarwal and W. Harshawardhan, Phys. Rev. A **50**, R4465 (1994).
- [42] K. W. Madison, M. C. Fischer, and M. G. Raizen, Phys. Rev. A **60**, R11767 (1999).
- [43] R. Diener and Q. Niu, J. Opt. B: Quantum Semiclass. Opt. **2**, 618 (2000).
- [44] L. D. Landau and E. M. Lifshitz Quantum Mechanics: Nonrelativistic Theory, Nauka, Moscow, 1963, p.173 (in Russian).
- [45] L. Allen and J. H. Eberly, *Optical Resonance and Two-level Atoms* (Wiley-Interscience, New York, 1975).
- [46] C. B. Adams, M. Sigal and J. Mlynek, Phys. Rep. **240**, 143 (1994).
- [47] R. J. Cook and A. F. Bernhardt, Phys. Rev. A **18**, 2533 (1978).
- [48] A. Zh. Muradyan, Izv. Akad. Nauk Arm. SSR, Fiz. **10**, 361 (1975).
- [49] A. F. Bernhardt and B. W. Shore, 23, 1290 (1981).
- [50] A. P. Kazantsev, G. I. Surdutovich and V. P. Yakovlev, Pis'ma Zh. Eks. Eks. Teor. Fiz. **31**, 542 (1980).
- [51] J. Dalibard and C. Cohen-Tannoudji, J. Opt. Soc. Am. B **2**, 1707 (1985).
- [52] P. J. Martin, P. L. Gould, B. G. Oldaker, A. H. Miklich and D. E. Pritchard, Phys. Rev. A **36**, 2495 (1987).
- [53] A. P. Prudnikov, Yu. A. Brichtnikov and O. I. Marichev. Integrals and Series, Nauka, Moscow, 1988, formula 5.7.5.11, p 660 (in Russian).
- [54] I. V. Romanenko and L. P. Yatsenko, Pis'ma Zh. Eks. Teor. Fiz. **63**, 920 (1996).
- [55] A. M. Ishkhanyan, Laser Physics **7**, 1225 (1997).
- [56] V. A. Grinchuk, E. F. Kuzin, M. L. Nagaeva, G. A. Ryabenko and V. P. Yakovlev, Pis'ma Zh. Eks. Teor. Fiz. **57**, 534 (1993).
- [57] A. P. Prudnikov, Yu. A. Brichtnikov and O. I. Marichev. Integrals and Series, Nauka, Moscow, 1988, formula 5.7.5.11, pp 665-667 (in Russian).
- [58] L. Allen, M. W. Beijersbergen, R. J. C. Spreeuw, and J. P. Woerdman, Phys. Rev. A **45**, 8185 (1992).

- [59] S. S. R. Oemrawsingh, J. A. W. van Houwelingen, E. R. Eliel, J. P. Woerdman, E. J. K. Verstegen, J. G. Kloosterboer, G. W. 't Hooft Appl. Opt., **43**, 688 (2004).
- [60] S. J. van Enk and G. Nienhuis, J. Mod. Opt. **41**, 963 (1994).
- [61] A. Muthukrishnan and C. R. Stroud Jr J. Opt. B: Quantum Semiclass. Opt. **4**, S73 (2002).
- [62] M. E. J. Friese, J. Enger, H. Rubinsztein-Dunlop, and N. R. Heckenberg, Phys. Rev. A **54**, 1593 (1996).
- [63] S. Kuppens, M. Rauner, M. Schiffer, K. Sengstock, W. Ertmer, F. E. van Dorsselaer, and G. Nienhuis, Phys. Rev. A **58**, 3068 (1998).
- [64] E. M. Wright, J. Arlt, and K. Dholakia, Phys. Rev. A **63**, 013608 (2001).
- [65] P. L. Gould, G. A. Ruff, and D. E. Pritchard, Phys. Rev. Lett. **56**, 827 (1986).
- [66] N. Tsukada, Phys. Rev. A **65**, 063608 (2002).
- [67] K. K. Das, G. J. Lapeyre, and E. M. Wright, Phys. Rev. A **65**, 063603 (2002).
- [68] Gh. -S. Paraoanu, Phys. Rev. A **67**, 023607 (2003).
- [69] M. R. Andrews, C. G. Townsend, H.-J. Miesner, D. S. Durfee, D. M. Kurn, and W. Ketterle, Science **275**, 637 (1997).
- [70] D. S. Hall, M. R. Matthews, C. E. Wieman, and E. A. Cornell, Phys. Rev. Lett. **81**, 1543 (1998).
- [71] G. Kalosakas and A. R. Bishop, Phys. Rev. A **65**, 043616 (2002).
- [72] J. Javanainen and M. Y. Ivanov, Phys. Rev. A **60**, 2351 (1999).
- [73] G. J. Milburn, J. Corney, E. M. Wright and D. F. Walls, Phys. Rev. A **55**, 4318 (1997).
- [74] J. R. Anglin and A. Vardi, Phys. Rev. A **64**, 013605 (2001).
- [75] G. L. Salmond, C. A. Holmes, and G. J. Milburn, Phys. Rev. A **65**, 033623 (2002).
- [76] C. Menotti, J. R. Anglin, J. I. Cirac, and P. Zoller, Phys. Rev. A **63**, 023601 (2001).
- [77] N. R. Thomas, A. C. Wilson, and C. J. Foot, Phys. Rev. A **65**, 063406 (2002).
- [78] T. G. Tiecke, M. Kemmann, Ch. Buggle, I. Shvarchuck, W. von Klitzing, J. T. M. Walraven J. Opt. B: Quantum Semiclass. Opt. **5**, S119-S123 (2003).
- [79] M. Wilkens, E. Schumacher, and P. Meystre, Phys. Rev. A **44**, 3130 (1991).
- [80] C. Keller, J. Schmiedmayer, A. Zeilinger, T. Nonn, S. Dürr, G. Rempe Appl. Phys. B:Lasers Opt. **69**, 303 (1999).
- [81] B. W. Shore, The Coherent Theory of Atomic Excitation (Wiley, New York, 1990), p. 1005.
- [82] D. M. Giltner, R. W. McGowan and S. A. Lee, Phys. Rev A **52**, 3966 (1995).
- [83] L. Bernstein, J. C. Eilbeck, and A. C. Scott, Nonlinearity **3**, 293 (1990).
- [84] M. Holthaus, Phys. Rev. A **64**, 011601 (2001).
- [85] A. R. Edmonds, *Angular Momentum in Quantum Mechanics*(University Press, Princeton, 1957).
- [86] A. Polkovnikov, S. Sachdev and S. M. Girvin, Phys. Rev. A **66**, 053607 (2002)).
- [87] D.H. Dunlap and V.M. Kenkre, Phys. Rev. B **34**, 3625 (1986).
- [88] G. S. Agarwal and W. Harshawardhan, Phys. Rev. A **50**, R4465 (1994).
- [89] F. T. Arecchi and E. Courtens and R. Gilmore and H. Thomas Phys Rev A **6**, 2211 (1972).
- [90] A. M. Perelomov, *Generalized Coherent States and their applications* (Springer, Berlin 1986).
- [91] Y. Castin and J. Dalibard, Phys. Rev. A **55**, 4330 (1997).

- [92] F. A. M. de Oliveira, M. S. Kim and P. L. Knight, V. Bužek, Phys. Rev. A **41**, 2645 (1990).
- [93] M. Kitagawa and M. Ueda, Phys. Rev. A **47**, 5138 (1993).
- [94] A. R. Kolovsky, Phys. Rev. Lett. **90**, 213002 (2003).
- [95] D. van Oosten, P. van der Straten, and H. T. C. Stoof, Phys. Rev. A **63**, 053601 (2001).
- [96] G. G. Batrouni, V. Rousseau, R. T. Scalettar, M. Rigol, A. Muramatsu, P. J. H. Denteneer, and M. Troyer, Phys. Rev. Lett. **89**, 117203 (2002).
- [97] J. I. Cirac, C. W. Gardiner, M. Naraschewski, and P. Zoller, Phys. Rev. A **54**, 3714 (1996).
- [98] J. Ruostekoski and D. F. Walls, Phys. Rev. A **58**, 50 (1998).
- [99] J. A. Dunningham, S. Bose, L. Henderson, V. Vedral and K. Burnett, Phys. Rev. A **65**, 064302 (2002).
- [100] A. P. Hines, R. H. McKenzie and G. J. Milburn, Phys. Rev. A **67**, 013609 (2003).
- [101] E. L. Bolda, S. M. Tan and D. F. Walls, Phys. Rev. Lett. **79**, 4719 (1997).
- [102] G. Nienhuis, J. Phys. A **34**, 7867 (2001).
- [103] A. J. Leggett and F. Sols, Found. Phys. **21**, 353 (1991).
- [104] J. A. Dunningham and K. Burnett, J. Phys. B **33**, 3807 (2000).
- [105] C. W. Gardiner, *Quantum Noise* (Springer, Berlin, 1991).
- [106] L. Mandel and E. Wolf, *Optical Coherence and Quantum Optics* (Cambridge University Press, Cambridge, England 1995).
- [107] T. Wong, M. J. Collett and D. F. Walls, Phys. Rev. A **54**, 3718 (1996).



Samenvatting

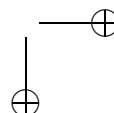
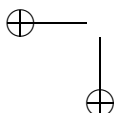
Sinds de komst van de quantummechanica is licht een belangrijk middel om de quantumeigenschappen van materie te bepalen en te begrijpen. Om de bouwstenen van de wereld op atomaire schaal (atomen, ionen en elektronen) te onderzoeken is het nodig om de thermische fluctuaties van de atomaire dynamica te beperken. Dit probleem is uitgebreid onderzocht in de afgelopen jaren, met als prominent voorbeeld succesvolle methoden om neutrale atomen te koelen en op te sluiten met de kracht van licht. Aan dit onderzoeksgebied is in 1997 de Nobelprijs voor natuurkunde verleend, die gezamenlijk werd toegekend aan W. D. Phillips, C. Cohen-Tannoudji en S. Chu. Het basismechanisme is de uitwisseling van impuls en energie tussen het licht en een atoom. De lichtkrachten die het atoom ondervindt kunnen zijn bewegingsvrijheid in de ruimte beperken, en bovendien de thermische fluctuaties in zijn snelheid verminderen.

Daarnaast vormen lichtvelden het belangrijkste middel om de quantumeigenschappen van neutrale atomen te sturen. Dit is in verscheidene toepassingen gerealiseerd. De belangrijkste toepassing is atomaire interferometrie, die tegenwoordig een aanzienlijk hogere gevoeligheid te zien geeft dan de meer conventionele, zuiver optische interferometrie. Een verdere toepassing van koude atomen, meer in het bijzonder koude ionen, wordt nagestreefd in opstellingen die de basis moeten vormen van onderdelen van quantumcomputers.

Een volgende belangrijke stap in het "meer quantummechanisch" maken van neutrale atomen is gezet in 1995, met de eerste experimentele demonstratie van een Bose-Einstein-condensaat (BEC) van alkali-atomen. Dit is een toestand van materie waarin alle atomen in eenzelfde quantumtoestand verkeren. In 2001 werd de Nobelprijs voor natuurkunde toegekend aan E. A. Cornell, W. Ketterle and C. E. Wieman, voor de realisatie van BEC in een ijel gas van alkali-atomen, en baanbrekend fundamenteel onderzoek van hun eigenschappen. De macroscopische bevolking van de laagste energietoestand werd bereikt door de atomen op te sluiten in licht, en door ze met behulp van afdamping tot extreem lage temperaturen te koelen. Op deze wijze kunnen de quantumeigenschappen van materie worden versterkt, en op macroscopische schaal worden onderzocht.

De meeste theoretische beschrijvingen van een systeem van koude atomen verwaarlozen de correlatie tussen de atomen. Maar een beschrijving van een BEC als een echt veeldeeltjessysteem vereist dat de wisselwerking tussen de atomen in rekening wordt gebracht. Het vroegere theoretische werk aan condensaten in een enkele mode maakte gebruik van het model van Gross, Pitaevski en Bogoliubov. De basisvergelijking van deze theorie beschrijft het systeem met behulp van een macroscopische golf functie, die de verdeling van de atomen over plaats en impuls beschrijft. Deze beschrijving is semiklassiek van aard, en is nauw verwant met de theorie van superfluiditeit. Maar in de praktijk kan een BEC quantumfluctuaties vertonen die niet in de semiklassieke theorie zijn vervat. Dit soort quantumeffecten is waarneembaar voor een BEC in meerdere modes, bijvoorbeeld in een optisch rooster.

In dit proefschrift bekijken we een aantal voorbeelden van fysische situaties waar lichtvelden worden gebruikt om condensaten en andere systemen van koude atomen met hoge



nauwkeurigheid te manipuleren. We beginnen met beschouwingen van enkele atomen, en breiden vervolgens de discussie uit tot veeldeeltjessystemen, zoals condensaten.

In Hoofdstuk 2 bekijken we de mogelijkheden om de toestand van een enkel atoom te prepareren en te sturen. Het atoom verkeert in een periodieke optische potentiaal met een helling. Meestal wordt een periodieke optische potentiaal gevormd door een staande golf van licht, die is samengesteld uit twee tegen elkaar in lopende golven. Het resultaat is een keten van potentiaalputten, waarbinnen een deeltje door het tunnелеffect de barrière tussen twee beledende putten kan passeren. Een systeem van atomen in een periodieke optische potentiaal wordt een optisch rooster genoemd. Wij beschouwen de situatie waarin behalve de periodieke potentiaal ook een uniforme kracht wordt opgelegd, die bovendien met de tijd kan variëren. We bepalen de dynamica van een deeltje bij een willekeurige begintoestand, met behulp van een exact oplosbaar model. Het gedrag van zo'n deeltje is rijk gestructureerd, en hangt sterk af van de beginverdeling van het deeltje over het rooster. Als het deeltje bijvoorbeeld aanvankelijk is gelokaliseerd in een enkele potentiaalput, dan beweegt het niet in de richting van de uniforme kracht, maar het spreidt zich slechts uit over het rooster, zonder dat zijn gemiddelde positie verandert. Als het deeltje aanvankelijk een redelijk welbepaalde quasi-impuls heeft, waarbij het verdeeld moet zijn over vele roosterplaatsen, dan zal het Bloch-oscillaties gaan vertonen. Daarbij vertonen de quasi-impuls en de gemiddelde positie van het deeltje een periodieke variatie in de tijd. Dit effect is aanvankelijk voorspeld voor elektronen in een kristal, maar het is waargenomen voor atomen in een optisch rooster. We geven een algemene beschrijving van de gemiddelde beweging en de spreiding van de toestand van een deeltje in een optisch rooster met een uniforme kracht.

Ook in Hoofdstuk 3 kijken we naar de wisselwerking van een enkel atoom met een periodieke optische potentiaal. Maar terwijl het in Hoofdstuk 2 ging over de dynamica van een atoom dat gevangen was in het rooster, gaat het nu om een vrij atoom, waarvan de golffunctie diffractie vertoont als het een staande golf van licht doorkruist. De belangrijkste resultaten kunnen worden begrepen uit de beginselen van behoud van energie en impuls. Als het atoom wisselwerkt met twee tegen elkaar in lopende golven, dan kan het een foton uit één lopende golf absorberen, en dat weer uitzenden naar de andere lopende golf. Zo kan een atoom in een staande golf een grote impuls oplopen, zonder dat er sprake is van spontane emissie. Dit is in tegenstelling tot het geval van een lopende golf, waar een atoom niet meer impuls kan opnemen dan de impuls $\hbar k$ van een enkel foton. Deze bekende resultaten gelden als een atoom voorafgaand aan de wisselwerking in de grondtoestand verkeert. Maar de situatie is anders wanneer het atoom in een superpositie verkeert van de grondtoestand en de aangeslagen toestand. We laten zien dat in dit geval de impulsoverdracht van de fotonen aan het atoom gedurende de wisselwerking met een lopende golf groter kan zijn dan $\hbar k$. Dit effect suggereert een belangrijke praktische toepassing. Het effect van diffractie kan worden gestuurd door een welgekozen afwisseling van staande en lopende golven te gebruiken.

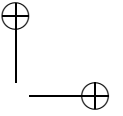
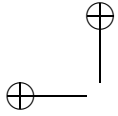
Terwijl de wisselwerking van een atoom met een staande golf van licht gepaard gaat met een uitwisseling van impuls tussen veld en atoom, kan de wisselwerking met een paar Laguerre-Gauss-bundels met tegengestelde heliceiteit leiden tot uitwisseling van impulsmoment. Dit is het gevolg van het feit dat de fotonen in een Laguerre-Gauss-bundel een baanimpulsmoment in de propagatierichting dragen. Ruimtelijk gezien vormt een paar van zulke bundels met tegengestelde heliceiteit een circulair optisch rooster, dat het gevolg is van een staande golf langs een cirkel. Zo'n circulaire staande golf heeft wezenlijke voordelen verge-

leken met een gebruikelijke lineaire staande golf. Een aanvankelijk gelokaliseerd golfpakket van een atoom wordt gesplitst in een superpositie van een naar links en een naar rechts draaiende component. Als het atoom is opgesloten in een ringvormige potentiaal, dan leiden de beide componenten tot interferentie. Karakteristiek voor het circulaire rooster is dat de componenten elkaar treffen zonder dat hun bewegingsrichting hoeft te worden omgekeerd. In gebruikelijke interferometrische opstellingen zijn altijd lichtvelden nodig die als spiegel dienen voor een atomair golfpakket. Dit schema voor atoominterferometrie zonder spiegelende lichtvelden wordt besproken in Hoofdstuk 4.

Vanaf Hoofdstuk 5 bekijken we condensaten in meerdere modes. Als modelsysteem nemen we het geval van een BEC in een dubbele potentiaalput. We vergelijken de dynamica van een BEC in de twee putten met de dynamica van atomen die aan een staande lichtgolf diffractie ondergaan. De aanleiding daarvoor is dat de Hamiltonianen in operatorgedaante er hetzelfde uitzien. Het verschil ligt in de commutatierregels van de operatoren. Bekende diffractieverschijnselen zoals de *Pendellösung*-oscillaties tussen tegengestelde impulsstanden in het geval van Bragg-diffractie hebben een analogon in het gedrag van de verdeling van de atomen in een BEC over de twee putten. Deze verdeling vertoont een oscillatie in het verschil in de atoomaantallen in de twee putten, tenminste als de koppeling tussen de putten zwak is vergeleken met de wisselwerking tussen de atomen. Als deze koppeling langzaam varieert in de tijd, dan kan een deel van de atomen adiabatisch van de ene put overgaan naar de andere.

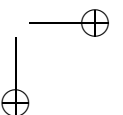
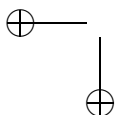
In Hoofdstuk 6 worden de eigenschappen van een BEC in een dubbele potentiaalput nader onderzocht in het geval van sterke wisselwerking tussen de atomen. Een gevoelige manier om de eigenschappen van een condensaat te bepalen is te zoeken naar resonanties in de respons van het systeem op een externe periodieke variatie van de parameters. In de buurt van de resonantiefrequenties is te verwachten dat de respons sterk met de frequentie zal variëren. De periodieke variatie kan worden gerealiseerd door de vorm van de potentiaal te moduleren. We vinden een resonante overgang tussen twee toestanden waarbij een enkel atoom uit het condensaat oscilleert tussen de putten. Het kan ook voorkomen dat meer dan twee toestanden resonant met elkaar zijn gekoppeld, zodat meer dan één atoom tussen de putten oscilleert. Als gevolg van deze resonantie-effecten kan men het aantal atomen in de putten beheersen door de sterkte en de frequentie van de modulatie van het energieverschil tussen de putten geschikt te kiezen. Ook de tunnelsnelheid tussen de putten kan door resonanties worden vergroot. Deze beschouwingen kunnen ook worden gegeneraliseerd tot een systeem met meer dan twee putten, zoals een condensaat in een optisch rooster.

In Hoofdstuk 7 behandelen we het probleem van de relatieve fase tussen de verschillende modes van een BEC. De relatieve fase wordt bepaald door de atomen waar te nemen die door de verschillende modes worden geëmitteerd. Daarbij worden de atomen uitgezonden door verschillende modes in de ingangskanalen van een bundelsplitser gestuurd, en zodoende in interferentie waargenomen. Eerst behandelen we het geval van een BEC in twee modes. Beide modes zenden atomen uit in de ingangskanalen van twee verschillende bundelsplitters, waarvan de uitgangskanalen worden gedetecteerd. De uitgangskanalen van een bundelsplitser corresponderen met twee tegengestelde relatieve fasen van de modes. De instelling van de bundelsplitters kan zo worden gekozen dat de paren van relatieve fasewaarden met elkaar in tegenspraak zijn. Ook bij meer dan twee modes treedt een dergelijk conflict op, wanneer ze met elkaar gekoppeld zijn in een cyclische structuur. We berekenen de statistiek van de



104 Samenvatting

verschillende mogelijke detectiehistories van alle uitgangskanalen, en we leiden af welke van die histories de grootste waarschijnlijkheid hebben. Het model laat zien dat bij elk van de histories met de grootste waarschijnlijkheid de relatieve fase uiteindelijk convergeert naar een van de elkaar tegensprekende waarden. Welke van de waarden uiteindelijk optreedt is een strikt quantumproces, dat zich dus niet laat voorspellen. Een dergelijk conflict treedt niet op bij een lineaire keten van modes, die buursgewijs door bundelsplitters zijn gekoppeld. Een gemeenschappelijke eigenaardigheid van de verschillende gevallen is dat een aanvankelijk gefactoriseerde toestand van de modes leidt tot een gecorreleerde toestand door alleen maar de vervalsproducten van de modes in interferentie te detecteren. Dit houdt in dat een quantummechanische verstrengeling ontstaat zonder dat de modes met elkaar in contact zijn geweest.



Սառը ատոմների և Բոզե-Էյնշտեյնի կոնդենստի կոհերենս դեկավարումը լուսային ալիքներով

Քվանտային մեխանիկայի ստեղծման առաջին օրերից լուսային դաշտերը լայնորեն օգտագործվել են միկրոաշխարհի (ատոմներ, էլեկտրոններ, իոններ և այլն) քվանտո-մեխանիկական հատկությունները ուսումնասիրելիս: Այդ հատկություններն ի հայտ բերելու համար էական է սահմանափակել մասնիկների ջերմային շարժումը: Այս պրոբլեմը երկար ժամանակ լայն քննարկման առարկա էր ժամանակակից ֆիզիկայում: Հետագայում, չեզոք մասնիկների սառեցման և գերման փորձերը պսակվեցին հաջողությամբ, որի համար 1997թ Նոբելյան մրցանակը ֆիզիկայից շնորհվեց ՌԻ. Ֆիլիպսին, Կ. Կոհեն-Տանուջին և Ս. Չուին: Այս փորձերի հիմքում ընկած է էներգիայի և իմպուլսի փոխանցումը լուսային փնջից ատոմին, որի արդյունքում ատոմի վրա ազդող ուժ է առաջանում: Դրա հաշվին սահմանափակվում է ատոմի տարածական շարժումը և միևնույն ժամանակ կրճատվում է շարժման ջերմային կոմպոնենտը:

Բացի գուտ ֆունդամենտալ հետաքրքրություն ներկայացնելուց, լուսային դաշտերը լայնորեն օգտագործվում են ատոմների քվանտո-մեխանիկական շարժումը բարձր ճշտությամբ դեկավարելու համար: Մինչ այժմ ատոմային ինտերֆերոմետրերը հանդիսանում են սառը ատոմների ամենակարևոր կիրառությունը: Նրանք ապահովում են շատ անգամ բարձր զգայնություն, քան իրենց լայնորեն տարածված օպտիկական անալոգները: Սառեցված ատոմների և հատկապես իոնների մյուս կարևոր կիրառությունը կապված է նրանց օգտագործման հետ քվանտային հաշվարկի սխեմաներում:

Սառեցված ատոմներն ավելի քվանտո-մեխանիկական դարձնելու ուղղությամբ հաջորդ քայլն արվեց 1995թ, երբ առաջին անգամ փորձում հնարավոր եղավ դիտել Բոզե-Էյնշտեյնի կոնդենսատը (ԲԷԿ): Արդեն 2001թ Նոբելյան մրցանակը ֆիզիկայից շնորհվեց Է. Կոհենիին, Վ. Կետերլիին և Կ. Վայմանին ԲԷԿ-ի ստացման և նրա ֆունդամենտալ հատկությունների ուսումնասիրության համար: Կիրառելով «գոլորշիացման» կոչվող սառեցման մեթոդները, հնարավոր եղավ սառեցնել ատոմական գազը այնպիսի ցածր ջերմաստիճանի, երբ ատոմների մեծ մասը զբաղեցնում են իրենց հիմնական միմասնիկային վիճակը՝ որոշակի քվանտային վիճակում ստեղծելով մակրոսկոպիկ բնակեցվածություն: Այսպիսով, ԲԷԿ-ում նյութի քվանտային հատկությունները ուժեղացվել են և կարող են դիտվել մակրոսկոպիկ մակարդակով: Ի հակադրություն սառը ատոմական գազի՝ ԲԷԿ-ը հանդիսանում է իրական բազմամասնիկային համակարգ և նրա հատկությունների տեսական նկարագրությունը տալիս միջատոմական փոխազդեցությունը ընդգրկելը էական է: ԲԷԿ-ի վերաբերյալ առաջին տեսական աշխատանքները հիմնված են

Գրոսս-Պիտասևսկի-Բոգոլյուբովի տեսության վրա, որն ինքնին կիսադասական է դիտարկում համակարգի հատկությունները: Սա սերտորեն կապված է գերհոսունության տեսության հետ: Միևնույն ժամանակ, ԲԷԼ-ը ուսումնասիրելիս կարող են ի հայտ գալ երևույթներ, որոնց համար կիսադասական նկարագրությունը բավական չէ: Այսպիսի երևույթներ արդեն դիտվել են բազմամոդ ԲԷԼ-ի համար, մասնավորապես, ԲԷԼ-ը օպտիկական բյուրեղում քննարկելիս:

Այս ատենախոսության մեջ մենք քննարկում ենք երևույթներ և ֆիզիկական իրավիճակներ, որտեղ լուսային դաշտերն են կիրառված սառեցված ատոմական գազի և ԲԷԼ-ի քվանտո-մեխանիկական վարքը բարձր ճշտությամբ ղեկավարելու համար: Առաջին գլուխները վերաբերվում են սառը ատոմական գազին, որից հետո մենք անդրադառնում ենք բազմամասնիկային համակարգերին ինչպիսին է ԲԷԼ-ը:

Գլուխ 2-ում մենք քննարկում ենք մասնիկի վիճակի պատրաստման և ղեկավարման խնդիրը թեքված օպտիկական բյուրեղում: Սովորաբար, օպտիկական բյուրեղը կազմվում է երկու հակադիր վազող ալիքները համադրելով: Այն իրենից ներկայացնում է պոտենցիալ հորների հաջորդականություն, որտեղ մասնիկները կարող են թունելային անցմամբ անցնել մի հորից մյուսը: Թեքված օպտիկական բյուրեղն իրենից ներկայացնում է դաշտ, որտեղ ատոմի նկատմամբ բացի օպտիկական բյուրեղից նաև համասեռ ուժ է կիրառված: Ճշգրտորեն լուծվող մոդելի հիման վրա ցույց է տրված, որ մասնիկը ցուցաբերում է հարուստ դինամիկա, և նրա սկզբնական վիճակը վճռորոշ է հետագա վարքի համար: Օրինակ, երբ մասնիկը սկզբում կենտրոնացած է օպտիկական բյուրեղի միայն մեկ հորում, չնայած նրա վրա ազդող որոշակի ուղղություն ունեցող ուժի, մասնիկի միջին կոորդինատը չի փոխվում, և մասնիկը հետագայում կարող է միայն սփռվել բյուրեղով մեկ: Երբ սկզբնական վիճակը իրենից ներկայացնում է այսպես կոչված Բլոխի վիճակ, որը նշանակում է, թե մասնիկը սկզբում սփռված է ամբողջ բյուրեղով և օժտված է որոշակի քուադրիմպուլսով, հետագայում մասնիկը ցուցաբերում է Բլոխի տատանումներ: Այս երևույթը իրենից ներկայացնում է մասնիկի տատանումներ տարբեր քուադրիմպուլսային վիճակների մեջ: Երևույթը կանխատեսվել է վաղուց, էլեկտրոնների համար բյուրեղում և դիտվել է միայն չեզոք ատոմների համար օպտիկական բյուրեղում: Ընդհանուր դեպքում կարելի է արագադրել պայման, որը բացատրում և բնորոշում է մասնիկի շարժման բնույթը թեքված օպտիկական բյուրեղում:

Գլուխ 3-ում մենք շարունակում ենք քննարկել ատոմի փոխազդեցությունը պարբերական պոտենցիալի հետ: Ի տարբերություն Գլուխ 2-ի, որտեղ մեկ գերված ատոմի դեպքն է դիտարկվում, այստեղ մենք դիտարկում ենք ազատ ատոմ, որը փոխազդում է տարածականորեն պարբերական լուսային փնջի կամ կանգուն ալիքի հետ: Հիմնական

արդյունքները կաող են մեկնաբանվել՝ հիմնվելով էներգիայի և իմպուլսի պահպանման սկզբունքների վրա: Երբ ատոմը փոխազդում է հակադիր տարածման ուղղությամբ վազող ալիքների հետ, այն կարող է կլանել ֆոտոն մի ալիքից և ճառագայթել մյուսի մեջ: Այսպիսով, ատոմը կարող է ձեռք բերել մեծ իմպուլս կանգուն ալիքի հետ փոխազդելով: Սա հակառակ է մի վազող ալիքի հետ փոխազդելության դեպքին, երբ ատոմի իմպուլսի փոփոխությունը չի կարող գերազանցել առանձին ֆոտոնի իմպուլսը: Այսպիսով, հետաքրքիր ֆիզիկական իրավիճակ է առաջանում, երբ հաշվի է առնվում ատոմի ներքին կառուցվածքը, այլ խոսքերով, դիտարկում ենք մոդելային երկմակարդակ ատոմ, որը փոխազդում է վազող ալիքի հետ: Եթե ատոմը մինչ փոխազդելությունը գտնվում է ենթամակարդակներից որևէ մեկում, արդյունքը որակապես նույնն է, ինչ որ նախորդ դեպքում: Որակապես այլ իրավիճակ է առաջանում, երբ ատոմը նախապես մինչև վազող ալիքի հետ փոխազդելը ենթամակարդակների որոշակի սուպերպոզիցիոն վիճակում է: Այդպիսի սուպերպոզիցիոն վիճակում ատոմը հայտնվում է, եթե այն փոխազդում է կանգուն ալիքի հետ: Կարելի է ցույց տալ, որ այս դեպքում մակարդակների միջև փոխանցված իմպուլսը ավելի մեծ է քան առանձին ֆոտոնի իմպուլսը: Այսպիսով, մի ֆոտոնանի պրոցեսը, որպիսին կարելի է դիտել ատոմի փոխազդելությունը վազող ալիքի հետ, առաջացնում է ատոմի իմպուլսի փոփոխություն, և փոփոխության չափը շատ անգամ կարող է գերազանցել առանձին ֆոտոնի իմպուլսը: Առաջարկվում է նաև երևույթի պրակտիկ կիրառությունը. ատոմի՝ կանգուն ալիքի վրա ցրման պատկերը կարելի է դեկավարելի ձևով փոփոխել՝ կիրառելով կանգուն ալիք+վազող ալիք հաջորդականությունը և ընտրելով կանգուն ու վազող ալիքի հետ փոխազդելության փուլերի տևողությունը:

Եթե փոխազդելությունը հակուղղված վազող ալիքների հետ բերում է ատոմի իմպուլսի փոփոխությանը, ապա փոխազդելությունը հակառակ պտույտի ուղղություն ունեցող Լազեր-Գաուսի (ԼԳ) ալիքների հետ բերում է նրան, որ ատոմի պտտական իմպուլսը (իմպուլս, որը կապված է ազիմուտային անկյան հետ) կարող է զգալի աճել: Այս երևույթը կապված է ԼԳ ալիքների՝ որոշակի պտտական իմպուլսով օժտված լինելու հատկության հետ: Սա մանրամասն քննարկված է Գլուխ 4-ում, որտեղ դիտարկում ենք ատոմի փոխազդելությունը հակառակ պտտական ուղղությամբ ԼԳ լուսային ալիքների հետ: Այս ալիքները ստեղծում են օպտիկական շրջանային դասավորված բյուրեղ, որն կարող է նաև կոչվել կանգուն ալիք ազիմուտային անկյան նկատմամբ: Այսպիսի շրջանային բյուրեղը մի շարք սկզբունքային առավելություններ ունի սովորական գծային բյուրեղի նկատմամբ: Օրինակ, երբ այն ազդում է անկյունային նեղ սեգմենտի վրա կենտրոնացած ատոմական ալիքային փաթեթի վրա, փաթեթը տրոհվում է հակառակ պտտման ուղղությամբ ալիքների: Եթե այդպիսի ատոմը գտնվում է գլանային սիմետրիա

ունենցող պոտենցիալ հորում, հակառակ պոտվող փաթեթները հատվում են և կարելի է գրանցել նրանց վերադրման ինտերֆերենցիոն պատկերը: Այսպիսով, հակառակ պոտվող ատոմական փնջերը իրար վերադրվում են առանց լրացուցիչ հայելի հանդիսացող դաշտի, որը միշտ առկա է ատոմական ինտերֆերոմետրերում և կիրառվում է ատոմական փնջերի ողողությունը շրջելու ու նրանց հետագա վերադրումը ապահովելու համար: Այս երույթը կարող է կիրառվել սկզբունքորեն նոր ատոմային ինտերֆերոմետրեր կառուցելու համար, որտեղ ընդհանրապես հայելիներ չեն օգտագործվում:

Սկսած Գլուխ 5-ից՝ մենք քննարկում ենք բազմամող ԲԷԿ-ներ: Որպես երկմող մողելային համակարգ՝ դիտարկում ենք ԲԷԿ, որը գերված է կրկնակի պոտենցիալ հորում: Մեր մոտեցումը հիմնված է այդպիսի հորում կոնդենսատի վարքի և կանգուն ալիքի վրա ատոմների ցրման միջև համանմանության վրա: Համապատասխան համիլտոնիանները ունեն միևնույն տեսքը, միայն բնութագրվում են տարբեր կոմուտացիոն աղբյուրություններով:

Ատոմի դիֆրակցիայի խնդրից հայտնի են մի շարք երևույթներ, ինչպիսին են, օրինակ, *Պենդլլոտունգ տատանումները*, որոնք ծագում են Բրեգի և ադիաբատորեն միացված կանգուն ալիքի վրա ցրման դեպքում: Այդ երևույթները համապատասխանում են համանման երևույթներին կրկնակի հորում կոնդենսատի համար մի այնպիսի ռեժիմում, երբ հորերի միջև թունելային անցման գործակիցը փոքր է ատոմների միջև փոխազդեցության հաստատունի նկատմամբ կամ հորերի միջև արգելքը ադիաբատորեն դանդաղ է միացվում: Երևույթներն ի հայտ են գալիս, երբ սկզբնական պահին աջ և ձախ հորերում պարունակվող մասնիկների թիվը զգալիորեն տարբեր է: Կոնդենսատի համար նշված երևույթները արտահայտվում են նրանում, որ աջ և ձախ հորերում պարունակվող մասնիկների թվի տարբերությունը օսցիլացվում է մի հորից մյուսը:

Հաջորդ, 6-րդ գլխում մենք շարունակում ենք ուսումնասիրել երկհոր պոտենցիալում ԲԷԿ-ի վարքը: Երբ կոնդենսատը կազմող ատոմների միջև փոխազդեցությունը ուժեղ է, համակարգը ցուցաբերում է ուժեղ ռեզոնանսներ, հետագայում այն շատ զգայուն է արտաքին պարբերական գրգռումների նկատմամբ: Պարզ է, որ ռեզոնանսների մոտակայքում (երբ արտաքին պարբերական գրգռման այդ հաճախականությունը մոտ է համակարգի սեփական ռեզոնանսային հաճախականություններից որևէ մեկին), համակարգի վարքը զգալիորեն կախված է գրգռման հաճախականությունից: Արտաքին պարբերական գրգռումը ընդգրկում ենք երկհոր գերող պոտենցիալի տեսքը պարբերականորեն փոխելով: Սկզբունքորեն, մի քանի ռեժիմներ կարող են դիտվել: Երկու մակարդակների միջև կարող է ծագել ռեզոնանս, որը համապատասխանում է այն պարզ դեպքին, երբ մեկ առանձին ատոմ տատանվում է հորերի միջև: Միևնույն ժամանակ, բազմամասնիկային ռեզոնանսներ են հնարավոր, երբ

մի քանի վիճակներ ռեզոնանսային ձևով կապված են, և մեկից ավելի ատոմներ են ռեզոնանսային ձևով անցնում մի հորից մյուսը: Օգտագործելով այդպիսի ռեզոնանսները՝ կարելի է ղեկավարելի ձևով փոխել մասնիկների միջին թիվը հորերում՝ փոփոխելով խնդրի համար էական հանդիսացող պարամետրերը, ինչպիսիք են պարբերական գրգռման հաճախականությունը, կրկնակի հորի տեսքը և այլն: Կիրառության տեսակետից հետաքրքիր է այն փաստը, որ ռեզոնանսներին մոտ թունելային անցմամբ մի հորից մյուսը անցնող մասնիկների թիվը զգալի աճում է: Կրկնակի հորի համար դուրս բերված մի շարք ռեզոնանսային էֆեկտները կարելի է ընդհանրացնել բազմամոդ համակարգի համար, ինչպիսին է, օրինակ, օպտիկական բյուրեղը:

Հաջորդ և վերջին գլխում մենք դիտարկում ենք բազմամոդ ԲԷԿ-ի մոդերի միջև հարաբերական փուլի հաստատման հարցը: Մոդերի միջև հարաբերական փուլը չափելու համար դիտարկվում է մոդերից ճարագայթվող մասնիկների ինտերֆերենցիոն պատկերը: Ինտերֆերենցիոն պատկերը կարելի է մոդելավորել գրանցելով մասնիկները այսպես կոչված «ալիքային բաժանարար»-ի միջոցով, որտեղ մասնիկները հավաքվում են երկու մուտքերում և հետագայում գրանցվում են երկու ելքերում:

Քննարկումը սկսում ենք երկմոդ համակարգ դիտարկելուց, որտեղ ճառագայթված մասնիկները գրանցվում են երկու իրարից տարբեր ալիքային բաժանարարներով: Խնդրի հետաքրքրությունը կայանում է նրանում, որ հատկություններով տարբեր բաժանարարներից ամեն մեկը առանձին, եթե մյուսը բացակայում է, պրոյեկտում է հարաբերական փուլը մի որոշակի արժեքի, որը որոշվում է միայն բաժանարի հատկություններով: Այսպիսով, տարբեր բաժանարարների գոյությունը կարող է բերել անհամատեղելի հարաբերական փուլերի: Նման իրավիճակ, երբ անհամատեղելի փուլեր կարող են ծագել, առաջանում է բազմամոդ համակարգում, որտեղ մոդերը դասավորված են շրջանաձև: Համակարգի վարքը քննարկում ենք ըստ բաժանարարի ելքերում մասնիկների գրանցման պատմության և ընտրում ենք այն պատմությունը, որը առավել հավանական է: Ըստ մեր մոդելի՝ հարաբերական փուլը հավասար հավանականությամբ կարող է գուգամիտել բաժանարարի հատկություններով որոշվող անհամատեղելի փուլերից որևէ մեկին: Միևնույն ժամանակ ցույց է տրված, որ հարաբերական փուլի գուգամիտելը կախված է գրանցող սարքից: Կարելի է մոդելավորել իրավիճակ կամ ընտրել այնպիսի գրանցող սարք, երբ հարաբերական փուլը չի գուգամիտում որևէ արժեքի, և փուլային բաշխման մաքսիմումը փոխվում է ժամանակի ընթացքում:



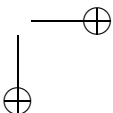
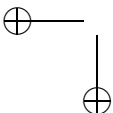
Curriculum Vitae

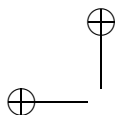
Hayk Haroutyunyan

Born on the 4th of February 1975 in Yerevan, Armenia.

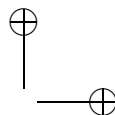
After receiving in 1998 my Ms degree in Physics with Major in Theoretical Physics and Minor in Computational Physics I started to work as a Research Assistant at the Engineering Center in Armenia studying Atom Optics in the group of prof. dr. A. Zh. Muradyan.

In 2000 I came to the Netherlands to start my PhD research in the group of Quantum Optics in Leiden University. I was involved in the theoretical research on properties of cold atoms and Bose-Einstein condensates supervised by prof. dr. G. Nienhuis. The results of my work were presented at the European Quantum Electronics Conferences (EQEC) in Nice, France (2000) and in Munich, Germany (2003), at the Workshop on the Theory of Bose-Einstein condensates held in Salerno (2001), at the conference on Atom Optics and Interferometry in Lunteren, the Netherlands (2002) and at the International Conference on Atomic Physics (ICAP) in Boston (2002). I have attended the summer school on Quantum Computation in Varenna, Italy (2002) and the summer school on Atomic Physics held in Boston (2002).



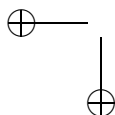


|

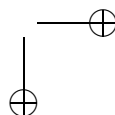


—

—



|





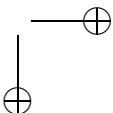

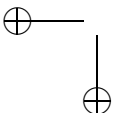
Acknowledgements

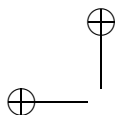
This thesis would not be complete without a word to everyone who helped me in preparing it in Leiden and back in Armenia.

First of all, I am grateful to Prof. Atom Muradyan for his great influence on my scientific and human skills. In my decision to pursue my PhD abroad I was assisted and supported by colleagues at the Engineering Center in Armenia, and I want to express my special thanks to Prof. Raphael Kazaryan.

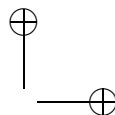
My work in Leiden wouldn't be possible without help and support of several people. I was dependent on the computer support of Arno van Amersfoort, René Overgauw and Leendert Prevo. Our two secretaries, Anneke Aschoff and Henriette van Leeuwen ensured that the rest of us could continue doing our research. I want to thank Anneke for her help and support in my long efforts to study the Dutch language. I have had long discussions and have learned a lot from my roommates Sergio, Matthijs, Andrea and Cyriaque, who were always very helpful and ready to discuss. I am thankful for discussions with other students in the group: Krista, Alexander, Marnix, Steven, Yngve, Jos, Sumant, Javier, Jorrit, Erwin, Nikolay, Graciana, Thijs, Peter.

Special thanks to the family van de Poll and Mrs Gemma Cranssen for their hospitality and for their help in understanding the habits, customs of the foreign country and again in my long struggle with the Dutch language.



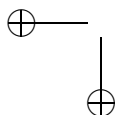


|

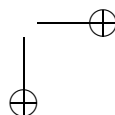


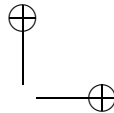
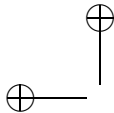
—

—



|





Publications

- *Momentum transfer for an optical transition in a prepared two-level atom*
A. Zh. Muradyan and H. L. Haroutyunyan Phys. Rev. A **62**, 013401 (2000).
- *Coherent control of atom dynamics in an optical lattice*
H. L. Haroutyunyan and G. Nienhuis Phys. Rev. A **64**, 033424 (2001).
- *Analogy between a two-well Bose-Einstein condensate and atom diffraction*
H. L. Haroutyunyan and G. Nienhuis Phys. Rev. A **67**, 053611(2003).
- *Phase dynamics of a multimode Bose-Einstein condensate controlled by decay*
H. L. Haroutyunyan and G. Nienhuis Phys. Rev. A **69**, 053621 (2004).
- *Diffraction by circular optical lattices*
H. L. Haroutyunyan and G. Nienhuis (accepted for Phys. Rev. A).
- *Resonances for coupled Bose-Einstein condensates*
H. L. Haroutyunyan and G. Nienhuis (accepted for Phys. Rev. A).

